

TRA 2.10/95-18

c.2

Field and Analytical Evaluation of the Effects of Tied PCC Shoulders and Widened Slabs on Performance of JPCP

Prepared for:

State of Colorado
Department of Highways
Research and Development Branch
4201 E. Arkansas Avenue
Denver, Colorado 80222


Submitted by:

ERES
CONSULTANTS, INC.

505 West University Avenue
Champaign, IL 61820-3915
(217) 356-4500

ERES Project No. 94-59-R1

October 1995

COLORADO STATE PUBLICATIONS LIBRARY
TRA2.10/95-18 c.2 local
Yu. H. Thomas/Field and analytical evalu

3 1799 00021 4445

REPORT DOCUMENTATION PAGE			FORM APPROVED OMB NO. 0704-0188
Public reporting burden for this collection of information is estimated to average 1 hour per response, including the time for reviewing instructions, searching existing data sources, gathering and maintaining the data needed, and completing and reviewing the collection of information. Send comments regarding this burden estimate or any other aspect of this collection of information, including suggestions for reducing this burden, to Washington Headquarters Services, Directorate for Information Operations and Reports, 1215 Jefferson Davis Highway, Suite 1204, Arlington, VA 22202-4302, and to the Office of Management and Budget, Paperwork Reduction Project (0704-0188), Washington, DC 20503.			
1. AGENCY USE ONLY (Leave Blank)	2. REPORT DATE October 1995	3. REPORT TYPE AND DATES COVERED Final Report, 2 Years	
4. TITLE AND SUBTITLE Effects of Tied Pcc Shoulders and Widened Slabs on Performance of JPCP			5. FUNDING NUMBERS
6. AUTHOR(S) H. Thomas Yu, Kurt D. Smith, M.L. Darter			
7. PERFORMING ORGANIZATION NAME(S) AND ADDRESS(S) Colorado Department of Transportation 4201 E. Arkansas Ave. Denver, Colorado 80222			8. PERFORMING ORGANIZATION REPORT NUMBER CDOT-DTD-R-95-18
9. SPONSORING/MONITORING AGENCY NAME(S) AND ADDRESS(S) Colorado Department of Transportation 4201 E. Arkansas Ave. Denver, Colorado 80222			10. SPONSORING/MONITORING AGENCY REPORT NUMBER CDOT-DTD-R-95-18
11. SUPPLEMENTARY NOTES Prepared in Cooperation with the U.S. Department of Transportation, Federal Highway Administration			
12a. DISTRIBUTION/AVAILABILITY STATEMENT No Restrictions: This report is available to the public through the National Technical Information Service, Springfield, VA 22161			12b. DISTRIBUTION CODE
13. ABSTRACT (Maximum 200 words) This study was conducted to evaluate the effects of widened slabs and tied concrete shoulders on the performance of PCC pavements. As part of this study, The Colorado Department of Transportation (CDOT) constructed three test sections in the westbound driving lanes of I-70 during the Summer of 1994. The experimental factors included in these sections are as follows: - Section1: Widened Slabs (14-ft) with tied PCC shoulder. - Section2: Widened Slabs (14-ft) with nontied PCC shoulder. - Section3: Standard Slabs (12-ft) with tied PCC shoulder. The analytical evaluation included the evaluation of the data collected from the instrumented slabs, the analysis of the FWD data, and fatigue analysis to determine the expected performance of the three JCP designs...			
14. SUBJECT TERMS tied shoulder widened slabs nontied shoulder			15. NUMBER OF PAGES 76
			16. PRICE CODE
17. SECURITY CLASSIFICATION OF REPORT Unclassified	18. SECURITY CLASSIFICATION OF THIS PAGE Unclassified	19. SECURITY CLASSIFICATION OF ABSTRACT Unclassified	20. LIMITATION OF ABSTRACT

**Field and Analytical Evaluation of
the Effects of Tied PCC Shoulder and
Widened Slabs on Performance of JPCP**

Final Report

H. Thomas Yu
Kurt D. Smith
M.I. Darter

ERES Consultants, Inc.
October 1995

Prepared for:
Colorado Department of Transportation

Disclaimer

The contents of this report reflect the views of the authors who are responsible for the facts and the accuracy of the data presented herein. The contents do not necessarily reflect the official views of the Colorado Department of Transportation or the Federal Highway Administration. This report does not constitute a standard, specification, or regulation.

Table of Contents

INTRODUCTION	1
ANALYSIS OF DATA FROM INSTRUMENTED SLABS	4
Curling Analysis	4
<u>Instrumentation and Data Collection</u>	4
<i>Curling Measurements</i>	4
<i>Temperature Measurements</i>	5
<u>Analysis</u>	10
Strain Analysis	15
<u>Instrumentation and Data Collection</u>	15
<u>Analysis</u>	18
<i>Temperature Effects on Load Strains at the Longitudinal Edge</i>	25
<i>Load Transfer Efficiency</i>	30
<i>Effects of Measurement Location and Load Placement on Load Strains</i>	32
Conclusion	37
PERFORMANCE EVALUATION AND MONITORING	38
Deflection Testing Using FWD	38
<u>Field Testing</u>	38
<u>Backcalculation</u>	39
<u>Load Transfer Efficiencies</u>	40
<u>Deflection Trends</u>	43
Fatigue Analysis	47
<u>Stress Calculations</u>	48
<i>Load Stress</i>	49
<i>Curling Stress</i>	52
<i>Combined Stress</i>	53
<u>Fatigue Damage Calculation</u>	54
<i>Temperature Distribution</i>	55
<i>Pass-to-Coverage Ratio</i>	56
<i>Fatigue Damage Distribution Across the Slab</i>	61
<u>Effects of Built-in Upward Curling on Performance</u>	64
<u>Expected Performance</u>	65
Long-Term Monitoring	70
SUMMARY	71
<u>Field Testing and Data Analysis</u>	71
<u>Expected Performance</u>	72
<u>Recommendations</u>	73
REFERENCES	75

Table of Contents
(Continued)

APPENDIX A: CORE TESTING RESULTS

APPENDIX B: SUMMARY OF FIELD STRAIN DATA

APPENDIX C: FWD DATA

INTRODUCTION

This study was conducted to evaluate the effects of widened slabs and tied concrete shoulders on the performance of portland cement concrete (PCC) pavements. As a part of this study, the Colorado Department of Transportation (CO DOT) constructed three test sections in the westbound driving lanes of I-70 during the summer of 1994. All three test sections are 11.25-in jointed plain concrete pavements (JPCP) with 15-ft joint spacing constructed on a 7-in asphalt concrete (AC) base which is the old pavement surface. The experimental factors included in these sections are as follows:

- Section 1: Widened slabs (14-ft) with tied PCC shoulder.
- Section 2: Widened slabs (14-ft) with nontied PCC shoulder.
- Section 3: Standard-width slabs (12-ft) with tied PCC shoulder.

The test sections are located 2 mi west of the Kansas-Colorado border, near Burlington. The site location is shown in figure 1. The exact location of the test sections are as follows:

- Section 1: Mile 449.0, Westbound, Station 1365+03 to 1359+90.
- Section 2: Mile 447.8, Westbound, Station 1302+10 to 1300+00.
- Section 3: Mile 446.9, Westbound, Station 1255+12 to 1249.97.

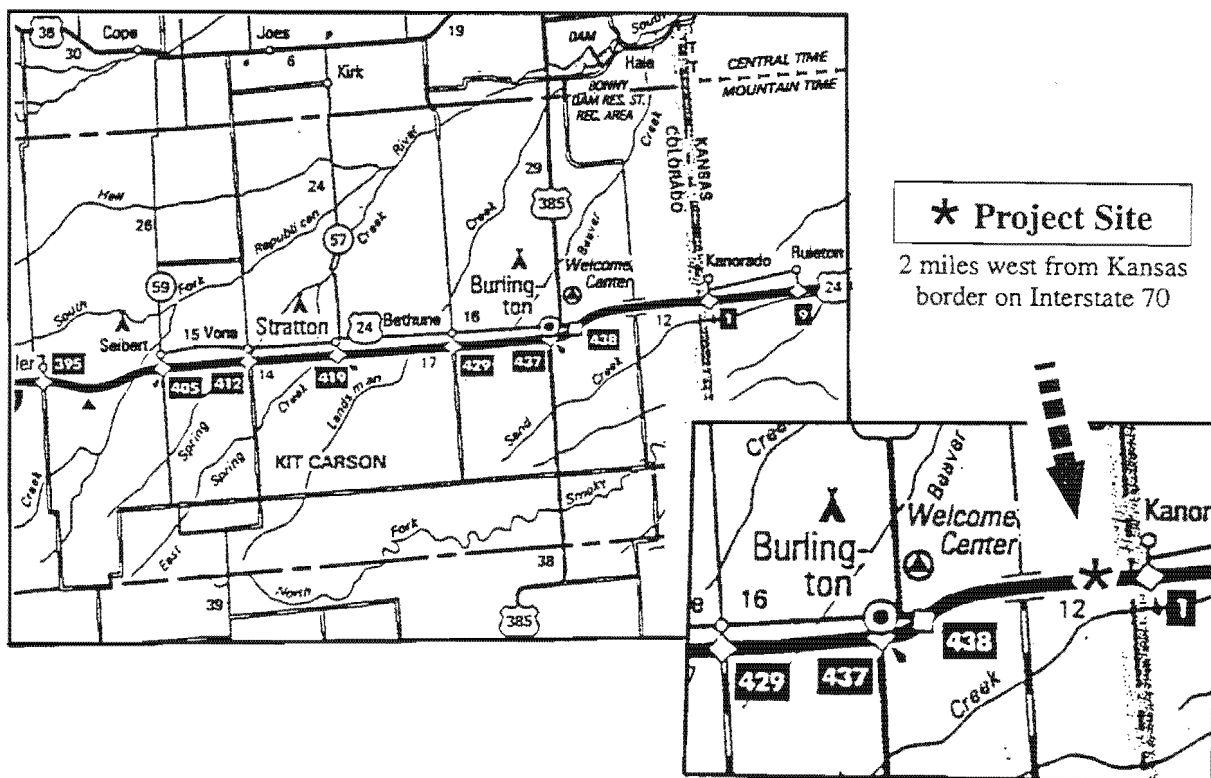


Figure 1. Illustration of the site location.

Through field testing, analysis, and long-term monitoring of these test sections, it is hoped that the effects of the widened slabs and tied concrete shoulders on performance of jointed concrete pavement (JCP) will be determined.

A number of States are using widened slabs and tied PCC shoulders in an effort to enhance the fatigue performance of JCP (*NCHRP Project 1-32*). The widened slabs are used extensively in Wisconsin and Minnesota. Wisconsin uses 14-ft and 15-ft wide slabs on the outside lane. Minnesota uses 13.5-ft and 14-ft wide slabs on the outside lane and 13.5-ft wide slabs on the inside lane. The other States that have used widened slabs include Iowa, Illinois, Indiana, and Texas. The widened slabs are typically provided on the outside lane, and 14-ft wide slabs are most common. AC shoulders are typically provided on widened-slab pavement sections.

The use of tied PCC shoulders is more prevalent than widened slabs, although the performance of the in-service tied PCC shoulder sections have been mixed (Smith et al. 1995). Improper design is responsible for the less-than-expected performance observed on many in-service tied PCC shoulder sections. The observed design deficiencies include excessive tiebar spacing and inadequate tiebar size to obtain good aggregate interlock, mismatch between shoulder and mainline pavement joints, and improper sawing of the lane-shoulder joint. Where properly designed and constructed tied PCC shoulders were provided, excellent performance has been observed. The States that have used tied PCC shoulders include Arizona, Florida, Georgia, Illinois, Michigan, Minnesota, North Carolina, New York, Ohio, and Wisconsin. California has used both tied and nontied PCC shoulders.

The structural responses of the test pavements were measured by instrumenting the test sections and by conducting falling weight deflectometer (FWD) testing. The analytical evaluation included the evaluation of the data collected from the instrumented slabs, the analysis of the FWD data, and fatigue analysis to determine the expected performance of the three JCP designs. The test sections will be monitored over their service life to validate the results of the analytical evaluation.

During the field testing conducted in July 1994, selected slabs were instrumented with dial gauges and surface-mounted strain gauges to measure the temperature and load induced deflections and strains. Pavement temperatures during the testing were monitored by installing thermocouples at several different depths in a pavement slab and recording the temperatures at regular intervals. Instrumentation and data collection were conducted by Construction Technologies Laboratories (CTL). The wheel loads were applied using a truck that was loaded to provide an 18-kip single axle load. Cores were also taken from each test section to obtain slab thickness, modulus of elasticity, and strength. The instrumented slabs provided valuable data on how PCC slabs constructed on a very stiff stabilized base (the old AC pavement) respond to temperature and wheel loads.

A thorough analysis was performed on the collected data to determine whether the measured structural responses of PCC pavement are consistent with the analytically obtained values. This was accomplished by evaluating the following:

- Curling at the slab corners and longitudinal edge.
- Load-induced edge strains at various temperature conditions.
- Strains at various transverse distances from the shoulder joint caused by the load placed at various locations.

The second part of the analytical evaluation was completed in May 1995, following the completion of the FWD testing. The focus of this part of the evaluation was to evaluate the effects of widened slabs and tied concrete shoulders on long-term performance of JCP. Considering the effects of traffic, slab curling, and slab design factors, a thorough fatigue analysis was conducted to determine the expected performance of the three JCP designs under evaluation. This report documents field testing, evaluation of the testing data, and analytical performance evaluation conducted under this study.

ANALYSIS OF DATA FROM INSTRUMENTED SLABS

Instrumented slabs were used in this study to characterize the structural response of the three pavement designs under evaluation and to verify that the deflections and stresses in PCC pavements can be determined adequately by analytical means. The instrumentation included the following:

- Dial gauges at the slab edges and corners to measure slab deflections due to temperature curling.
- Surface-mounted strain gauges installed along the slab edges and wheelpath to measure the load-induced strains under an 18-kip single axle load.

The evaluation of the deflection and strain measurements taken from the instrumented slabs are presented in this chapter.

Curling Analysis

Temperature differences between the top and bottom of PCC slabs cause the pavement slabs to curl. The direction (lifting or dropping of the slab corners) and amount of curling depends on the sign and magnitude of the temperature gradient. If the slab surface is hotter than the bottom (as typically is the case during a sunny day) the slab curls downward; if the surface is colder than the bottom, the slab curls upward (corners lifted). Curling is a direct result of the through-thickness differences in the amount of thermal expansion or contraction of concrete caused by the through-thickness temperature differences. The amount of curling depends on the temperature gradient and the slab length.

Significant bending stresses can result from curling because the self-weight of concrete restrains curling. Curling stresses at certain times of day can equal or exceed load stresses in typical jointed concrete highway pavements. Accurate determination of the effects of curling, therefore, is very important to JCP performance predictions.

Instrumentation and Data Collection

Curling Measurements

In this study, curling was measured directly using dial gauges installed at the corners and longitudinal edge of shoulder slabs. This was accomplished by anchoring reference rods 6 ft below the pavement surface, thus isolating the rods from the movements of upper layers, and measuring the movements of the slab corners and edge with respect to the reference rods using dial gauges. The dial gauges were mounted on the slabs with the probe end bearing on the reference rod to give the readings of the relative movements. The dial gauge installation is shown in figure 2.

The curling measurements were taken at about 30 min intervals throughout the day, starting early in the morning (6:23 a.m. on 7/12/94 and 5:30 a.m. on 7/13/94) until late afternoon (5:40 p.m. on 7/12/94 and 6:00 p.m. on 7/13/94). The curling measurements are summarized in tables 1 and 2. The curling measurements given in these tables are

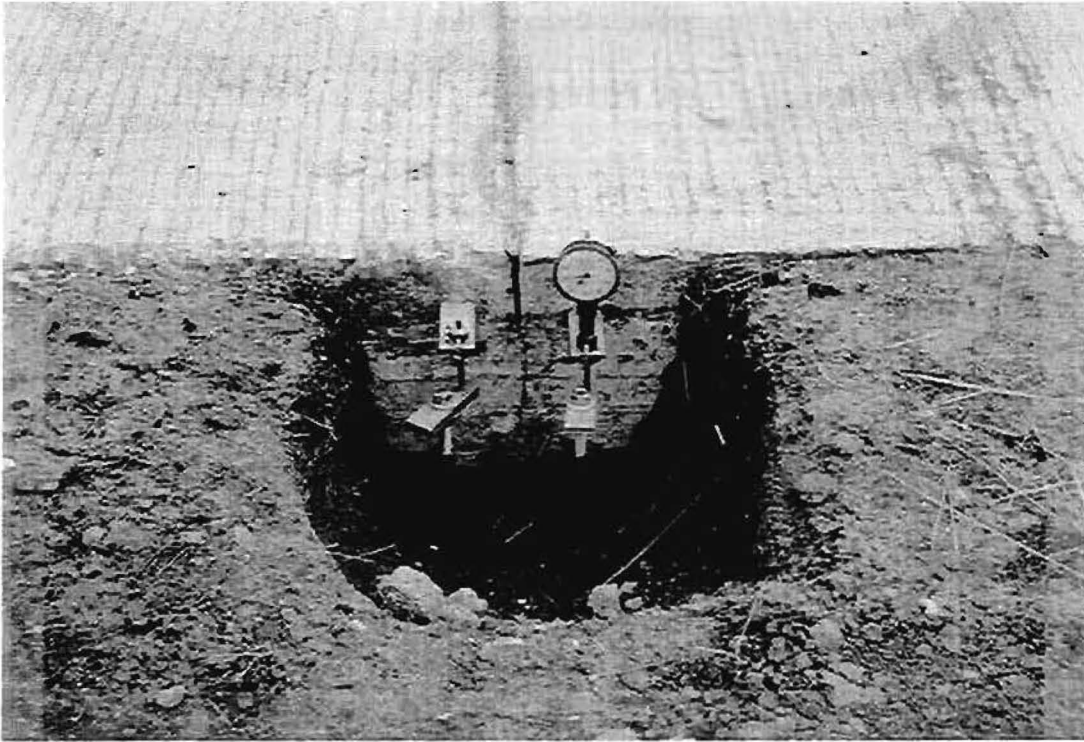


Figure 2. Dial gauge installed at a slab corner for curling measurements.

relative values. Because only the changes in the elevation at the monitoring points can be measured, whether the slab is curled up or down cannot be determined from the field measurements. The slabs are not necessarily flat at zero temperature gradient because moisture gradients also affect curling and some residual curling may have been built in during construction. The smallest number from each set of dial gauge readings was used to determine the amount of curling at each location.

Similar magnitudes of curling were observed on both days. Several of the readings of 32 on the leave corner curling shown in table 1 were caused by a frozen dial gauge. Because no wheel loads were applied, the curling of the approach corner should not be different than that of the leave corner. This is shown better in table 2 than in table 1. The curling reversed (indicating that the point of maximum effect of positive temperature gradients had been reached) at 2:45 p.m. on July 12th and at 3:35 p.m. on the 13th.

Temperature Measurements

The temperature gradients in the slabs were monitored by installing thermocouples at five different depths in a pavement slab (top, middle, bottom, and at 1/4 points) and recording temperatures at 30 min intervals. The temperature data are given in tables 3 and 4. Figure 3 illustrates the through-thickness temperature variations at different times of the day. As shown in this figure, temperature gradients can be highly nonlinear at certain times of the day; however, because the maximum negative (5:30 a.m.) and maximum positive (2:00 p.m.) gradients are fairly linear, the simple difference between top and bottom temperatures was used in the analysis.

Table 1. Curling measurements taken on July 12, 1994.

Time 7/12/94	Temp Diff, ofF	Dial Gauge Readings, mils			Curl, mils		
		Leave	Approach	Mid Slab	Leave	Approach	Mid Slab
6:23	-12.5	305	276	441	73	77	27
6:35	-11.7	306	279	442	72	74	26
7:01	-9.9	310	280	442	68	73	26
7:31	-7.9	314	285	445	64	68	23
8:02	-5.8	320	290	446	58	63	22
8:29	-3.5	325	296	449	53	57	19
8:57	-0.8	330	303	450	48	50	18
9:28	3.0	331	310	454	47	43	14
10:10	7.4	346	320	456	32	33	12
10:36	9.6	346	325	460	32	28	8
11:12	12.5	346	333	462	32	20	6
11:45	14.9	346	337	464	32	16	4
12:16	16.8	346	343	465	32	10	3
12:38	18.5	346	345	466	32	8	2
14:45	19.9	378	353	468	0	0	0
15:40	15.0	377	351	467	1	2	1
16:41	10.4	370	344	465	8	9	3
17:30	8.8	365	340	464	13	13	4
17:40	8.0	358	338	462	20	15	6

Table 2. Curling measurements taken on July 13, 1994.

Time 7/13/94	Temp Diff, °F	Dial Gauge Readings, mils			Curl, mils		
		Leave	Approach	Mid Slab	Leave	Approach	Mid Slab
5:30	-11.9	310	284	445	75	74	25
5:50	-11.0	310	285	445	75	73	25
6:35	-10.0	311	286	446	74	72	24
7:18	-7.5	315	291	447	70	67	23
8:07	-2.0	325	298	450	60	60	20
8:53	3.0	334	308	452	51	50	18
9:32	6.8	344	313	456	41	45	14
10:14	11.5	353	327	459	32	31	11
10:51	15.7	361	335	462	24	23	8
11:55	19.5	371	345	465	14	13	5
12:40	21.9	377	351	467	8	7	3
13:58	23.2	382	356	469	3	2	1
14:40	21.4	384	357	469	1	1	1
15:35	20.6	385	358	470	0	0	0
16:14	17.4	381	355	468	4	3	2
16:48	13.4	378	350	466	7	8	4
18:01	6.6	366	339	463	19	19	7

Table 3. Temperature data for July 12, 1994.

Time	Top					Bottom	Difference
	Air	1	2	3	4	5	
6:25	62.3	61.0	64.1	67.8	71.6	73.5	-12.5
6:55	61.7	63.1	64.6	67.6	67.8	73.3	-10.2
7:25	66.3	64.9	65.6	68.0	68.2	73.1	-8.2
7:55	67.2	66.9	66.8	68.4	68.5	73.0	-6.1
8:25	69.6	69.0	68.2	69.0	68.4	72.9	-3.9
8:55	72.1	71.8	69.8	69.6	68.7	72.8	-1.0
9:25	74.7	75.6	72.1	70.6	69.2	72.7	2.9
9:55	76.0	78.5	73.9	71.4	70.6	72.5	6.0
10:25	77.5	81.5	75.9	72.3	70.9	72.3	9.2
10:55	78.7	84.2	77.9	73.5	71.2	72.5	11.7
11:25	79.7	86.7	80.0	74.8	71.6	72.6	14.1
11:55	81.1	89.7	82.4	76.5	72.7	73.3	16.4
12:25	82.9	92.0	84.9	78.5	73.5	74.2	17.8
12:55	90.8	94.0	86.7	79.8	74.3	74.8	19.2
13:25	87.3	95.7	88.2	81.0	75.3	75.1	20.6
13:55	89.1	97.0	89.7	82.3	76.4	75.8	21.2
14:25	87.3	98.6	91.1	83.7	77.5	76.5	22.1
14:55	85.5	96.0	91.9	84.9	78.6	77.2	18.8
15:25	90.3	95.3	90.9	85.4	79.1	77.7	17.6
15:55	85.8	94.3	91.5	86.0	80.7	78.6	15.7
16:25	86.0	93.1	90.7	86.1	81.2	78.9	14.2
16:55	84.4	90.8	89.8	86.1	81.9	79.5	11.3
17:25	85.4	88.9	88.6	85.9	82.0	79.7	9.2
17:41	84.6	88.3	88.0	85.7	82.3	80.3	8.0

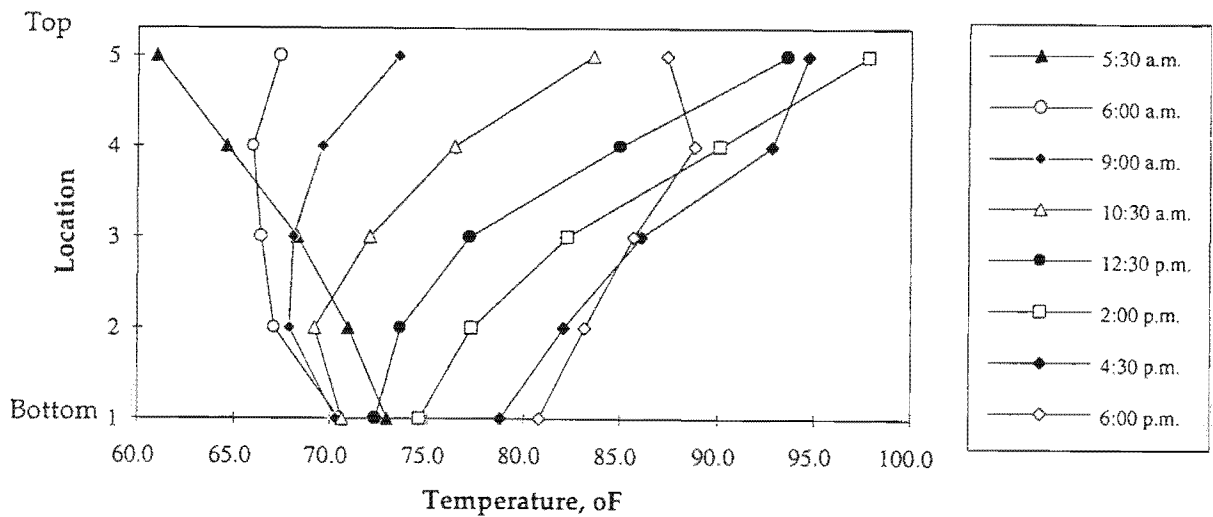


Figure 3. Through-thickness temperature variations.

Table 4. Temperature data for July 13, 1994.

Time	Air	Top				Bottom	Difference
		1	2	3	4	5	
5:28	68.2	61.0	64.6	68.3	70.9	72.9	-11.9
5:58	67.0	60.7	63.7	67.4	71.0	71.7	-11.0
6:28	66.7	61.1	63.6	66.6	69.3	71.5	-10.4
6:58	66.4	62.7	63.9	66.3	67.4	71.1	-8.4
7:28	66.4	64.9	64.8	66.2		70.7	-5.8
7:58	66.6	67.4	66.0	66.4	67.1	70.5	-3.1
8:28	67.2	70.5	67.6	67.4		70.3	0.2
8:58	68.1	73.5	69.6	68.1	67.9	70.3	3.2
9:28	69.0	77.1	71.6	69.1	68.5	70.3	6.8
9:58	70.2	80.6	74.0	70.4		70.5	10.1
10:28	71.3	83.6	76.4	72.0	69.2	70.6	13.0
10:58	72.6	86.5	78.6	73.4	69.9	70.8	15.7
11:28	74.2	89.0	80.8	74.9		71.3	17.7
11:58	75.9	91.6	83.0	75.7	71.0	71.8	19.8
12:28	77.3	93.6	85.0	77.2	73.6	72.3	21.3
12:58	78.9	95.4	86.9	79.5		72.9	22.5
13:28	80.3	96.5	88.6	81.0		73.6	22.9
13:58	81.8	97.8	90.1	82.3	77.3	74.6	23.2
14:28	83.4	97.4	91.0	83.7	78.8	75.9	21.5
14:58	84.2	97.9	91.6	84.9		76.5	21.4
15:28	85.0	98.0	92.3	85.4	80.1	77.1	20.9
15:58	86.2	96.8	93.1	86.0		77.8	19.0
16:28	87.4	94.7	92.8	86.1	82.1	78.8	15.9
16:58	87.8	92.2	92.0	86.1	82.8	79.8	12.4
17:28	87.6	90.1	90.4	85.9		80.4	9.7
17:58	86.8	87.5	88.8	85.7		80.4	7.1
18:01	87.0	87.4	88.8	85.7	83.2	80.8	6.6

The temperature differences between the top and bottom of the slab at different times of the day are shown in figure 4. The temperature conditions on July 12th and 13th were very similar, and caused very similar curling, as illustrated in figure 5. The maximum temperature gradients ranged from -14 °F to +22 °F on July 12th and from -12 °F to +23 °F on July 13th.

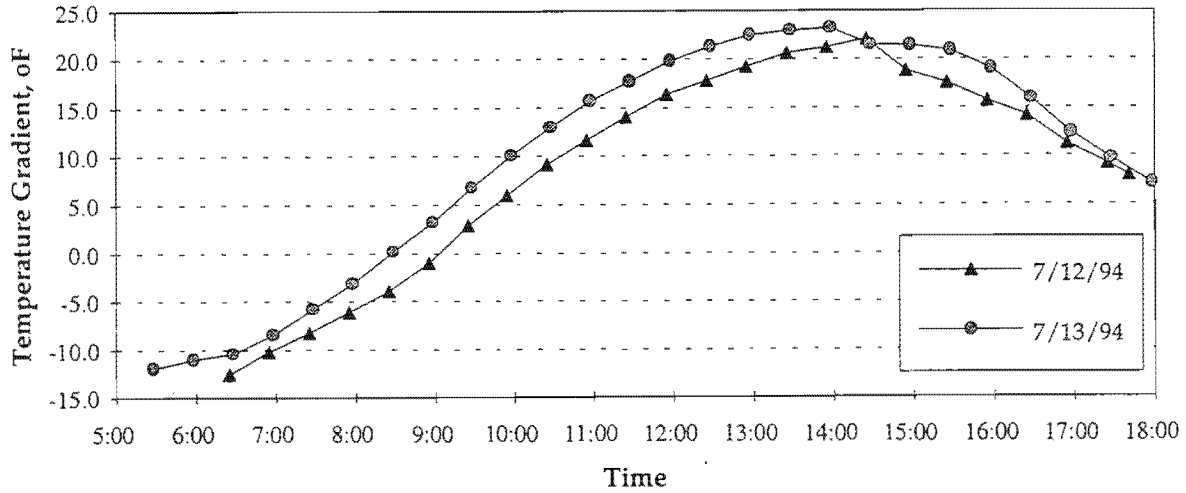


Figure 4. Temperature gradients through the test slabs on 7/12/94 and 7/13/94.

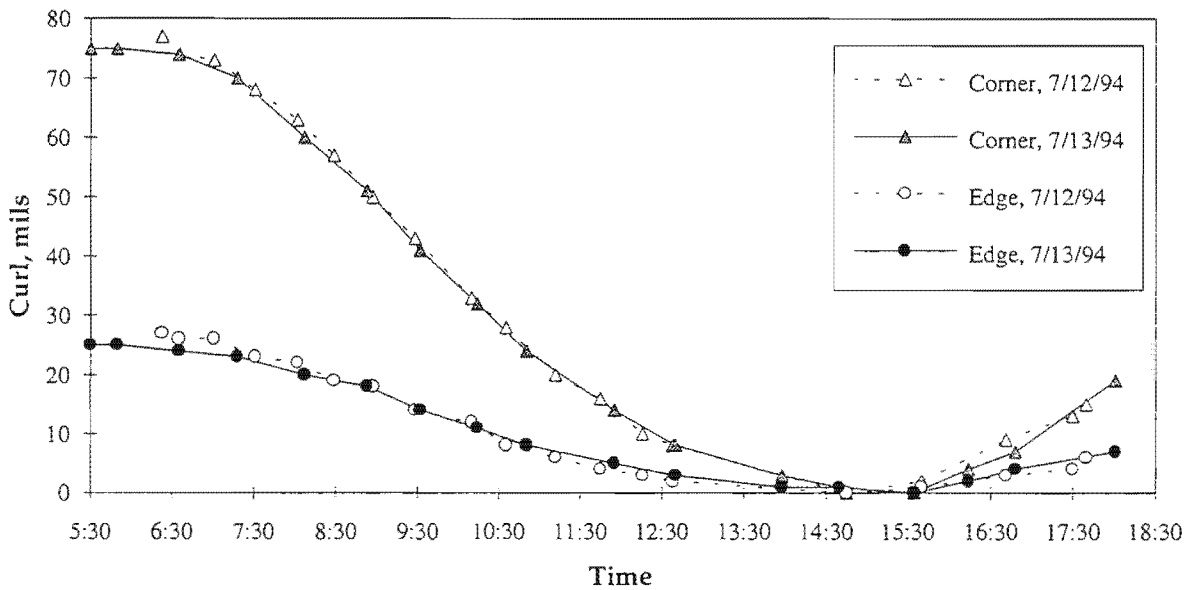


Figure 5. Measured curling.

Analysis

Curling of PCC slabs constructed on a stabilized base is a difficult phenomenon to analyze. The difficulty is that curling can cause the pavement slab to lift off the stabilized base. Many finite element programs for PCC pavements allow analysis of two-layered systems; however, in almost all cases, this is accomplished by converting the two-layer system to a structurally equivalent single-layer system. This conversion is feasible only if one of the following can be assumed:

- The two layers are fully bonded.
- The two layers are fully unbonded and they assume the same deflection profile.

Because the two pavement layers are not actually modeled as two separate layers, most finite element programs, including ILLI-SLAB, are not capable of analyzing the independent actions of the two layers.

Many finite element programs for PCC pavement analysis do model the separation between the PCC slab and the subgrade in the curling analysis; however, if the base is sufficiently stiff (with respect to the PCC slab), the separation between the slab and the base has a very different effect on the structural response of the pavement system than the separation between the slab and subgrade, even if the base is in full contact with subgrade. In general, however, the effects of layer separation need to be considered only when analyzing unbonded concrete overlays and PCC pavements constructed on a very stiff base (such as lean concrete or cement stabilized bases). If the base stiffness is significantly less than that of the PCC slab, the base does not significantly affect the structural response of the whole system and it may be simply ignored in the analysis. Even on pavements with moderately stiff bases, the layer separation does not have a significant effect on load stresses and deflections.

In the curling analysis for this study, however, the ability to model the layer separation is very important, because the calculated pavement response values that need to be matched to the measured values are the deflections due to temperature curling only. With no applied wheel load, the deflections at the slab corners are very sensitive to the support condition. Hence, the ability to model the independent action of the two pavement layers is very important.

Until recently, the separation between the slab and the base could only be modeled using 3-D finite element programs. The most recent version of ILLI-SLAB, ILSL2, incorporates a new approach to analyzing the layer separation problem (Khazanovich 1994). The new approach, developed by a Russian researcher (Totsky 1981), models the multi-layered pavement system resting on subgrade as a series of springs and plates. In finite element analysis of PCC pavements, the subgrade is typically modeled as distributed springs (Winkler foundation) and the slab is modeled as a medium-thick plate (Kirchhoff plate). The Totsky approach uses the same models for the slab and the foundation but models the two pavement layers as separate plates (Kirchhoff plates) and places springs between the two layers to model the contact conditions between the two layers and the layer compressibility (which is ignored in the Kirchhoff plate model). The

springs between the two pavement layers, the interface springs, are assumed to resist compression only.

The curling problem in the Totsky model is solved iteratively. The analysis begins with all of the interface springs in compression (compression due to the selfweight of the slab) then the pavement layers are allowed to curl. If any of the springs are in tension at the end of the first iteration, those springs are removed and the system reanalyzed. The iteration continues until an equilibrium condition has been reached. The interface springs that have been removed during the solution process represent the layer separation. The use of Totsky model incorporated in ILSL2 allows a very accurate modeling of the curling problem.

The following parameters were used in analyzing the test slabs:

- PCC Slab
 - Elastic modulus, $E_c = 3,000$ kpsi
 - Poisson's ratio, $\mu_c = 0.15$
 - Thickness, $h_c = 11.5$ in

- AC Base
 - Elastic modulus, $E_{AC} = 700$ kpsi
 - Poisson's ratio, $\mu_{AC} = 0.35$
 - Thickness, $h_{AC} = 7$ in

- Subgrade
 - Modulus of subgrade reaction, $k = 180$ psi/in

The PCC modulus represents the average of the values obtained from core testing. The core testing results are given in appendix A. The slab thickness obtained from the cores ranged from 11.5 to 11.8 in, and averaged 11.6 in. Other parameters were obtained from the design information provided by CO DOT.

The curling data obtained on July 13th were used in the comparisons. As shown in table 4, the maximum temperature gradients measured on July 13th were -12 °F and +23 °F. Because only the relative curling values are available, the comparison had to be made on the basis of the range of curling deflections (i.e., the difference between the curling deflection at the maximum negative temperature gradient and that at the maximum positive gradient). The range of measured curling at the slab corners was 75 mils.

To obtain the range of calculated curl, two ILSL2 runs were made using the Totsky model for the temperature gradients -12 °F and +23 °F. The Totsky model assumes that the two pavement layers are unbonded and does not consider any interface friction. Therefore, the slab is free to lift off the base during upward curling, and downward curling is not restrained by any frictional forces at the slab-base interface in this model. Even under these conditions, however, the range of the calculated corner curling from this initial analysis was only 42 mils.

One limitation of the ILSL2 implementation of the Totsky model is that it can only model one slab. One possible source of additional deflection at the outer corners and edges is the rigid body rotation of the slab. This can occur because of the restraint imposed by the interior slab at the longitudinal joint (the lane-shoulder joint in this case, because the free edge curling was measured at the free edge of a shoulder slab). This effect was modeled by applying a strip load on the elements along the lane-shoulder joint, which has the effect of providing some restraint against the upward movement of the lane-shoulder joint. The consideration of the slab rotation resulted in a slight increase in the calculated curling: the range of calculated curling increased to 48 mils. Clearly, not all physical effects are accounted for in the analytical model.

Within the range of temperature gradients to which the pavement was subjected during the field testing, the large curling deflections measured at the slab corners and longitudinal edge seemed possible only if the curling was allowed to occur with the least amount of restraint. The slab faces the least amount of resistance to curling during upward curling because only the slab edges need to be lifted for this to occur. This means the slab must have some initial upward curling (i.e., the slab is curled up at zero temperature gradient).

Several factors can cause the slab to curl up, including the following:

- Large positive temperature gradient during construction—if the concrete has any positive temperature gradient when it hardens, the slab will curl up when the slab cools. Because the slab was flat when it had a positive temperature gradient, the removal of this gradient has the same effect as applying a negative temperature gradient. Studies have shown that the magnitude of this is 2.5 °F/in (which translates to a temperature difference of 29 °F between the top and bottom for the test slabs) or more in many highway pavements (Eisenmann and Leykauf 1990a). Temperature gradients at hardening of up to about 4 °F/in were observed during construction of SHRP C-206 test sections, where high early-strength mixes were used (Whiting et al. 1994).
- Differential shrinkage of concrete—field moisture measurements have shown that surface shrinkage of concrete occurs only to a depth of about 2 in; the rest of the pavement remains at 80 percent saturation or higher (Eisenmann and Leykauf 1990b). The net effect of this phenomenon is an equivalent total temperature gradient of about -2.5 °F for the test slabs.
- Moisture gradients in the slabs. A difference in the moisture content between the top and bottom also causes the slab to curl. Moisture contents in pavement slabs are typically higher at the bottom than at the top, causing upward curling of the slabs.

Assuming that the test slabs do have a significant amount of built-in negative temperature gradient, a number of temperatures were tried to match the calculated curling to measured curl. Residual temperature gradients of -10 °F, -20 °F, and -25 °F were tried, and the best match was obtained with a residual temperature gradient of -20 °F. The use of a -25 °F gradient led to an excessive amount of calculated curling and -10

°F did not give enough. Although this analysis was performed with a limited number of field measurements, the use of a -20 °F residual temperature gradient gave an excellent match between the calculated and measured curling values.

The calculated and measured curls are summarized in table 5 and plotted in figure 6. Because the measured curling values are relative values, they have to be shifted to match the calculated values. The measured curling values were shifted down by matching the most positive curling values. The zero adjusted curling values are shown in figure 7.

Table 5. Comparison of measured and calculated curl.

Temp Diff, oF	Measured Curl, mils						Calculated Curl mils	
	Normalized		Zero Adjusted		Curl-Lag Adjusted		Corner	Edge
-12.0	75.0	25.0	66.0	19.0	66.0	19.0	65.8	15.2
-6.0	67.4	22.3	58.4	16.3	47.4	13.1	50.1	10.8
0.0	56.4	19.1	47.4	13.1	33.8	8.7	34.3	5.4
6.0	42.8	14.7	33.8	8.7	22.0	4.7	19.4	0.4
12.0	31.0	10.7	22.0	4.7	8.9	0.2	7.4	-2.7
18.0	17.9	6.2	8.9	0.2	-5.7	-4.8	-2.5	-4.8
23.0	3.3	1.2	-5.7	-4.8	-9.0	-6.0	-9.2	-6.0
21.0	0.0	0.0	-9.0	-6.0				

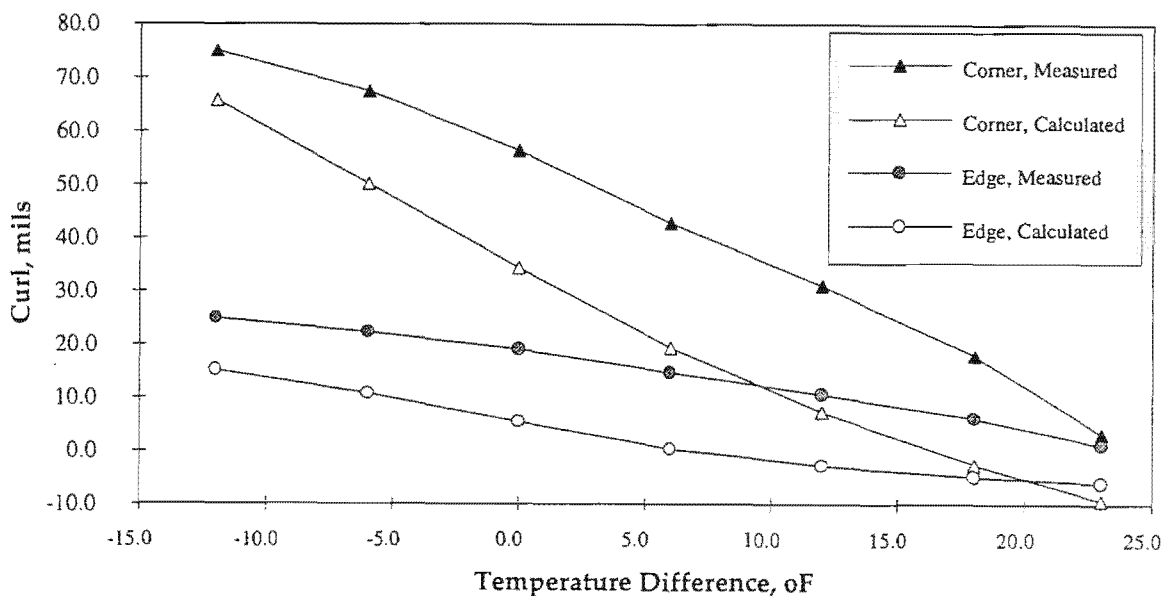


Figure 6. Comparison of calculated and measured curl.

Although the end values match, figure 7 still does not show a good agreement between the measured and calculated curl. This may be explained by examining table 2. Table 2 shows that the minimum curling lags the maximum positive temperature gradient by about 1.5 hrs. The suspected cause of this effect is the nonlinear temperature gradients illustrated in figure 3. If the measured curling is adjusted for the curl lag effect, an excellent match is obtained, as shown in figure 8.

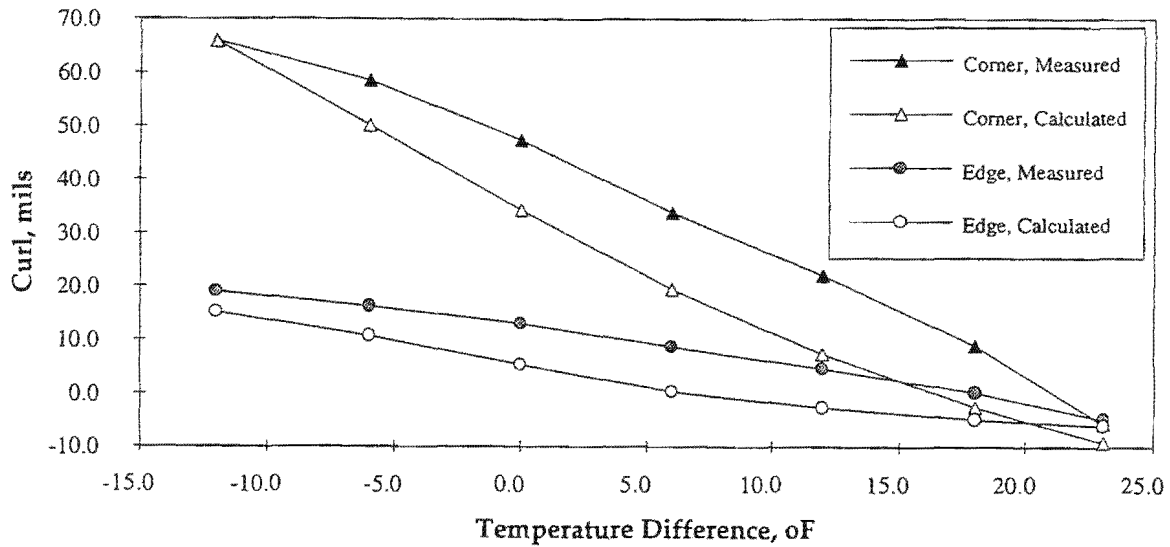


Figure 7. Comparison of measured and calculated curl, zero adjusted.

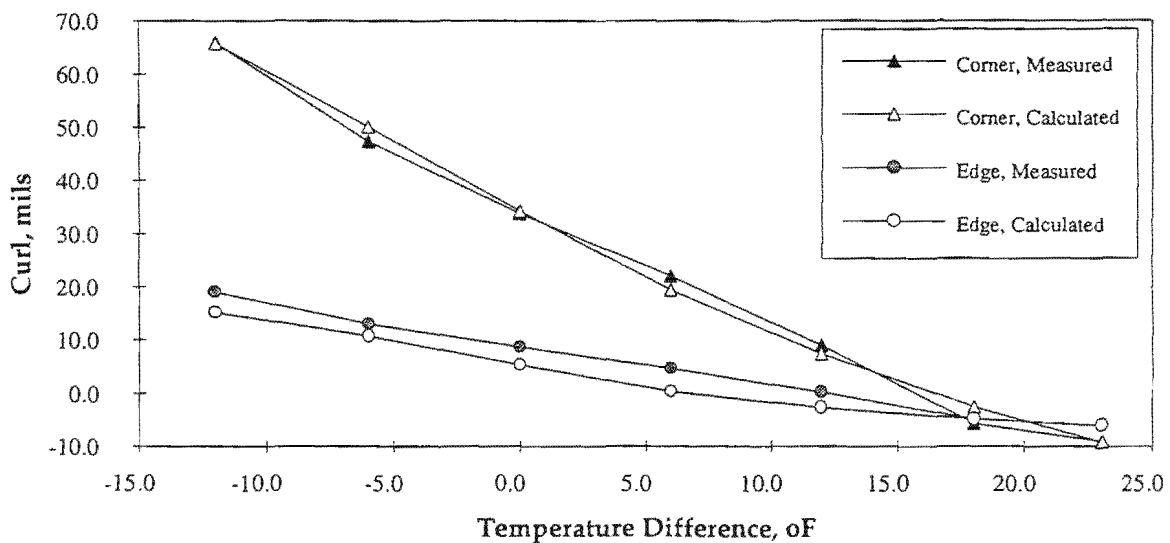


Figure 8. Comparison of measured and calculated curl, zero and curl-lag adjusted.

According to the curling analysis, the actual temperature gradient of -12 °F to +23 °F has the effect of a -32 °F to +3 °F temperature gradient on the pavement slabs because of the built-in temperature gradients. This shift in temperature gradients has a drastic effect on the critical bending stresses at the longitudinal edge and a correspondingly significant effect on fatigue life predictions. The bending stresses resulting from high positive temperature gradients can often equal or exceed the load stresses; however, the curling analysis conducted for this study suggests that this high effective positive temperature gradient may not occur in many pavements because they are counteracted by the residual temperature gradients.

Because fatigue of concrete is an exponential function of the ratio of the applied stress to PCC modulus of rupture (σ/M_R), the virtual removal of curling stresses would lead to drastically increased fatigue life. Since the effects of residual temperature gradients are not considered in existing fatigue pavement models, a new fatigue model that considers this effect may be needed to perform accurate performance predictions.

Many assumptions were made in this analysis, some less conventional than others; however, these assumptions were made on a rational basis and all can be supported with either field measurements or previous research. The analysis performed for the strain measurements further confirms the validity of the assumptions made. The field measurements provided seemingly conflicting data. If the assumptions made in this analysis were random or invalid, it would not have been possible to match both the curling and strain measurements. The introduction of the residual temperature gradient is unconventional, but ample evidence supports the presence of substantial negative residual temperature gradients in concrete highway pavements, perhaps the most convincing of which are the curling values measured in this study.

Strain Analysis

Instrumentation and Data Collection

Surface-mounted strain gauges were used to measure load-induced strains at the free edge (of a shoulder slab), at longitudinal edges of the lane-shoulder joint (for 12-ft tied, 14-ft tied, and 14-ft nontied sections), and at the outer wheel path of the 14-ft slab sections. The instrumentation layout is shown in figures 9, 10, and 11. The wheel load was applied using a truck that was loaded to provide an 18-kip single-axle load. The strain gauges installed on the tied 14-ft slab are shown in figure 12. A close-up of the mounted strain gauges is shown in figure 13. Figure 14 shows the instrumented slab being loaded by an 18-kip single axle.

The strain data were obtained using automated data acquisition equipment that was capable of sampling 20,000 times per second. The measurements were taken at both creep speed and under static conditions to see the effects of dynamic loading, and at various times throughout the day to evaluate the effects of temperature variations on load strains.

Examples of the collected data from the tied 14-ft slab, nontied 14-ft slab, tied 12-ft slab, and free edge sections are shown in figures 15, 16, 17, and 18, respectively. In these

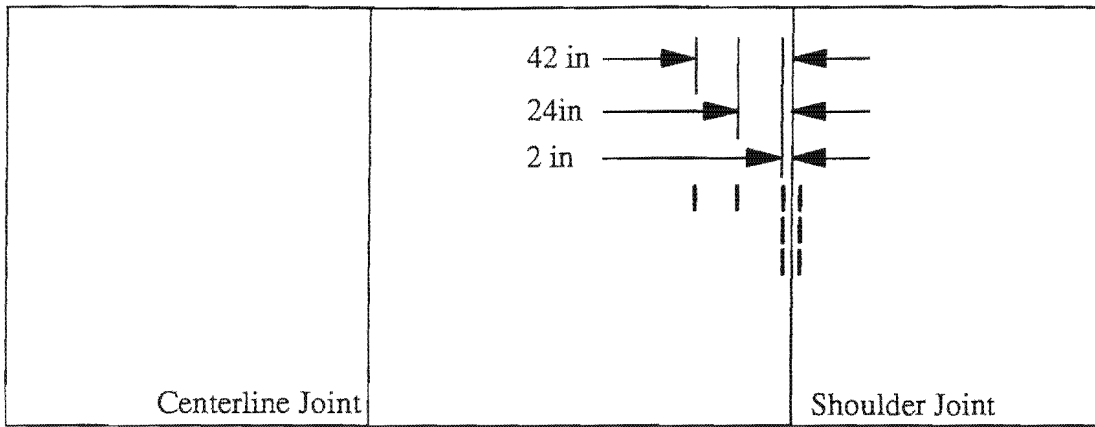


Figure 9. Instrumentation layout for the tied and non-tied 14-ft lane sections.

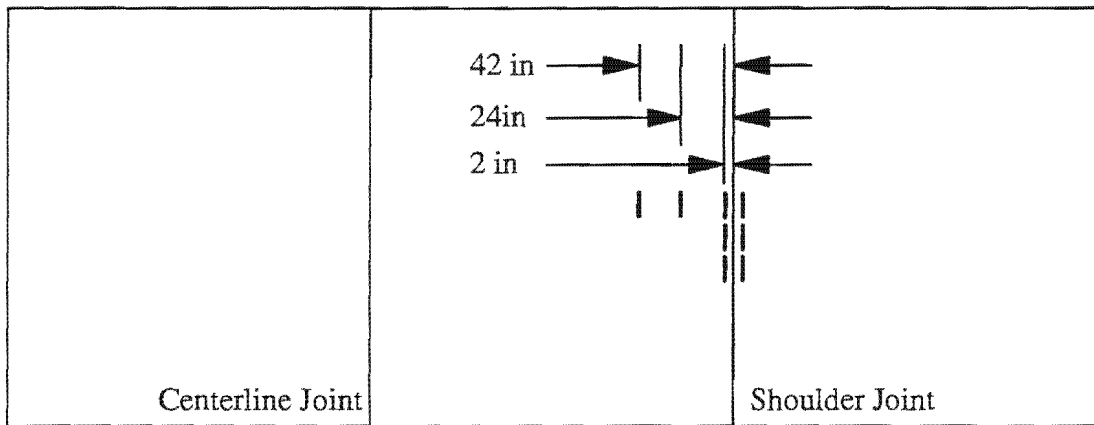


Figure 10. Instrumentation layout for the tied 12-ft lane section.

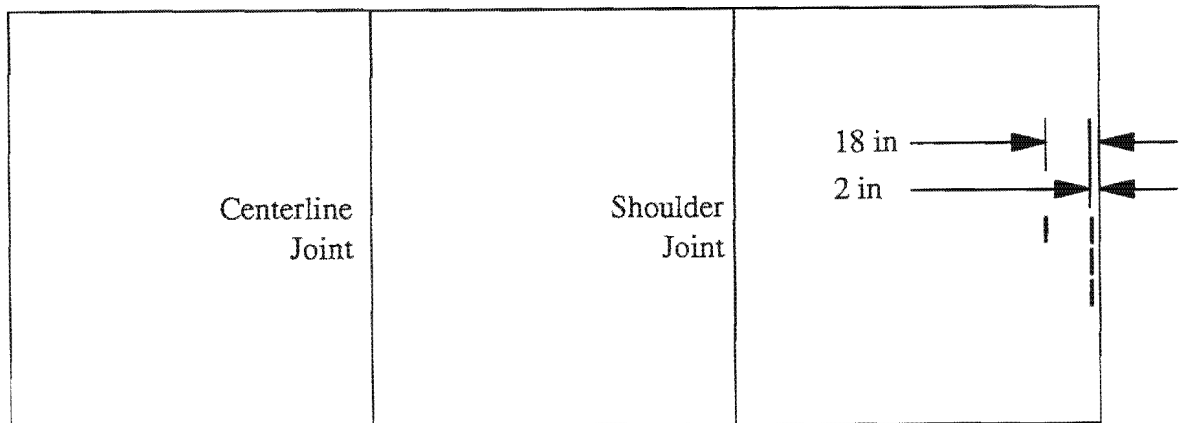


Figure 11. Instrumentation layout for the free edge.

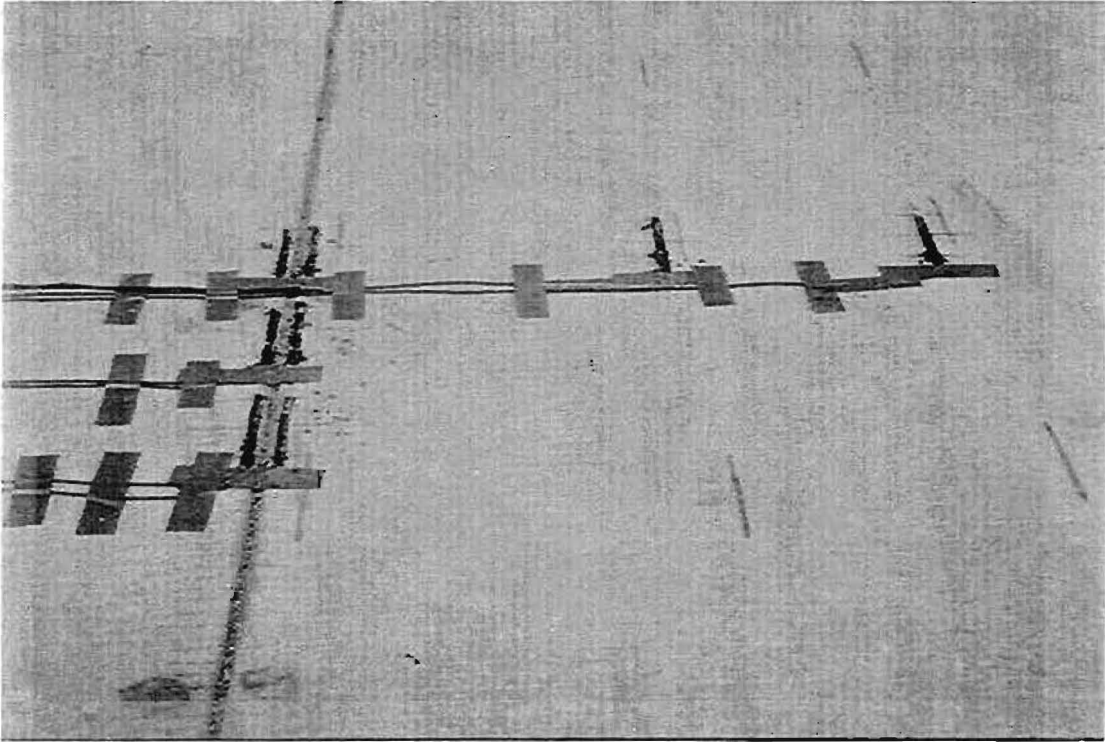


Figure 12. Strain gauges installed on the 14-ft slab section.

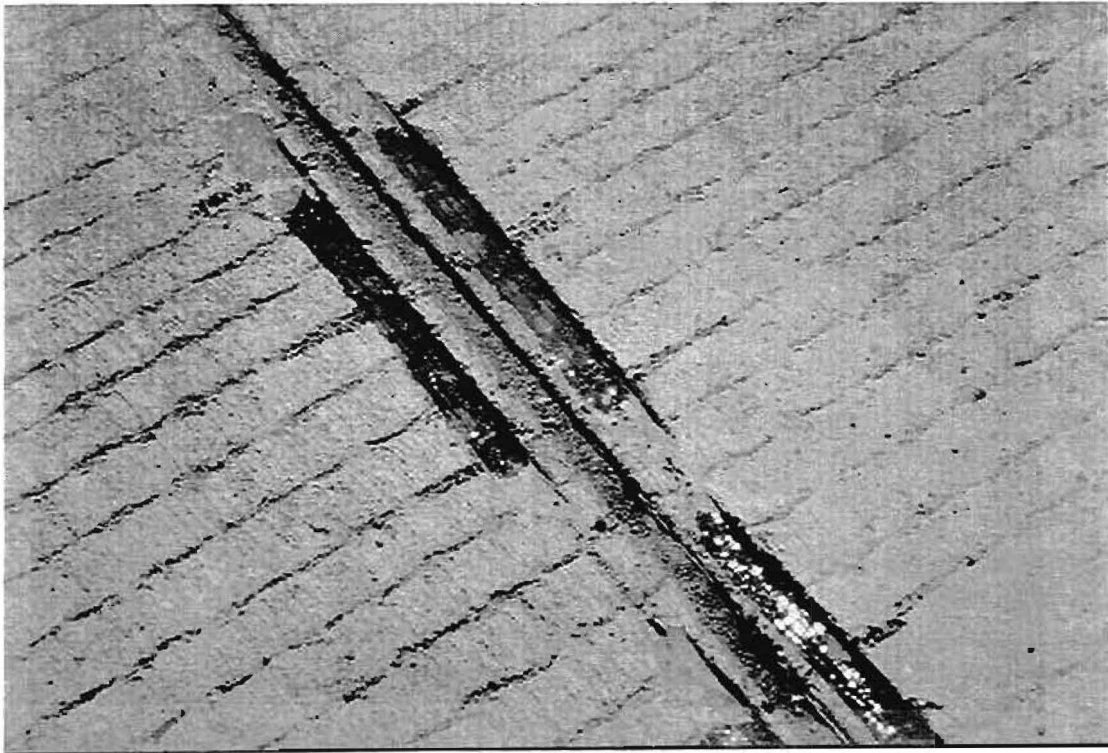


Figure 13. Close-up of the surface-mounted strain gauges.

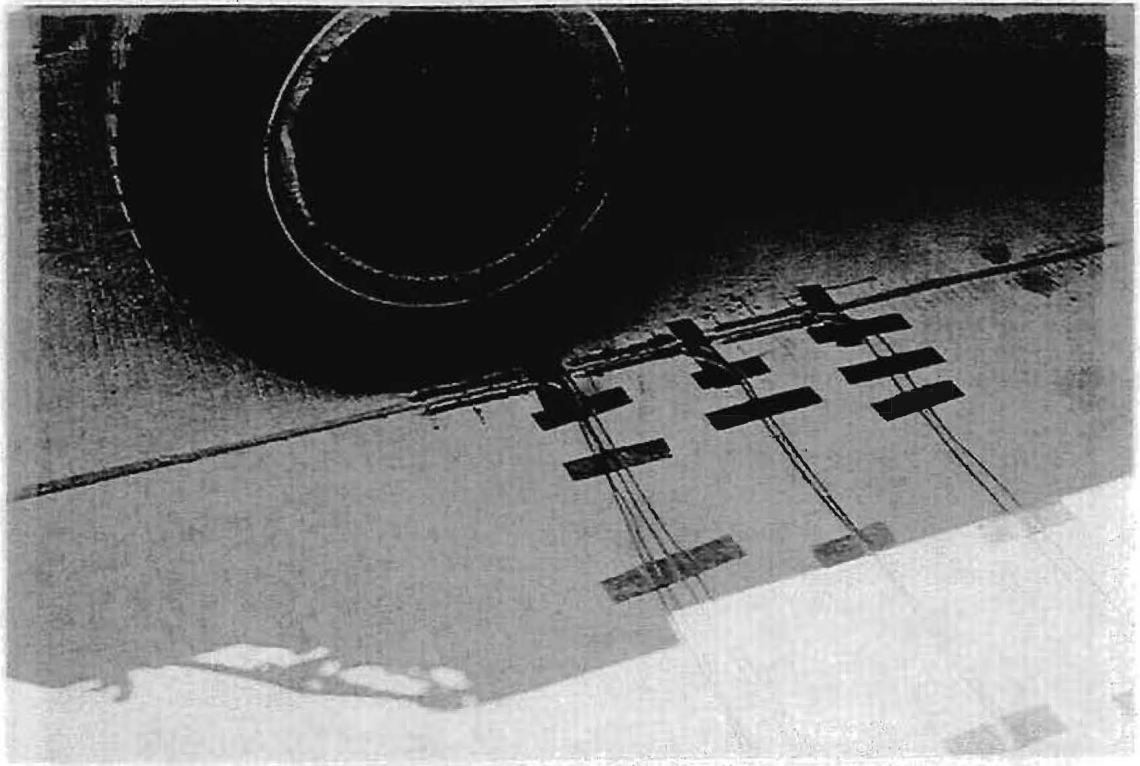


Figure 14. Instrumented slab being loaded by an 18-kip single axle.

figures, the measured strains are plotted against the sampling number, which is directly related to time. As expected, as the front axle of the loaded truck approaches the strain gauge, the strain first increases slightly (indicating tension at the surface), drops to the maximum negative value (compression at the slab surface due to slab bending), and then increases to the maximum positive value (the strain gauge is now located between the front and rear axle of the loaded truck). As the rear axle approaches the strain gauge, the strain rapidly drops to the second maximum negative value (the strain due to the 18-kip axle load) before dissipating as the truck axles move away from the gauge. The field measurements of the maximum strains due to the rear axle load are summarized in appendix B.

Analysis

The load strains at both the free edge and along the lane-shoulder joint were analyzed. The effects of the following factors on load strains need to be evaluated in this analysis:

- Temperature gradient.
- Load transfer efficiency.
- Load location (transverse placement of load).
- Strain location (strains at various locations across the pavement).

The temperature effects were evaluated using the edge strain data only; the remaining factors were evaluated at zero effective temperature gradient condition. This

Figure 15. Example strain vs time plot for the 14-ft tied PCC shoulder section.

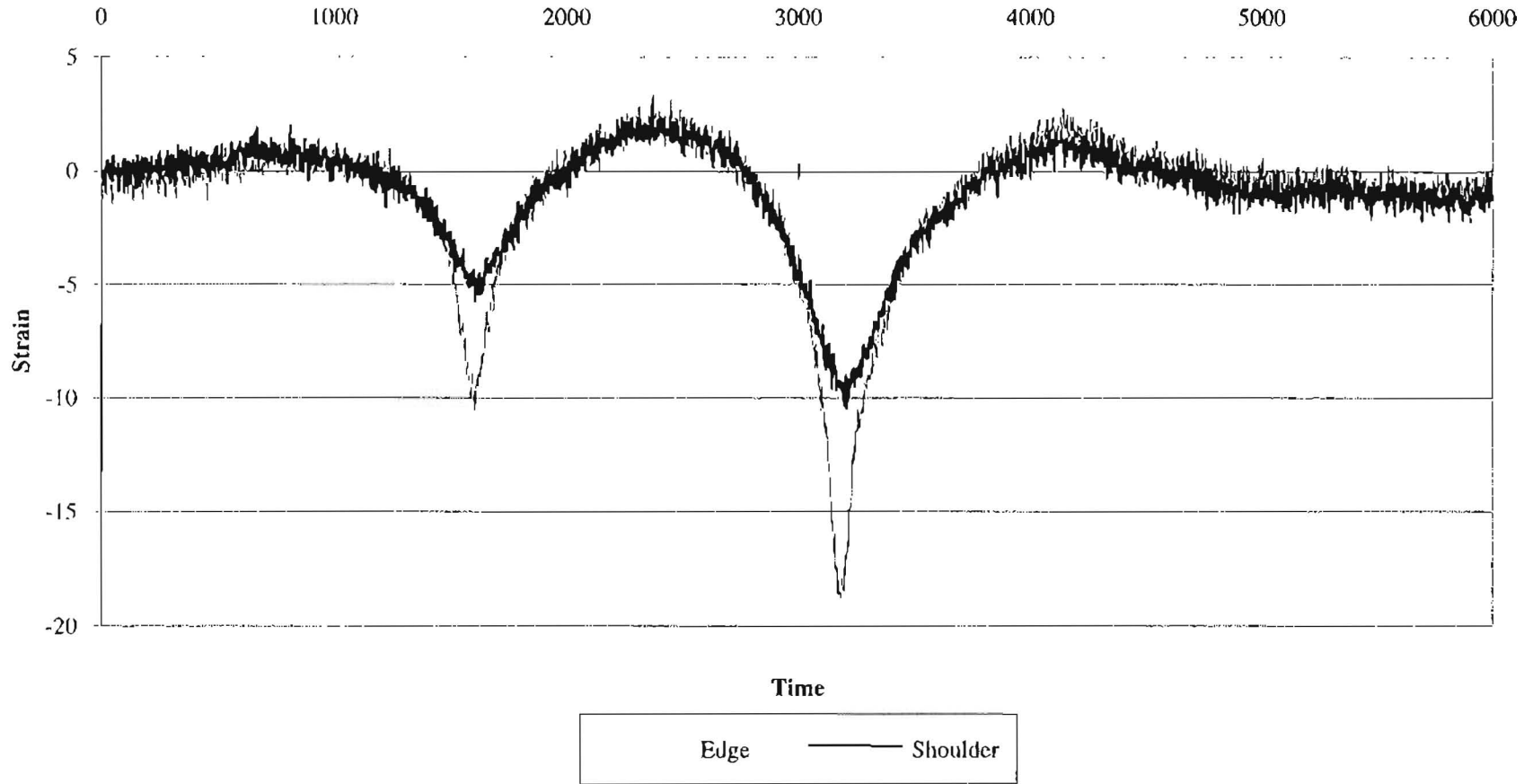


Figure 16. Example strain vs time plot for the 14-ft non-tied PCC shoulder section.

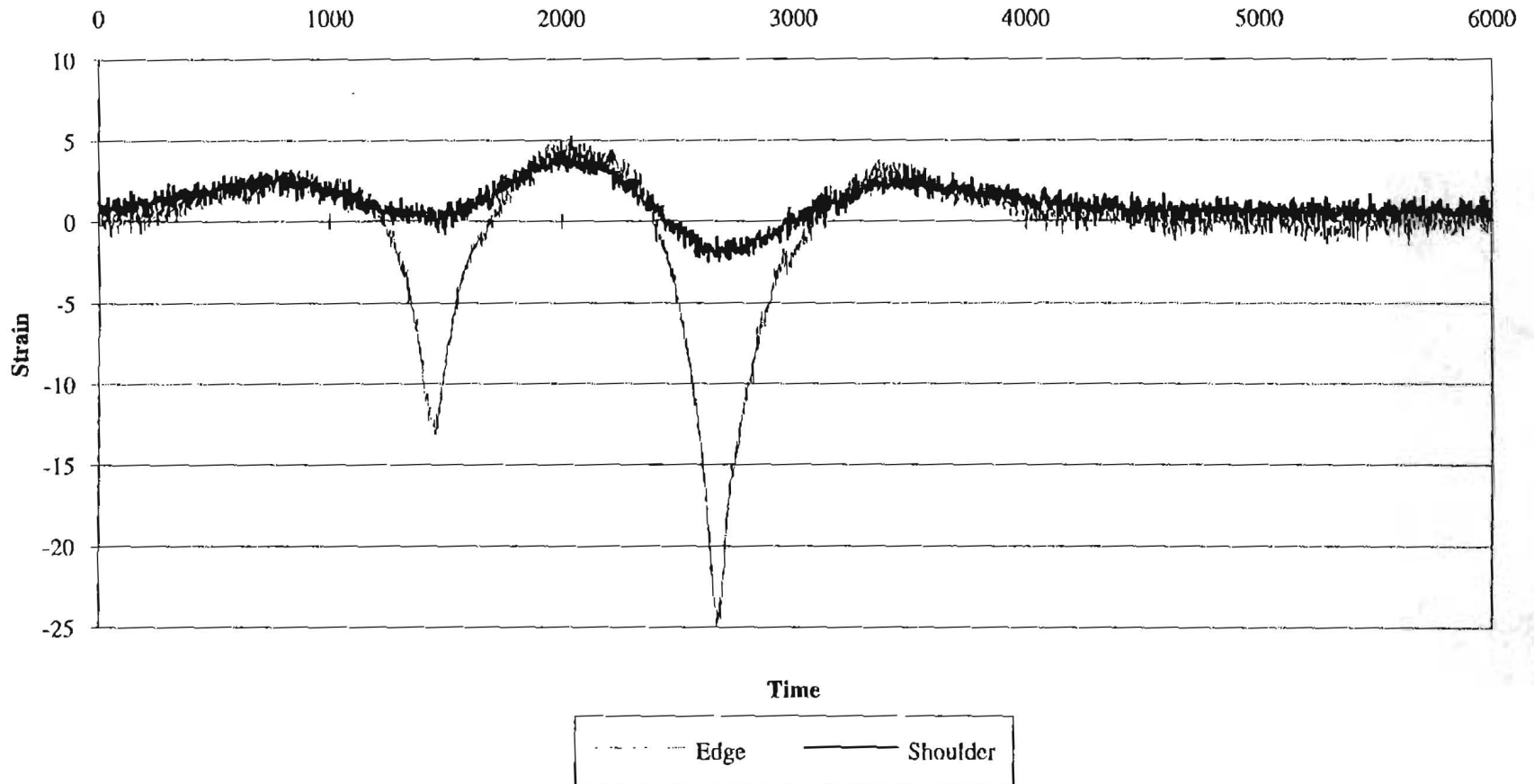


Figure 17. Example strain vs time plot for the 12-ft tied PCC shoulder section.

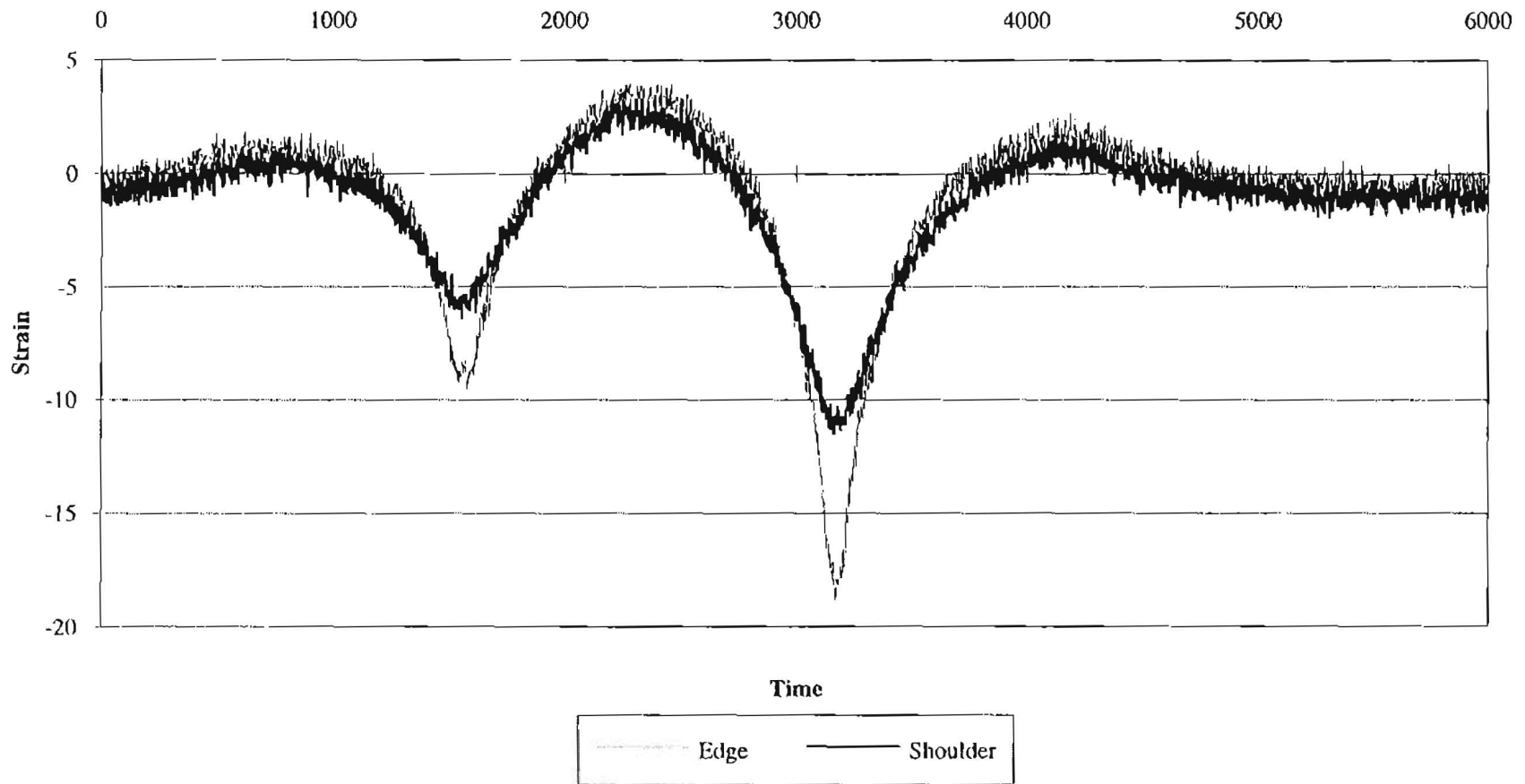
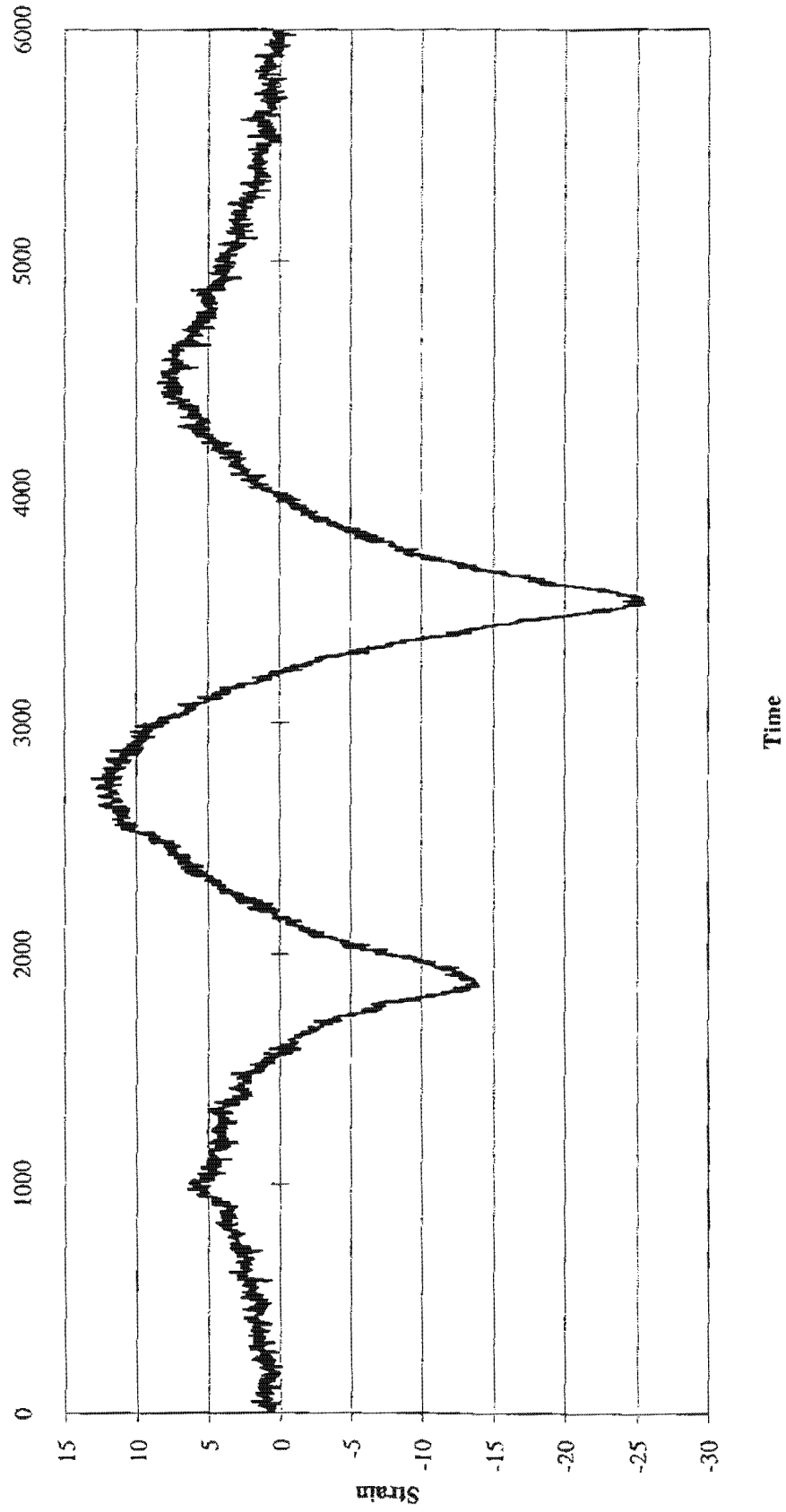


Figure 18. Example strain vs time plot for the free edge..



combination of analyses reduces the number of cases that must be evaluated without limiting the scope of analysis.

The lateral placement of load and the location of strain measurements affect the strain magnitudes. Because the intent of these measurements is to demonstrate that the strains at the interior locations can be adequately determined using analytical means, comparisons made at one condition would satisfy this objective. In addition, the evaluation of the temperature effects showed that temperature gradients do not significantly affect the load strains.

It is important to note that only the wheel load-induced strains were measured during the field testing. The measurement of combined strains is extremely complicated and cannot be accomplished reliably using only the surface-mounted strain gauges. The analysis of the temperature effects, therefore, was also limited to the evaluation of the temperature effects on wheel load-induced strains only. The only significant effect of temperature gradients on wheel load-induced strains is that the temperature gradients affect the support condition of the PCC slab.

The preliminary analysis of measured strains has shown that for the load strains to be as low as the measurements show, the effective stiffness of the pavement structure has to be very close to that exhibited when the AC base is bonded to the PCC slab. The equivalent thicknesses of two-layer systems for bonded and unbonded interface conditions can be determined using equations 1 and 3, respectively (Ioannides et al. 1992).

$$h_{e \text{ Bonded}} = \left(h_1^3 + \frac{E_2}{E_1} h_2^3 + 12 \left[\left(x - \frac{h_1}{2} \right)^2 h_1 + \frac{E_2}{E_1} \left(h_1 - x + \frac{h_2}{2} \right)^2 h_2 \right] \right)^{1/3} \quad (1)$$

where

- $h_{e \text{ Bonded}}$ = effective thickness of two bonded layers, in.
- h_1 = PCC slab thickness, in.
- h_2 = AC base thickness, in.
- E_1 = PCC modulus of elasticity, psi.
- E_2 = AC modulus of elasticity, psi.
- x = depth to natural axis, in (determined using equation 2)

$$x = \frac{E_1 h_1 \frac{h_1}{2} + E_2 h_2 \left(h_1 + \frac{h_2}{2} \right)}{E_1 h_1 + E_2 h_2} \quad (2)$$

$$h_e = \left(h_1^3 + \frac{E_2}{E_1} h_2^3 \right)^{1/3} \quad (3)$$

Where

$h_{e \text{ Unbonded}}$ = effective thickness of two unbonded layers, in.

As given earlier, the test sections have the following structural properties:

- PCC Slab
 - Elastic modulus, $E_c = 3,000$ kpsi
 - Poisson's ratio, $\mu_c = 0.15$
 - Thickness, $h_c = 11.5$ in
- AC Base
 - Elastic modulus, $E_{AC} = 700$ kpsi
 - Poisson's ratio, $\mu_{AC} = 0.35$
 - Thickness, $h_{AC} = 7$ in
- Subgrade
 - Modulus of subgrade reaction, $k = 180$ psi/in

For the above system, the effective pavement layer thickness is 14.5 in if the pavement layers are bonded (equation 1) and 11.7 in if they are unbonded (equation 3).

The bonded thickness determined above (14.5 in) corresponds to the effective single slab thickness that is needed to obtain the measured strain response. Some of the ways that this effective thickness can result include the following:

- The slab and the AC base act as if they are bonded when subjected to wheel loads.
- The slab is considerably thicker than 11.5 in.
- The base is considerably stiffer.

The second scenario can be dismissed, because none of the cores from the test sections measured more than 11.8 in. The structural stiffness of the base may be increased by either increasing its thickness or its modulus. The base modulus used in the design (700 kpsi) represents a relatively high value for AC. At this modulus value, the base would have to be 18.7 in thick to provide the effective slab thickness of 14.5 in. Even if the base modulus were 1,000 kpsi, the base would have to be 16.6 in thick to provide the required effective slab thickness. Clearly, these are not likely scenarios.

Based on the above discussion, the only reasonable model that provides the required effective slab thickness is the bonded base-slab interface model. Numerous field evaluations have shown that an actual bond between the base and slab is not necessary

for the pavement system to exhibit bonded behavior; friction between the base and slab is often sufficient to produce bonded behavior, particularly in thicker pavements. On one airfield pavement, FWD testing results showed that the pavement system exhibits bonded behavior even though the stabilized base is first ground and polyethylene sheets are placed between the pavement layers to deliberately provide a smooth, slip interface. Hence, the model in which the slab is allowed to lift off the base when the pavement is subjected only to temperature gradients but exhibits bonded response when the system is subjected to wheel loads is plausible, and appears to be the only reasonable model that explains the measured pavement responses.

For the no effective temperature gradient condition (+20 °F measured gradient), the calculated free edge strain for the bonded interface condition was 32×10^{-6} (32 $\mu\epsilon$). The free edge strains measured throughout the day ranged from 24.3 $\mu\epsilon$ to 31.4 $\mu\epsilon$. The test slab was subjected to different temperature gradients at different times of the day. The following analysis was conducted to determine the effects of temperature gradients on load strains.

Temperature Effects on Load Strains at the Longitudinal Edge

Curling affects the slab support condition. Because the portion of the slab that is lifted off the base is obviously not in contact with the base, that portion of the slab cannot be modeled as being bonded to the base. This problem again involves the separation of the two pavement layers, but the Totsky model could not be used directly to solve this problem because it does not consider the interface friction.

The Totsky model, however, could be used to analyze the case in which the slab is subjected to a very large temperature gradient—the condition in which the pavement layers remain separated even when the wheel load is applied. At the other extreme is the condition in which the effective temperature gradient is zero; in this case, a bonded interface may be assumed and the system analyzed using ILLI-SLAB. The cases that lie between these two extremes may be analyzed using the following procedure:

1. Run a series of analyses using the Totsky model with a temperature gradient and determine the load at which the two pavement layers come in contact at the loaded nodes (the closure load).
2. Analyze the pavement system using the Totsky model with only the temperature gradient to determine the curling stress component of the combined load-curling stress.
3. Subtract the curling stresses from the combined stresses at the closure load to determine the load-only stresses resulting from the closure load.
4. Obtain the stresses due to the remaining load (i.e., the balance of the wheel load after subtracting the closure load) by using ILLI-SLAB with no temperature gradients.
5. Add the stresses determined in steps 3 and 4 to obtain the total stress.

This procedure assumes that the Totsky model is accurate up to the point where the two pavement layers come in full contact and that the system exhibits bonded behavior once the contact has been established. It is further assumed that the pavement structure is fully supported at the closure load (i.e., no gaps exist under the pavement). The strain due to the loads beyond the closure load is determined without temperature gradients based on the last assumption.

Using this procedure, the edge strains at various temperature gradients were determined and compared to the measured values. Table 6 shows the results of the edge strain calculations at various temperature gradients. The closure load is shown in terms of the applied pressure. The total load area used in the analysis is 96 in², corresponding to two 6-in by 8-in rectangular areas. Because the total wheel load is 9 kips, the pressure at the full load is 93.75 psi. Each rectangular area represents the contact area of a tire; center-to-center spacing between the two loaded areas was 12 in, and the load was placed 2 in away from the edge to model the actual location of truck tires during the testing.

Table 6. Calculated load strains at various temperature gradients.

Actual temperature gradient, °F	Effective temperature gradient, °F	Closure load, psi	Load strain, $\mu\epsilon$
-12	-32	70	36.0
0	-20	30	33.5
+10	-10	10	33.5
+23	3		32

This analysis showed that the load strains are not significantly affected by temperature gradients. The calculated load strain at +23 °F actual temperature gradient (3 °F effective) represents the theoretical minimum, because this strain was determined assuming full bond and no temperature effects (zero closure load). The calculated load strain at -12 °F actual temperature gradient (-32 °F effective) is the maximum expected strain. Note that the difference in the calculated strains at the two extreme conditions is only 4 $\mu\epsilon$. According to this analysis, the load strain increases slightly with the increasing magnitude of negative temperature gradient.

The measured strains at the longitudinal edge are summarized in table 7, along with the calculated strains. At the lane-shoulder joints, the load strains are distributed between the mainline slab and the shoulder slab. The amount of strain picked up by the shoulder slab is determined by the load transfer capacity of the joint. The strains on either side of the joint should sum to the free edge strain. However, on the nontied 14-ft slab section, the small amount of strain measured from the shoulder slab is the result of the base deflection, and not load transfer; therefore, the free edge strain for this section is

Table 7. Summary of measured and calculated load strains.

Section	Time	Temp	Measured Strain, Creep*			Measured Strain, Static*			Calculated Strain*
		Diff, °F	Slab	Shoulder	Combined	Slab	Shoulder	Combined	
Tied 14 ft	7:00	-8.4	19.4	9.9	29.3	22.6	11.6	34.2	35.0
	9:10	4.4	13.6	4.5	18.1	11.8	1.2	13.0	33.5
	11:25	17.7	12.4	1.0	13.4	8.3	-5.9	2.4	32.5
	15:10	21.3	14.3	3.6	17.9	8.1	-2.2	5.9	32.0
	17:10	11.5	25.3	14.4	39.7	18.7	11.5	30.2	33.5
Non-tied 14 ft	7:46	-4.2	25.6	2.2	27.8	27.8	3.6	31.4	33.5
	9:50	9.1	19.0	-2.3	16.7	16.0	-7.3	8.7	33.5
	12:08	20.3	17.7	-3.2	14.5	11.6	-13.0	-1.4	32.0
	15:50	19.6	20.9	5.1	26.0	23.7	1.1	24.8	32.0
	17:36	8.8	24.2	3.7	27.9	29.8	3.7	33.5	33.5
Tied 12 ft	6:15	-10.8	19.6	9.6	29.2	18.0	9.6	27.6	35.0
	8:15	-1.5	17.8	10.4	28.2	15.7	9.7	25.4	33.5
	10:30	13.0	15.4	5.6	21.0	12.3	3.4	15.7	33.5
	14:20	20.9	17.9	10.3	28.2	12.8	5.2	18.0	32.0
	16:30	15.9	21.8	12.0	33.8	18.3	11.3	29.6	32.5
Free Edge	6:25	-10.4	26.6		26.6	26.3		26.3	35.0
	8:30	0.2	24.3		24.3	24.5		24.5	33.5
	10:42	14.3	26.1		26.1	27.9		27.9	33.5
	14:30	21.5	31.4		31.4	30.0		30.0	32.0
	16:50	13.6	30.3		30.3	31.2		31.2	33.5

*Strains are in millionths

simply the strain measured from the mainline slab. In figures 19 through 22, the equivalent free edge strains (combined slab and shoulder strains for the tied shoulder sections, and the edge strains for the free edge and nontied shoulder sections) are plotted against the time of measurement.

For all sections, the last measurement of the day gave the highest strains. The last measurements also closely matched the calculated strains in most cases. With the exception of the 12 ft tied shoulder section, statically measured strains matched the calculated values better. On the two widened-slab sections, the first static measurements of the day closely matched the calculated values.

Other measured strains deviated substantially from the calculated values. This discrepancy could not be explained analytically, and the deviations are well beyond the range of normal measurement errors (about $\pm 2 \mu\epsilon$). In all cases except for the free edge section, the most discrepancy occurred during the midday (from about 8:00 a.m. to 4:00 p.m.). This behavior is difficult to understand, because no consistent factor could be found that might explain the observed behavior. The temperature gradients between

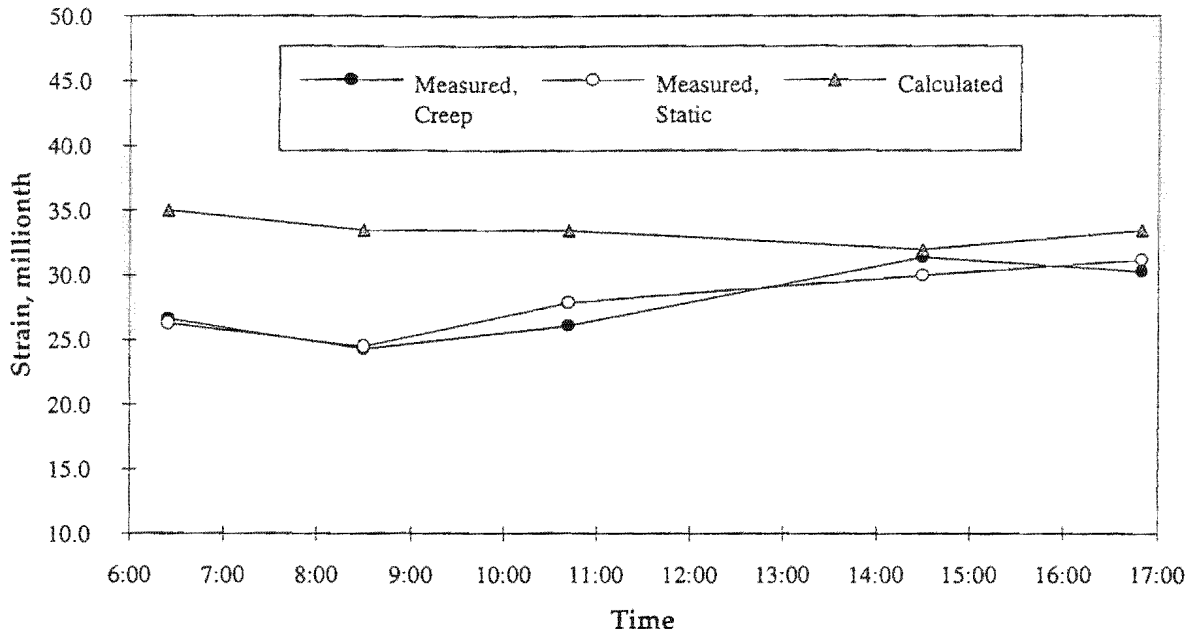


Figure 19. Comparison of measured and calculated strains, free edge section.

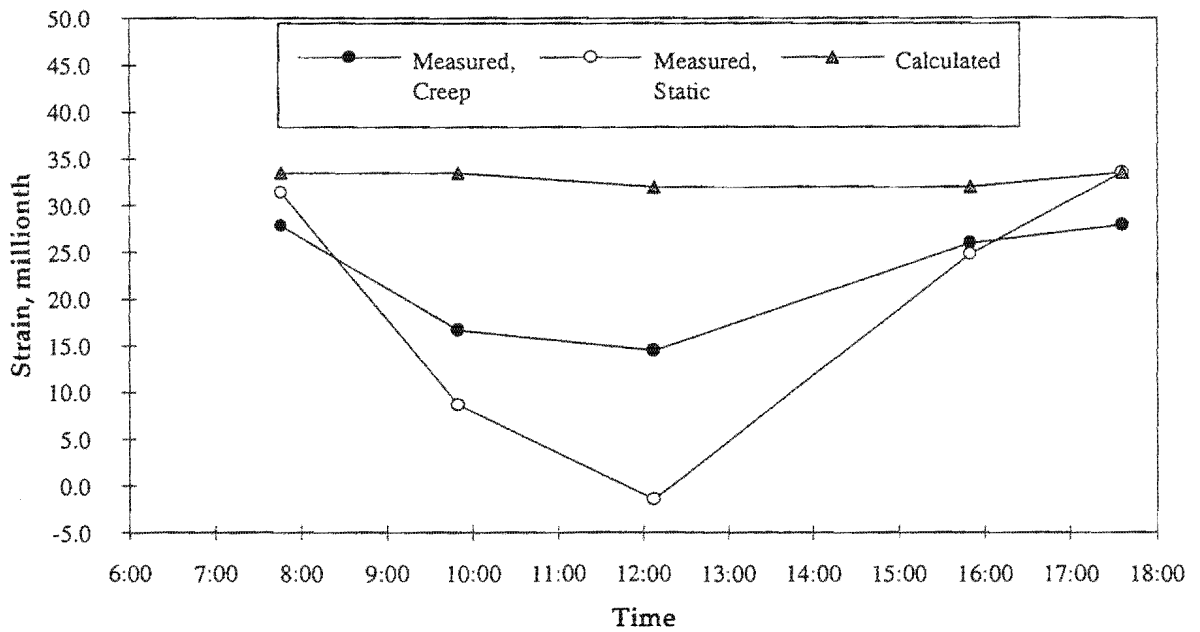


Figure 20. Comparison of measured and calculated strains, 14-ft nontied shoulder section.

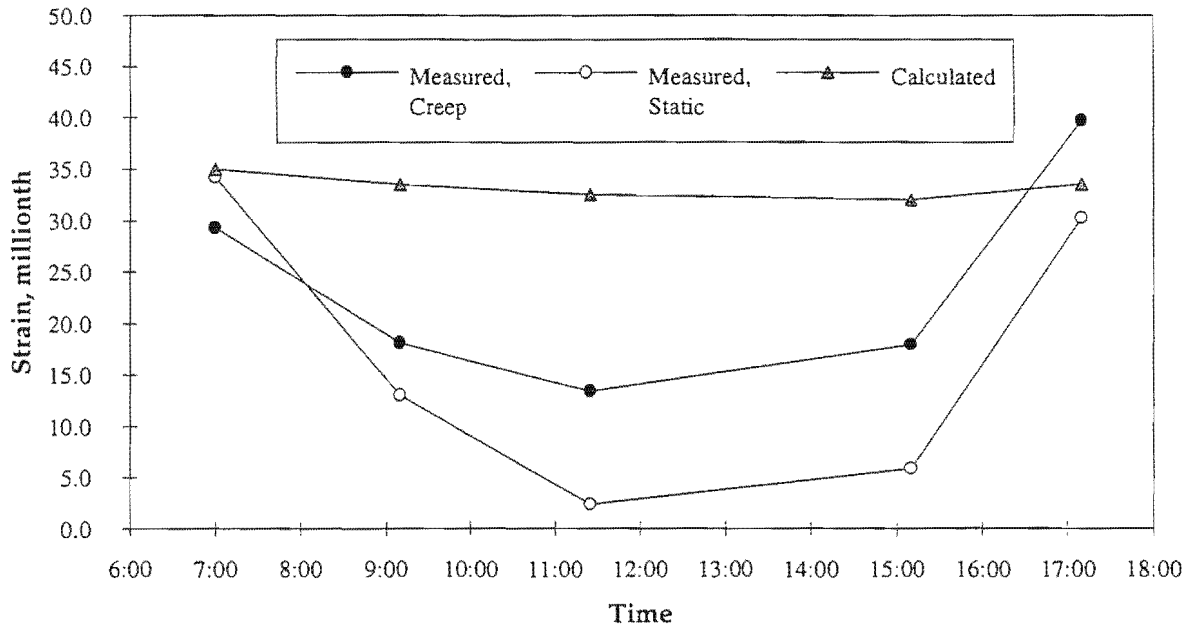


Figure 21. Comparison of measured and calculated strains, 14-ft tied shoulder section.

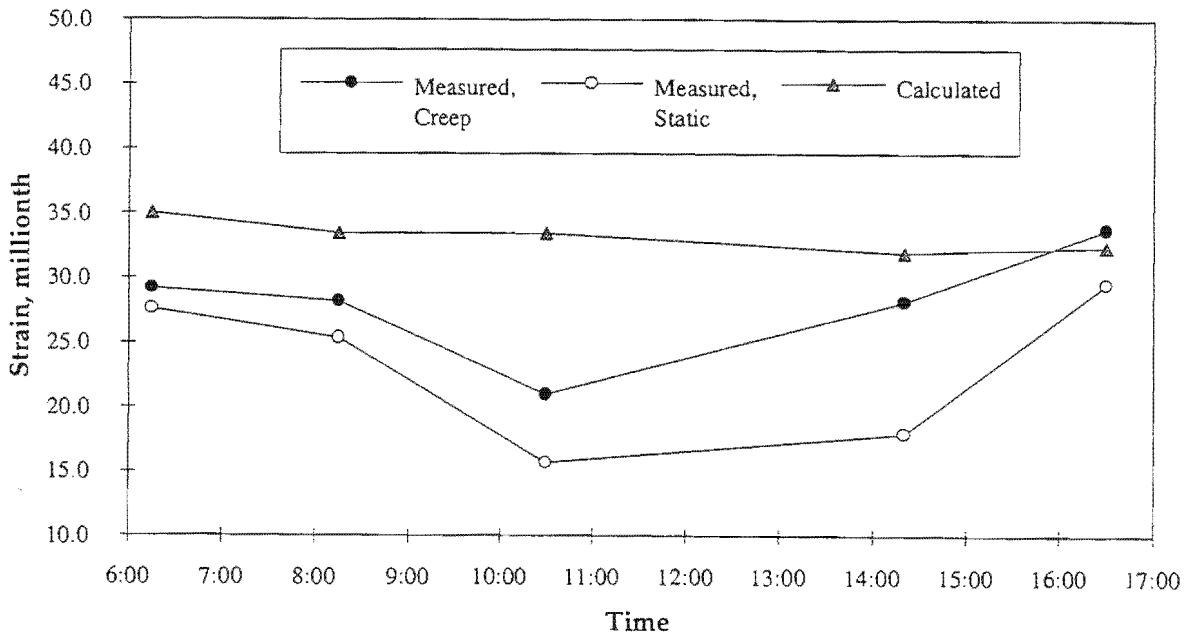


Figure 22. Comparison of measured and calculated strains, 12-ft tied shoulder section.

10:00 a.m. and 11:30 a.m. are not significantly different than those between 4:00 p.m. to 5:30 p.m., yet the measured strains from the two periods are substantially different.

Some of the strains measured during the midday do not appear reasonable. For example, a large negative strain (-13 $\mu\epsilon$, static) was measured at 12:08 p.m. from the shoulder of the nontied 14-ft section (table 7). The measured strain at that time on the loaded side was 11.6 $\mu\epsilon$. The static strains measured at 11:25 a.m. and 3:10 p.m. from the tied 14-ft section are also questionable. The loaded and unloaded side strains measured at 11:25 a.m. were 8.3 $\mu\epsilon$ and -5.9 $\mu\epsilon$, respectively, and those measured at 3:10 p.m. were 8.1 $\mu\epsilon$ and -2.2 $\mu\epsilon$, respectively. These values suggest that the tied lane-shoulder joint had no capacity to transfer load. However, the stress load transfer efficiency (LTE_s) values for this section determined from the 7:00 a.m. and 5:10 p.m. measurements were 51 percent and 61 percent, respectively. In any case, if the lane-shoulder joint had very poor LTE, the measured edge strains should have been much higher; if the LTE is close to 50 percent, the shoulder cannot have a negative strain. The magnitudes of these strains are also unreasonably small.

The measured strains matched the calculated strains reasonably well at the maximum negative temperature gradient (actual) and at moderately high positive temperature gradient. Recalling that the minimum slab curling lagged the maximum positive temperature gradient by about 1 hr (possibly due to nonlinear temperature gradients), it is possible that the last strain measurements of the day represent the strain at the highest positive effective temperature gradient. The magnitudes of the measured strains at the two extreme gradients are very similar, as the analytical evaluation has shown.

Further analysis is needed to determine whether the intermediate temperature gradients can substantially reduce load strains. However, this seems highly unlikely, because the measured midday strains are about half those of the maximum measured strains in each section. Although the trend seems consistent in all sections, a more likely cause of the observed discrepancies is equipment problems.

Load Transfer Efficiency

Load transfer efficiency refers to the ability of a pavement joint to transfer part of the load from the loaded slab to the adjacent, unloaded slab. A high LTE is desirable at transverse joints and lane-shoulder joints (if a tied PCC shoulder is provided) to reduce the critical bending stresses in the mainline slabs. As a part of the load is transferred from the loaded slab to an adjacent slab, the stresses in the loaded slab are reduced by the amount of load transferred.

LTE may be defined in terms of either deflection or stress (or strain) as follows:

$$LTE_s = \frac{\delta_u}{\delta_L} \quad (4)$$

$$LTE_{\sigma} = \frac{\sigma_u}{\sigma_L} \quad (5)$$

where

- LTE_{δ} = deflection LTE.
- δ_u = unloaded side deflection.
- δ_L = loaded side deflection.
- LTE_{σ} = stress LTE.
- σ_u = stress in the unloaded slab.
- σ_L = stress in the loaded slab.

The two LTEs are related, but they are not the same. In general, LTE_{σ} is considerably lower than LTE_{δ} . The significant difference in the two measures of LTE has to do with the deflected shape of the two sides. The load transfer at pavement joints is achieved primarily through shear. Although some moment transfer is possible when heavy dowels are used, most of the load transfer is still achieved through shear. Therefore, the deflected shape of the loaded and unloaded sides is very different. The deflection at the joint face can be matched without having the deflections at the locations further away from the joint of the unloaded side matching the deflections at the corresponding locations of the loaded side. Hence, the amount of load needed to cause the unloaded side to match the deflection of the loaded side at the joint face is considerably less than that being carried by the loaded side, and the amount of load transferred is considerably less than that indicated by the deflection LTE.

Deflection load transfer is more commonly measured, because it can be easily measured in the field using an FWD. To perform a stress analysis, however, LTE_{σ} is required. The relationship between LTE_{δ} and LTE_{σ} can be established from analytical results. Figure 23 shows such a relationship established using ILLI-SLAB. The load

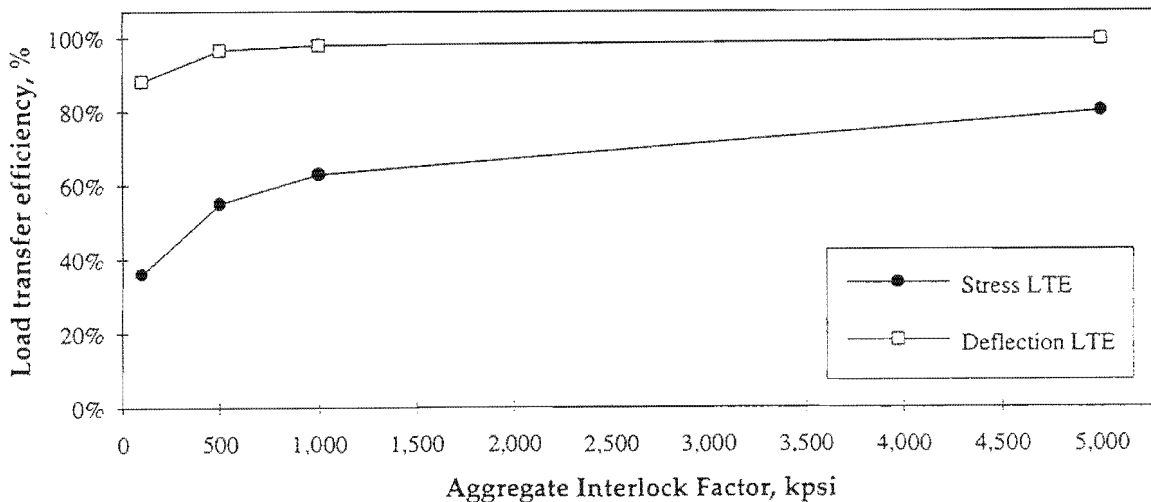


Figure 23. Stress and deflection load transfer efficiencies.

transfer at the lane-shoulder joint was modeled using aggregate interlock. The aggregate interlock factor is the stiffness of the joint in shear. The different aggregate interlock factors correspond to joints with different LTE.

The LTE determined from the measured strain values is summarized in table 8. These are LTE_g . The suspected reason for the negative LTE values and very small LTE values is again the instrumentation problem. The strain gauges may not have been zeroed properly. If the midday slab strains are shifted to match the maximum readings of the day and the shoulder strains shifted by the same amount, very consistent results are observed. Ignoring the negative values and the very small values calculated for the tied 14-ft section, the average LTE of the two tied shoulder sections was 55 percent. The LTE_g of 55 percent corresponds to an LTE_s of about 96 percent. This is a fairly high value for shoulder LTE, but it's not uncommon. Figure 23 shows that the aggregate interlock factor corresponding to the LTE_g of 55 percent is about 500 kpsi. This value was used to model the lane-shoulder joint in analyzing the slab system for the evaluation of the strains measured at interior locations and the effects of load location on strains at various locations.

Effects of Measurement Location and Load Placement on Load Strains

The load strains measured from the 14-ft tied, 14-ft nontied, and 12-ft tied shoulder sections were evaluated to determine if the strains at various distances away from the slab edge and those due to loads placed at different locations could be accurately determined by analytical means. To allow this evaluation, the strain data were collected for the following combinations of measurement and load locations:

Table 8. Measured load transfer efficiencies.

Section	Time	Temp Diff, °F	Measured Strain, Creep*			Measured Strain, Static*		
			Slab	Shoulder	LTE	Slab	Shoulder	LTE
Tied 14 ft	7:00	-8.4	19.4	9.9	51%	22.6	11.6	51%
	9:10	4.4	13.6	4.5	33%	11.8	1.2	10%
	11:25	17.7	12.4	1.0	8%	8.3	-5.9	-71%
	15:10	21.3	14.3	3.6	25%	8.1	-2.2	-27%
	17:10	11.5	25.3	14.4	57%	18.7	11.5	61%
Non-tied 14 ft	7:46	-4.2	25.6	2.2	9%	27.8	3.6	13%
	9:50	9.1	19.0	-2.3	-12%	16.0	-7.3	-46%
	12:08	20.3	17.7	-3.2	-18%	11.6	-13.0	-112%
	15:50	19.6	20.9	5.1	24%	23.7	1.1	5%
	17:36	8.8	24.2	3.7	15%	29.8	3.7	12%
Tied 12 ft	6:15	-10.8	19.6	9.6	49%	18.0	9.6	53%
	8:15	-1.5	17.8	10.4	58%	15.7	9.7	62%
	10:30	13.0	15.4	5.6	36%	12.3	3.4	28%
	14:20	20.9	17.9	10.3	58%	12.8	5.2	41%
	16:30	15.9	21.8	12.0	55%	18.3	11.3	62%

*Strains are in millionths

- Load placed at the edge: strains at
 - Shoulder
 - Edge

- Load placed 24 in from the edge: strains at
 - Shoulder
 - Edge
 - 24 in from the edge

- Load placed 42 in from the edge: strains at
 - Shoulder
 - Edge
 - 24 in from the edge
 - 42 in from the edge

Figures 24 and 25 illustrate the distribution of edge load stresses across the PCC slab with and without a tied concrete shoulder. These figures are based on finite element analysis results assuming 55 percent LTE_c. The load for the edge-loading condition was actually placed 2 in away from the edge to correlate the calculated strains to the measured values. The stresses are about 30 percent higher if the load is placed at the outer edge. As figures 24 and 25 show, the addition of the tied concrete shoulder greatly reduces the maximum bending stress in the slab (from 97 psi to 66 psi, or 32 percent reduction).

Whereas the edge stress profiles are significantly different for different loading conditions in the nontied concrete shoulder section (figure 25), those for the tied concrete section (figure 24) show very similar maximum stresses and stress distribution under the load for all three loading conditions. This is because the addition of the tied concrete shoulder provides support along the longitudinal edge, creating the support condition that is close to the slab interior even for the loads placed very close to the edge.

The tied PCC shoulder does not provide a significant reduction in stresses when the load is placed far away from the pavement edge. Whereas the tied PCC shoulder reduced the maximum bending stress by 32 percent when the load was placed at the edge, the stress reduction due to the addition of tied PCC shoulder is only about 5 percent when the load is placed 42 in from the pavement edge. Hence, on widened slab sections, where the critical location for fatigue damage is directly under the outer wheelpath, the tied PCC shoulder does not provide much advantage. In terms of fatigue damage, even 5 percent reduction in stress can be significant; however, because the stress levels are already so low on widened slab sections, the additional 5 percent reduction in stress does not provide any performance advantage.

The comparison of the measured and calculated values of load strains at various distances away from the lane-shoulder edge and for various loading conditions is given in table 9 and shown in figures 26 through 28. Because the primary effect of interest for this comparison is the relative magnitudes of strains (with respect to the edge strain under the edge loading condition), the measurements that gave the best fit in the

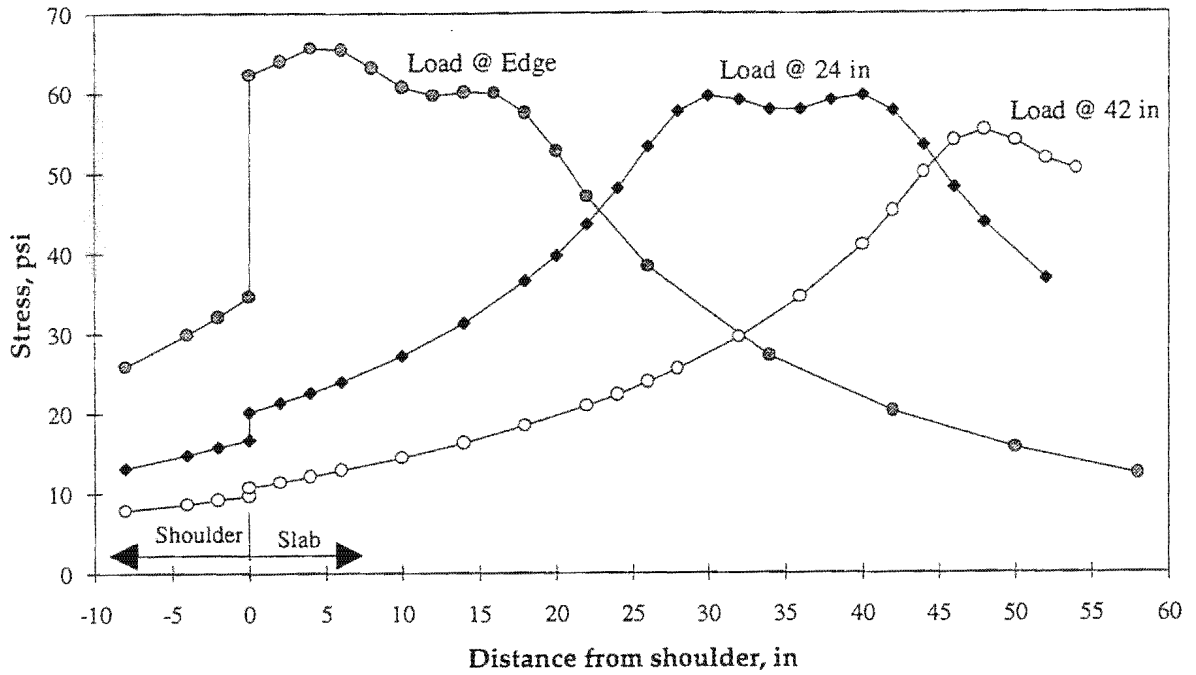


Figure 24. Edge stress profile at midslab, tied shoulder sections.

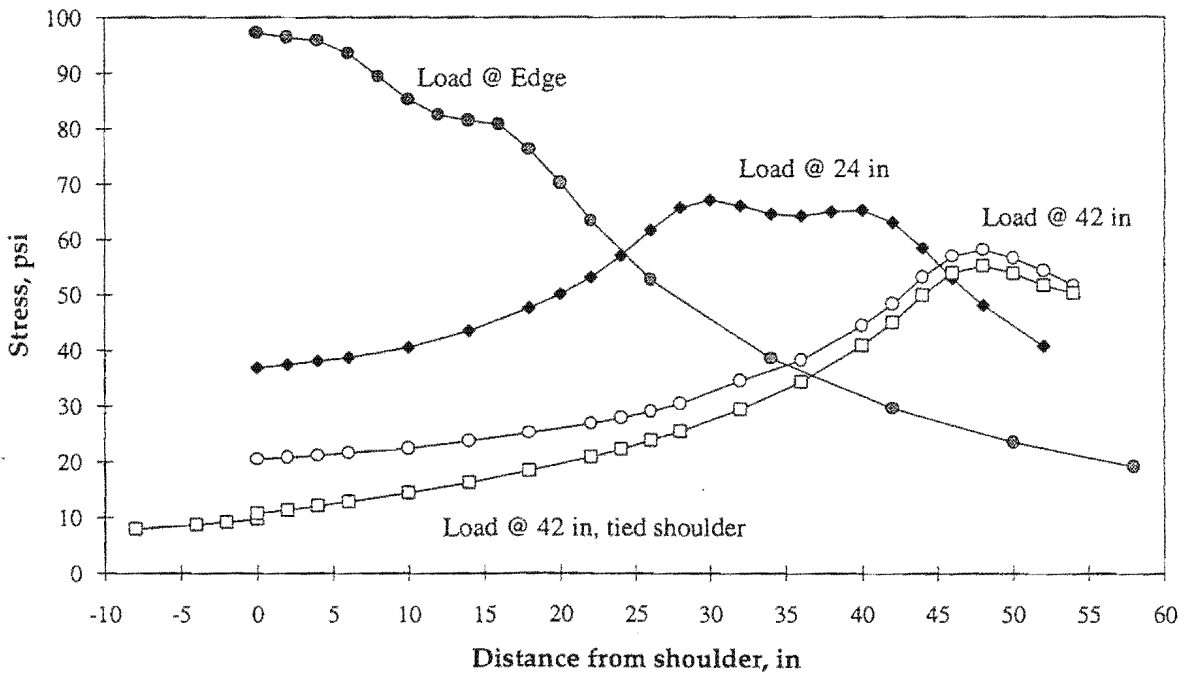


Figure 25. Edge stress profile at midslab, free edge.

Table 9. Comparison of measured and calculated strains due to load placed at various locations.

Section	Load Location	Measured Strain, millionths				Calculated Strain, millionths			
		Shoulder	Edge	24 in	42 in	Shoulder	Edge	24 in	42 in
14 ft Tied	Edge	12	23			12	21		
	24 in	5	6	15		6	7	15	
	42 in	3	4	8	19	3	4	7	14
14 ft Non-tied	Edge	4	28			3	29		
	24 in	2	8	17		2	10	17	
	42 in	0	4	9	14	1	5	8	15
12 ft Tied	Edge	12	22			12	21		
	24 in	3	5	18		6	7	15	

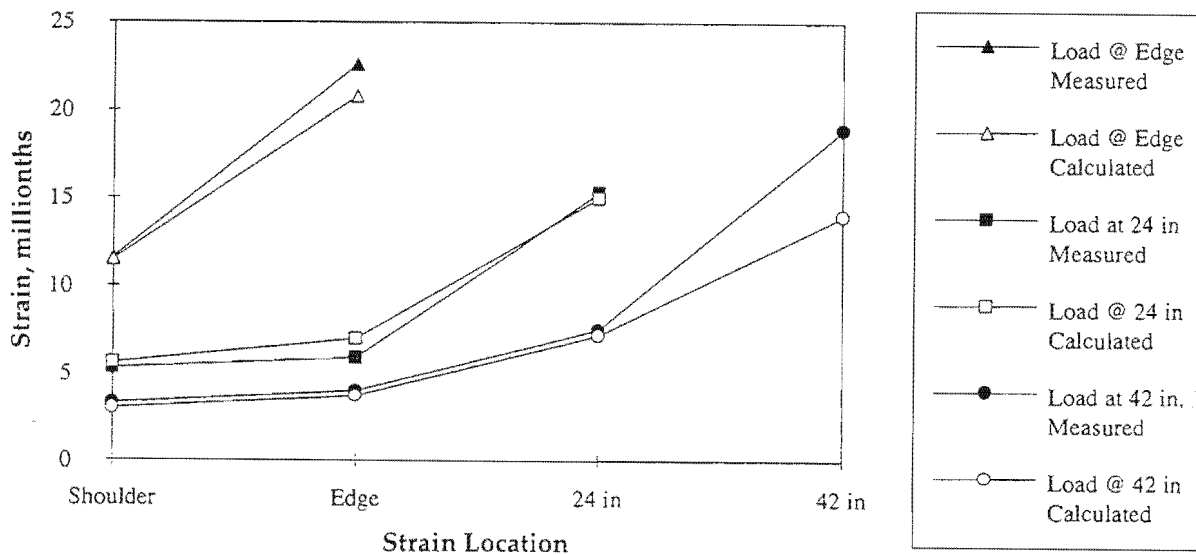


Figure 26. Comparison of measured and calculated strains at various locations (14-ft tied shoulder section).

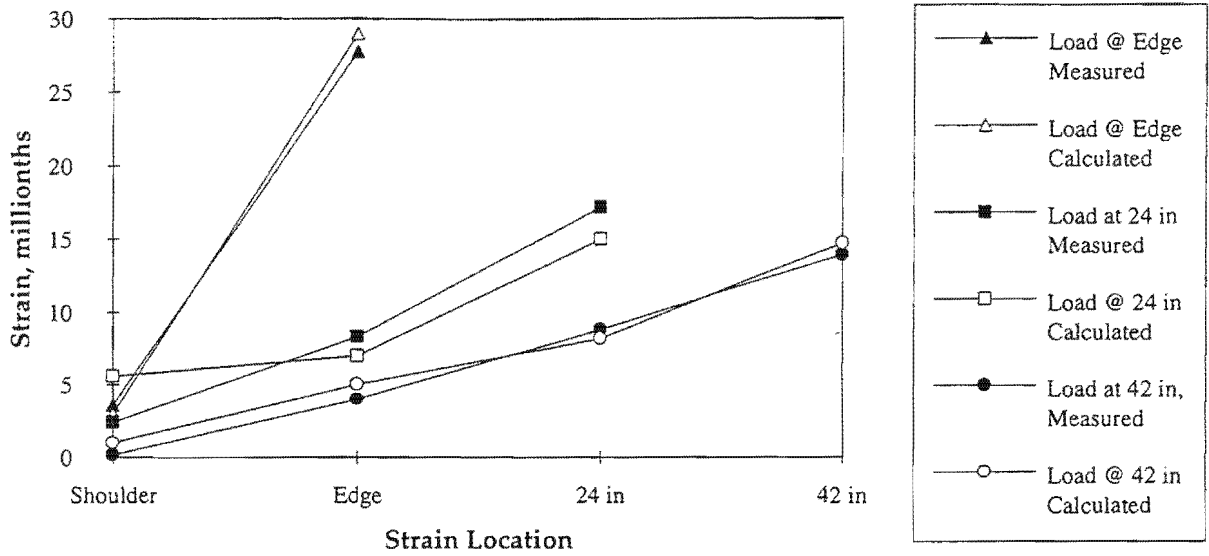


Figure 27. Comparison of measured and calculated strains at various locations (14-ft nontied shoulder section).

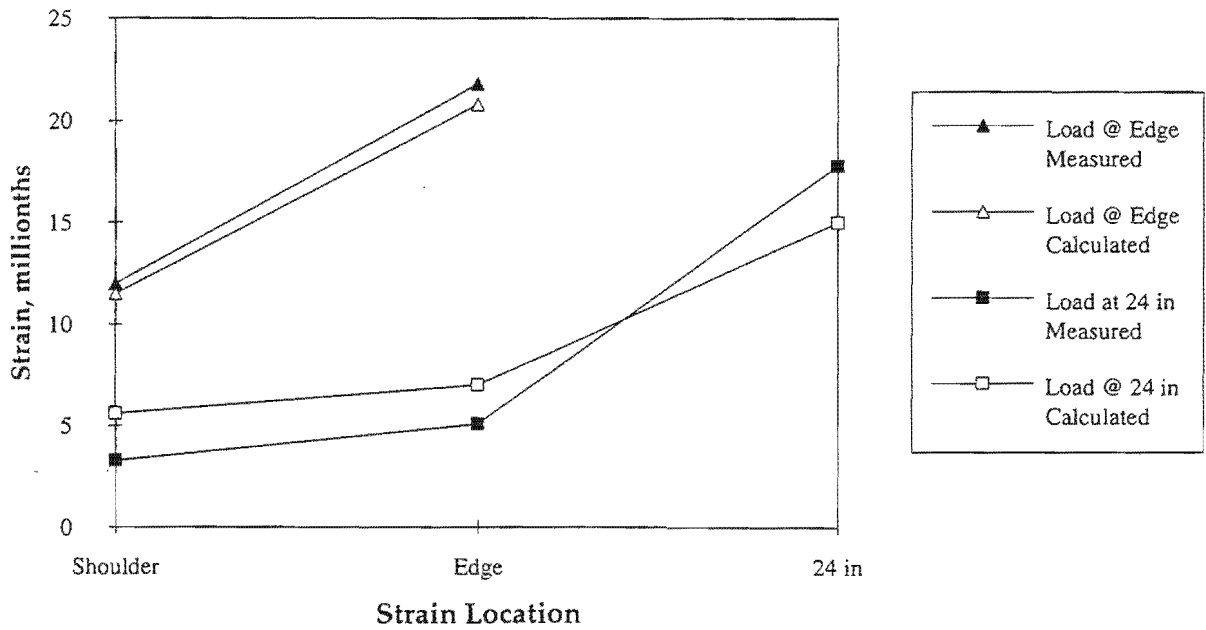


Figure 28. Comparison of measured and calculated strains at various locations (12 ft tied shoulder section).

comparison of the edge strains (see figures 20, 21, and 22) were used in this evaluation. The calculated values were obtained using ILLI-SLAB, modeling the two pavement layers with a full bond and ignoring the temperature effects. As figures 26 through 28 show, the measured values compared reasonably well with the calculated values.

Conclusion

The analysis of the data obtained from the instrumented slabs has shown that the strains (therefore stresses) in PCC pavements can be determined reliably by analytical means. The analytical work conducted for this evaluation has also shown that the addition of tied PCC shoulder does not significantly reduce the critical stresses in the slab when widened slabs are provided.

Another important finding of this evaluation, but one not directly related to the objectives of this study, is that there may be significant built-in upward curling in PCC slabs, resulting from residual temperature gradients and moisture gradients. The built-in upward curling of PCC slabs could significantly affect the fatigue performance of PCC pavements by counteracting the high positive temperature gradients that are responsible for most of the fatigue damage in PCC pavements.

PERFORMANCE EVALUATION AND MONITORING

This sections describes the testing and analysis conducted to determine the expected performance of the pavement sections evaluated under this study and provides recommendations for long-term monitoring of the test sections. FWD testing was conducted to obtain the data needed for the analysis, and the expected performance was determined based on fatigue analysis.

Deflection Testing Using FWD

FWD testing was conducted to achieve the following:

- Determine foundation modulus (modulus of subgrade reaction, k).
- Determine load transfer efficiencies across transverse joints and lane-shoulder joints.
- Determine load response of the in-place pavement structure. The effects of the old AC pavement beneath the PCC slabs and residual curling on structural response of the concrete pavement was evaluated.

The Colorado Department of Transportation performed the testing, using the department's Foundation Mechanics equipment.

Field Testing

The deflection testing was conducted on May 8, 1995. Three passes were made with the FWD to conduct the following tests:

- Transverse edge at the outer wheelpath—to determine LTE across the transverse joints.
- Longitudinal edge, halfway between the two transverse joints—to determine LTE across the lane-shoulder joint.
- Slab center—to obtain deflection basin for backcalculation.

The sensors were located at 0, 8, 12, 18, 26, 36, and 60 in from the center of the load plate, and four drops were made at each testing point (12-kip seating drop, followed by 9 kip, 12-kip, and 16-kip drops) to detect any nonlinear response. This sensor placement and testing sequence is similar to the SHRP LTPP procedure, except the sensor located at 26 in is nonstandard (the standard is 24 in), and the SHRP procedure required three drops at each load level. The sensor at 26 in was placed there because of the equipment limitation. A single drop was made at each load level, rather than three, to facilitate the testing process. This procedure was found to be adequate in all previous FWD testing work conducted by ERES; however, the analysis conducted for this study has shown that testing with three drops at each load level may be desirable for detecting loss of support under pavement slabs due to slab curling (further discussion on this topic will follow).

The weather during the testing was rainy with overcast skies, and conditions remained fairly constant throughout the day. The air temperature ranged from 47 °F to 59 °F. For the purposes of detecting the presence of residual curling discussed earlier,

the FWD testing conducted at various temperature conditions (different temperature gradients through the slabs) would have been useful. However, the weather conditions on the day of testing did not allow such validation to take place.

Backcalculation

The backcalculation was performed using a new procedure developed at ERES. This procedure employs closed-form solutions to the problem of deflection of slabs on Winkler foundations to determine the elastic properties of the slab and the foundation. The solution is found by minimizing the error between the measured and calculated deflections at the sensor locations as follows:

$$F(E, k) = \sum_{i=0}^n \alpha_i (w(r_i) - W_i)^2 \quad (6)$$

where:

- α_i = weighing factors.
- $w(r_i)$ = calculated deflection at sensor i.
- W_i = measured deflection at sensor i.

This procedure was developed and rigorously validated under a recent FHWA study conducted by ERES to evaluate the performance of experimental rigid pavements (Smith et al. 1995). The backcalculation was performed using the new procedure rather than an area-based procedure, which is more common, because of the nonstandard sensor spacing.

The new backcalculation procedure also incorporates the provision for the consideration of the effects of stabilized bases. The pavement system consisting of two layers above subgrade is analyzed by taking an assumed value for the ratio between the elastic modulus of the slab and the base and then analyzing the system as having either fully bonded or fully unbonded interface. The backcalculation results are then examined, and the more reasonable of the results given by the bonded and unbonded assumptions are taken as the representative moduli values.

The backcalculation results are given in table 10. The results clearly show the bonded response of the pavement structure. The average backcalculated PCC modulus (E_c) for the 14-ft tied and the 12-ft tied sections is 3.2 million psi. The backcalculated E_c for the 14-ft nontied section is higher (4.3 million psi), but the higher E_c is most likely due to thickness error. The structural response of concrete pavements is very sensitive to slab thickness. If the thickness used in backcalculation is less than the actual slab thickness the resulting backcalculated E_c will be substantially greater than the actual value.

The pavement parameters actually obtained from backcalculation are the radius of relative stiffness ℓ and subgrade modulus of reaction k . The E_c can be determined from ℓ if the slab thickness and k are known using equation 7.

Table 10. Backcalculation results.

	E_c Assuming Nonbonded Interface, ksi				E Assuming Bonded Interface, ksi				Subgrade k psi/in			
	Mean	Min	Max	Std Dev	Mean	Min	Max	Std Dev	Mean	Min	Max	Std Dev
14-ft tied	6,152	5,258	6,922	447	3,122	2,668	3,512	227	193	176	210	9.5
14-ft nontied	8,381	7,351	9,169	518	4,253	3,730	4,651	263	174	152	195	12.3
12-ft tied	6,398	5,200	7,532	621	3,246	2,638	3,822	315	154	137	169	9.7

$$E = \frac{\ell^4 12(1 - \mu^2)k}{h^3} \quad (7)$$

where

- E_c = PCC elastic modulus, psi.
- ℓ = radius of relative stiffness, in.
- μ = Poisson's ratio.
- k = modulus of subgrade reaction, psi/in.
- h = slab thickness, in.

This equation was obtained by rearranging the definition of ℓ . As shown in this equation, the backcalculated E_c is a function of h^3 . Therefore, relatively small changes in slab thickness can significantly affect the backcalculated E_c . The average E_c obtained by core testing is 3 million psi.

The average backcalculated k is 174 psi/in. This is consistent with the value used in the design. The k varies slightly from section to section, but for the critical stresses in the pavement slab, the variation is insignificant.

Load Transfer Efficiencies

The FWD testing was conducted at both transverse joints (in the outer wheelpath) and at the lane-shoulder joint (at mid slab, or halfway between transverse joints) to determine LTE. The transverse joints were tested with the load plate on the leave slab and then again with the load plate on the approach slab at each joint that was tested. The deflection LTE was determined using equation 4. In determining the LTE across the lane-shoulder joint, a correction factor was applied to the unloaded-side deflections because they were measured closer to the joint than the loaded side. The unloaded-side deflections were measured by manually placing the sensor next to the joint, across from the loaded-side sensor that was placed 12 in away from the load plate. The

measurements were taken about 2 in away from the joint (rather than equidistant from the joint across the loaded-side sensor) because of accessibility constraints. Based on ILLISLAB analysis, the unloaded-side deflection was divided by 1.12 to obtain the deflection 6 inches away from the joint. The results are shown in figures 29 and 30; the measured deflections and the LTE values are listed in tables C2 and C3 in appendix C. The values shown in figures 29 and 30 are the average of all of the drops made at each testing point.

The testing results show that, other than the fact that the nontied shoulder section had somewhat lower LTE across the lane-shoulder joints, the different pavement designs did not lead to appreciably different LTEs at transverse and longitudinal joints. The average deflection LTE across the lane-shoulder joint for the tied PCC shoulder sections was 84 percent, and the average for the nontied section was 81 percent. The average deflection LTE across the transverse joints was 80 percent.

The deflection LTEs based on FWD testing results correspond to stress LTE of about 25 to 28 percent. These LTEs are somewhat less than those determined based on strain measurements, but they are more consistent than the LTEs based on strain measurements and are more representative of the actual condition, because they represent the average value for 10 slabs, rather than 1. The LTEs obtained from FWD testing were used in the performance predictions.

The high deflection LTEs measured across the lane-shoulder joint in the nontied section may be attributed to the presence of the stiff AC layer beneath the slabs. Significant load transfer can be obtained through the base in a stabilized base section.

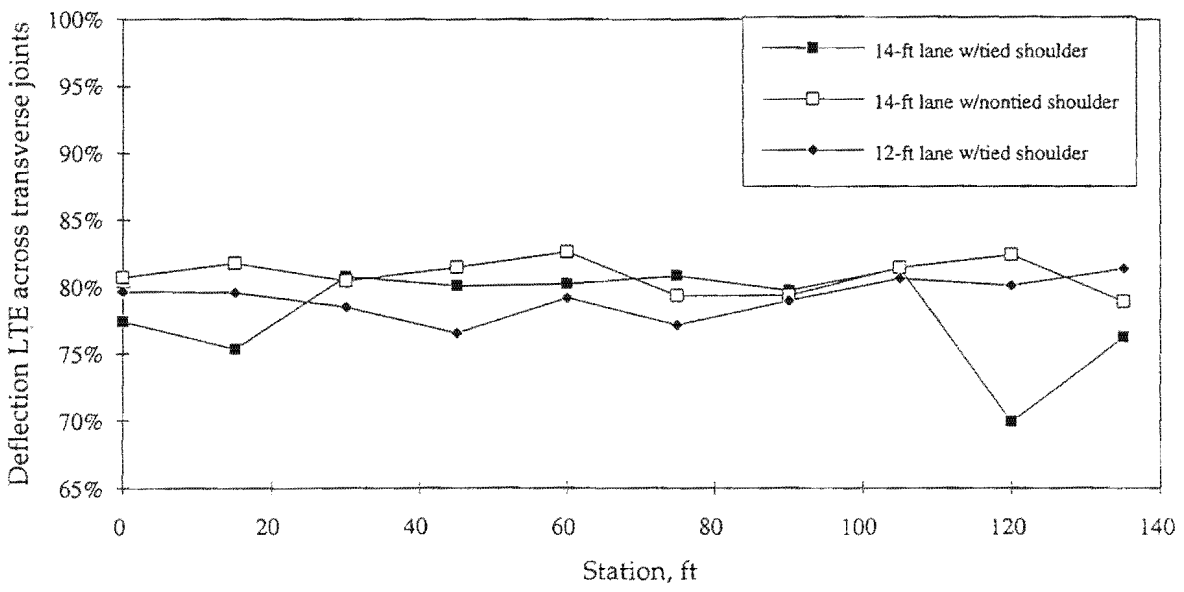


Figure 29. Deflection load transfer efficiency across transverse joint.

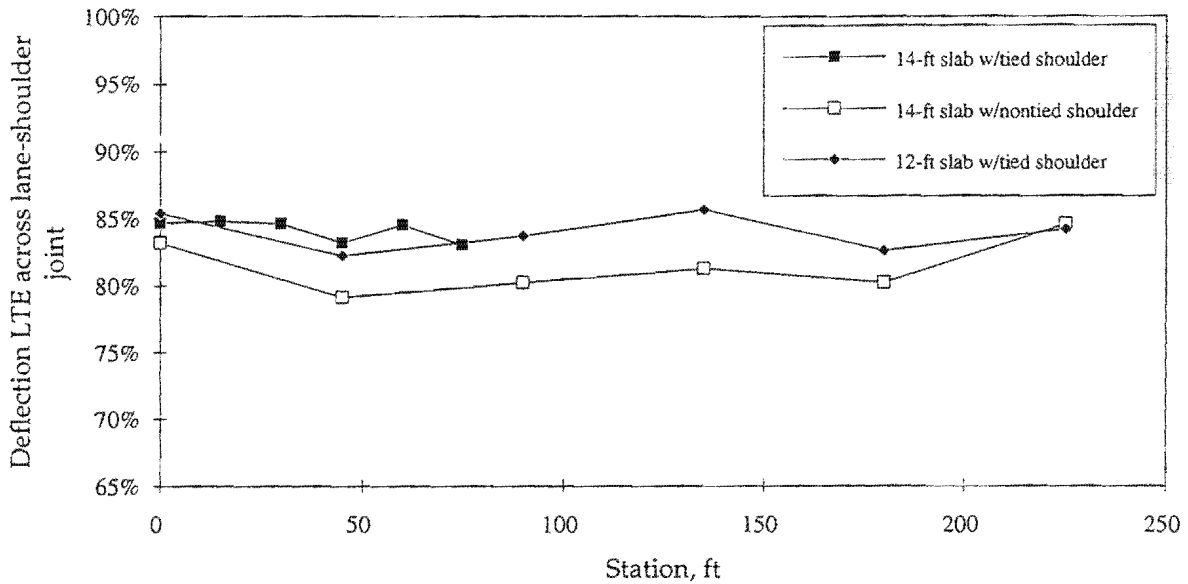


Figure 30. Deflection load transfer efficiency across lane-shoulder joint.

The lane-shoulder joint in the nontied section was sawed full-depth. The cores cut through this joint verified that the saw cut does extend the full slab thickness. Therefore, any load transfer exhibited at this joint is a result of the load transfer achieved through the stabilized base. Because of the significant role played by the AC layer in transferring load across pavement joints, similar LTEs may be expected at all joints; however, the doweled transverse joints are expected to provide better long-term performance. The LTE provided solely by stabilized bases do not provide the same degree of stress LTE as either aggregate interlock or dowels and may not be as reliable over the long term.

The greater variability observed on LTE at transverse joints appears to be due largely to measurement errors. The deflections near slab edges and corners are highly sensitive to the load location; the closer the load is to the slab edge, the higher the deflection will be. The sensitivity of the measured LTE to the load location is even greater because the sensor used to measure the unloaded-side deflection is located a fixed distance away from the load center. Consequently, if the load plate is placed closer to the edge, the sensor for the unloaded-side deflection will be placed farther away from the edge, leading to lower deflection readings of the unloaded-side. The LTE determined based on such measurements will be lower than the actual, because the calculation is based on the higher loaded-side deflection and the lower unloaded-side deflection. The reverse is true if the load plate is placed farther away from the joint. The unloaded-side sensor would be placed closer to the joint, leading to higher deflection readings and resulting in higher calculated LTE. Ideally, the loaded- and unloaded-side sensors should be placed equidistant from the joint to obtain accurate LTE values.

The relationship between deflection LTE and stress LTE is illustrated in figure 23. The stress LTE may be determined from the deflection LTE using the following regression equation (Seiler 1993):

$$\begin{aligned} \text{Log}_{10}(\text{LTE}_{\sigma}) = & 0.064787 + 0.0047221\text{LTE}_{\Delta} + 0.00089586\text{LTE}_{\Delta}^2 \\ & - 0.16478 \times 10^{-4}\text{LTE}_{\Delta}^3 + 0.89222 \times 10^{-7}\text{LTE}_{\Delta}^4 \end{aligned} \quad (8)$$

where

- LTE_{σ} = Stress LTE, percent.
- LTE_{Δ} = Deflection LTE, percent.

Deflection Trends

The maximum deflections under 9,000 lb load at transverse joints, lane-shoulder joints, and interior locations are shown in figures 31, 32, and 33. The most consistent results were obtained from the testing conducted at the interior locations. The differences in the interior deflections among different test sections may be attributed to the differences in the pavement layer thicknesses and subgrade support (k).

The deflections at transverse and longitudinal joints showed greater variability because they are sensitive to the placement of the load plate with respect to the slab edge; the closer the load plate is to the pavement edge, the higher the deflection. Figure

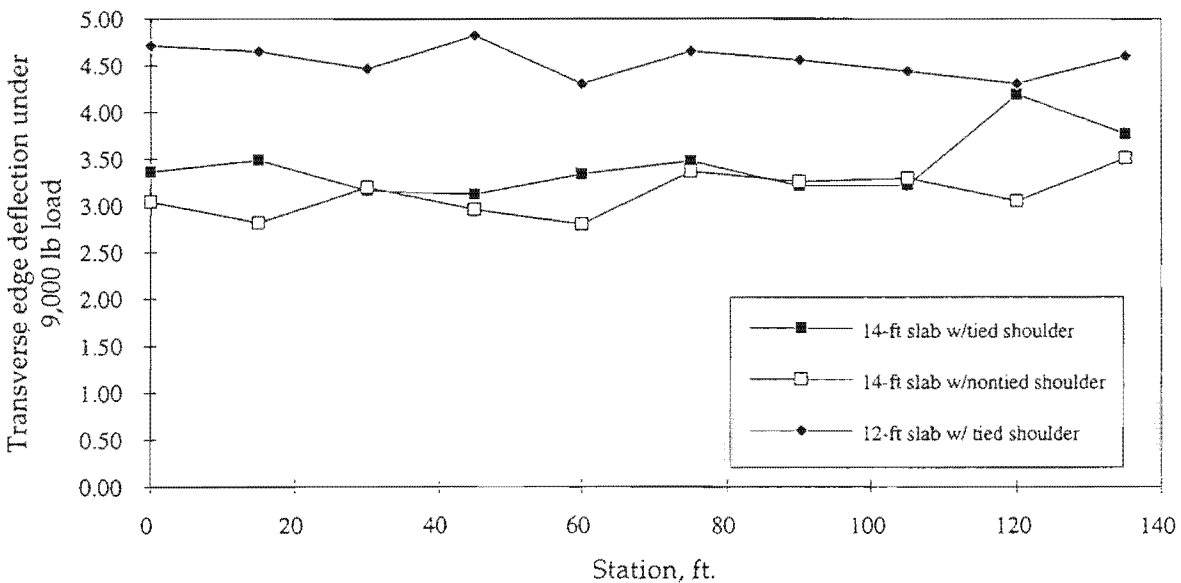


Figure 31. FWD deflections at transverse edges.

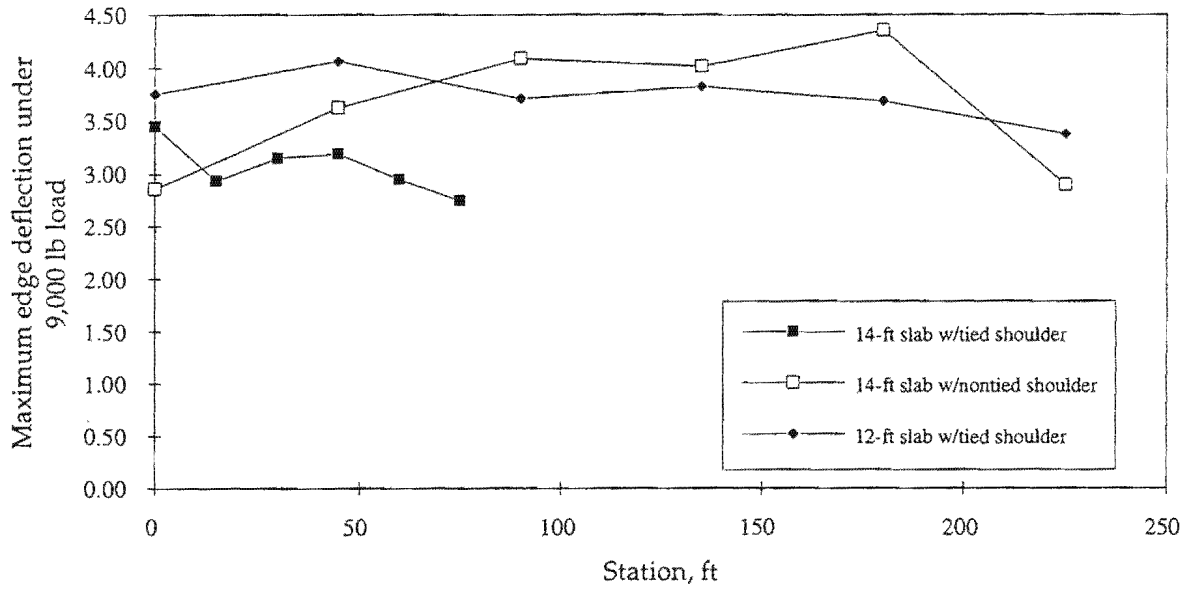


Figure 32. FWD deflections at the lane-shoulder joint.

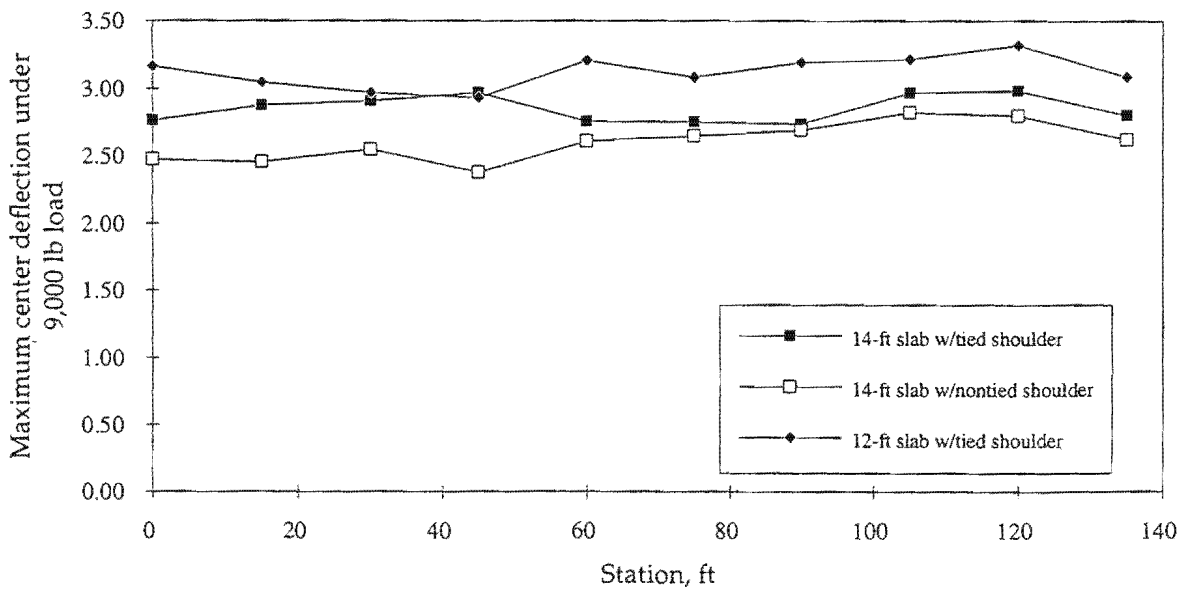


Figure 33. FWD deflections at the slab centers.

31 shows that the deflections at transverse joints are significantly higher in the 12-ft tied shoulder section than in either of the two widened-slab sections. This is simply because the outer wheelpath (where the deflection measurements were taken) is much closer to the slab corner in a standard-width section than in the widened-slab sections. Corner deflections are normally about twice those of edge deflections.

The magnitude of deflections at all locations indicated bonded response of the pavement structure (i.e., monolithic behavior of the PCC slab and the AC layer). The analysis of data from the instrumented slabs showed that curling may cause parts of PCC slabs to lift off the foundation, but the slabs can reestablish contact under load and provide bonded response. The slabs were found to have a considerable amount of built-in upward curling. The FWD testing results verified the bonded response of the pavement structure, but the presence of the built-in curl could not be confirmed.

The FWD testing conducted at different load levels showed that the slabs were very much flat when they were tested. Curling can cause lifting of either slab edges or slab center. The upward curling of the slab causes the slab edges and corners to lift up, whereas the downward curling causes the slab center to lift up. The resulting loss of support at the affected locations can be detected using the FWD by testing the slabs at different load levels. The loss of support leads to nonlinear response of slab deflections to load (i.e., the deflections are not directly proportional to the load levels). The nonlinear response is easily detected by plotting the deflections measured under different load levels against the applied load level.

The representative load response at different locations is shown in figures 34, 35, and 36. The loss of support would be indicated by the smaller relative deflection at higher load levels and positive intercept of the line drawn through the data points in the deflection versus load plot. Figure 34 shows a positive intercept for the testing conducted at transverse edge, but the magnitude of the intercept is very small. Figures 35 and 36 show a slight decrease in the deflection with respect to load for the deflections under a 16,000 lb load, but again the magnitude is very small.

The loss of support due to curling cannot exist at both the slab center and the slab corners at the same time for obvious reasons. The slab has to be resting on the foundation at some point. From the load response shown in figures 34 through 36, we may conclude that the slabs are flat. In all three figure, linear response is shown and the intercept (the extrapolated deflection at zero load) is very close to zero.

The temperature gradient through the slab was not measured during FWD testing, but it may be assumed to be close to zero, because the conditions during testing were overcast sky and rain with the air temperature ranging from 47 °F to 56 °F, close to the soil temperature at that time of the year. Under these temperature conditions, the slabs are expected to be curled up due to the built-in curl (as shown by the analysis of the instrumented slabs). One possible reason that the built-in curl was not detected may be the absence of moisture gradient through the slab due to the wet surface conditions during testing.

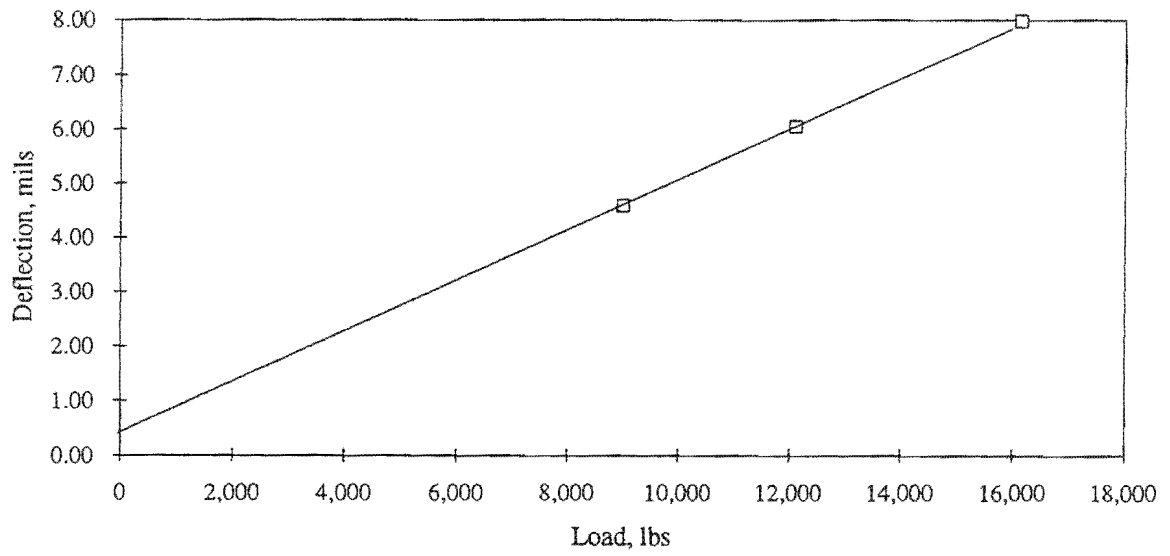


Figure 34. Representative load response of slab deflections at the transverse edge.

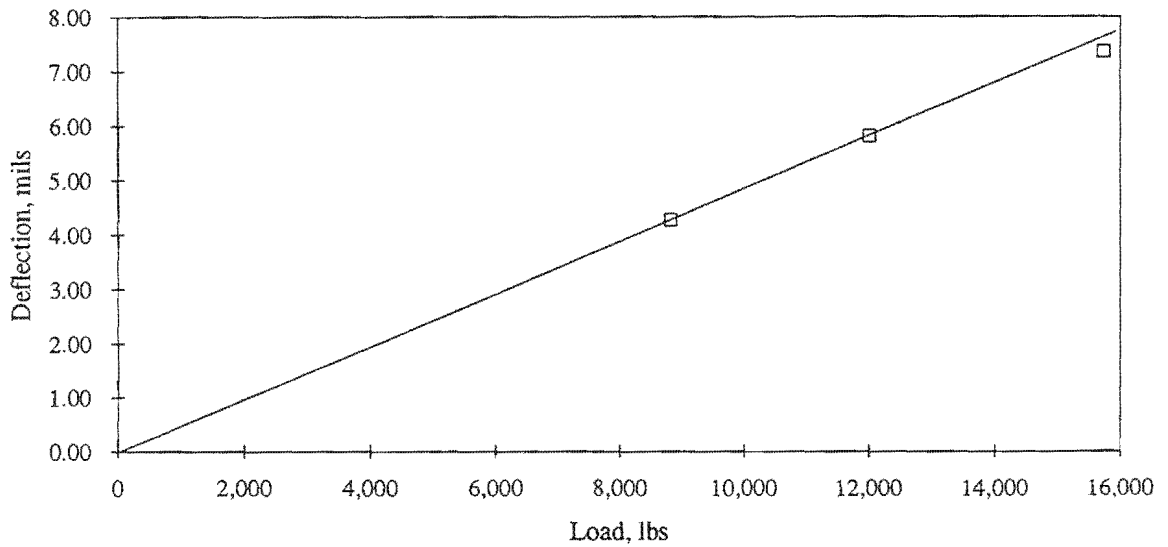


Figure 35. Representative load response of slab deflections at the lane-shoulder edge.

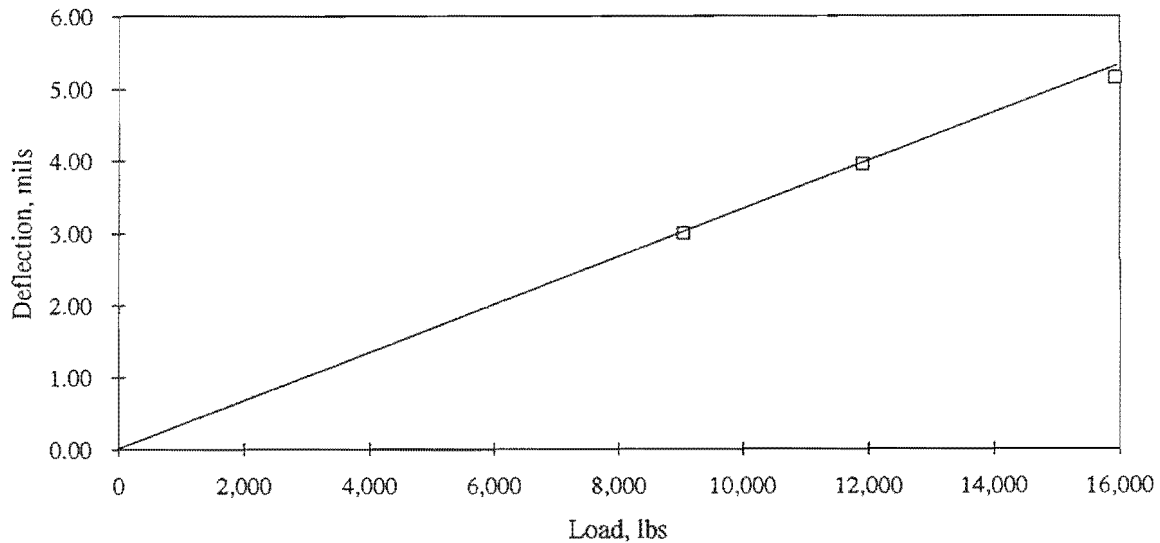


Figure 36. Representative load response of slab deflections at the slab center.

Fatigue Analysis

The long-term performance of the test sections was evaluated by performing a fatigue analysis. Several assumptions were made in this analysis to ensure that reliable, conservative results were obtained:

- The structural contribution of the AC layer was ignored. Although the field testing results showed that the pavement structure exhibits bonded behavior, the long-term reliability of this bonded behavior is poor, particularly at the slab corners and edges, where large deflections occur. The widened-slab sections may be expected to maintain the bonded behavior better, because the critical location for fatigue damage occurs in the wheelpath (rather than at the longitudinal edge), but the bonded response should not be depended on to provide adequate performance when no special efforts were made to ensure the bond between the pavement layers. A recent study conducted for the FHWA (Smith et al. 1995) showed that most of the stabilized base sections did not give bonded performance, although the FWD testing results showed bonded response at the slab centers. One possible explanation for the observed discrepancy may be that the effective bond is easily lost at the slab edges and corners, where deflections are considerably higher than at the slab center. Over 270 in-service PCC pavements were evaluated in that FHWA study.

- For the analysis of transverse cracking that occurs as a result of accumulated fatigue damage at the longitudinal edge, the effects of built-in curling were ignored. The built-in upward curling of the slabs counteract the positive temperature gradients at the longitudinal edge. The maximum stress at the longitudinal edge occurs at the highest positive temperature gradient. The magnitude of built-in curling can be quite variable even within a single project because a significant portion of the built-in curling is caused by the temperature gradient during construction (at time of concrete hardening), and concrete is placed throughout the day under continuously variable temperature conditions in a typical paving operation. Because the built-in curling reduces the critical stress at the longitudinal edge and the amount of built-in curling is variable, the most conservative estimate of the accumulated fatigue damage is made by ignoring the effects of built-in curling.
- For the analysis of the cracking that may occur near slab corners under the corner loading condition, the case of maximum built-in curl was considered. The critical stress under corner loading occurs at the maximum negative temperature gradient, and the effects of the built-in upward curling is additive to the curling due to negative temperature gradients. Hence, the case of the maximum built-in curl was considered for the evaluation of top-down cracking due to corner loading.

The fatigue analysis was performed for the cases where the cracking initiates at the bottom of the slab, either at the longitudinal edge (in the case of standard-width lanes) or directly under the outer wheelpath (widened-slab). These are typically the locations where the fatigue cracking initiates in concrete slabs, unless a large, built-in upward curling is present in the slab. If the slabs are initially curled up to a significant degree, then the tensile stress at the slab surface under corner loading can become more critical. The magnitudes of stresses under the corner-loading conditions were determined and compared to those under the edge-loading conditions, but a detailed fatigue analysis was not performed for the corner-loading condition because of limitations in the available tools for the analysis of this mode of failure and because the maximum stresses under the corner-loading conditions were comparable to those under edge-loading condition. The details of the fatigue analysis conducted for this study are presented in the following.

Stress Calculations

The stresses under the edge-loading condition were determined using the regression equations developed under NCHRP Project 1-26 (Salsili 1993). These equations are based on the results given by the finite element program ILLI-SLAB, and they provide an accurate and efficient means of determining the combined stress due to axle loads and slab curling under edge-loading condition. The regression equations make it feasible to analyze the large number of cases necessary to adequately address the effects of temperature gradients on fatigue damage.

Load Stress

The NCHRP 1-26 equations utilize Westergaard's edge stress equation for a circular load and various adjustment factors to reproduce the results given by the ILLI-SLAB finite element program. The equation for the load stress has the following form:

$$\sigma_{load} = f1 * f2 * f3 * f4 * \sigma_e \quad (9)$$

where

- σ_{load} = Load stress, psi.
- f1, f2, f3, f4 = Adjustment factors for slab size, stabilized base, widened slab, and tied concrete shoulder.
- σ_e = Stress obtained using Westergaard's edge load equation for circular loads, psi.

The equivalent single-axle radius (ESAR) concept is used to handle multiple wheel loads, and adjustments are made to account for the slab size effect, widened slab, tied concrete shoulder, and presence of a stabilized base. The ESAR is the equivalent single wheel radius of a multiple wheel load that will produce the same stress intensity at the critical location. The application of the ESAR concept allows the use of a closed-form solution to determine the maximum stress under a multiple wheel load.

The edge load stress is calculated using the equation given in Westergaard's 1948 paper for circular load given below, substituting the radius of the applied load with the equivalent single axle radius (Westergaard 1948):

$$\sigma_e = \frac{3(1 + \mu)P}{\pi(3 + \mu)h^2} \left[\ln \frac{Eh^3}{100ka^4} + 1.84 - \frac{4\mu}{3} + \frac{1 - \mu}{2} + 1.18(1 + 2\mu) \frac{a}{\ell} \right] \quad (10)$$

where

- P = Total applied load, lb.
- μ = Poisson's ratio.
- E = Modulus of elasticity of PCC, psi.
- h = Slab thickness, in.
- k = Modulus of subgrade reaction, psi/in.
- a = Radius of the applied load, in.
- ℓ = Radius of relative stiffness, in, defined as follows:

$$\ell = \left[\frac{Eh^3}{12(1 - \mu^2)k} \right]^{0.25} \quad (11)$$

where

- E = Modulus of elasticity of PCC, psi.
- h = Slab thickness, in.
- μ = Poisson's ratio.
- k = Modulus of subgrade reaction, psi/in.

The equivalent single-axle radius for the dual wheel load is obtained using the following equation:

$$\begin{aligned} \frac{a_{eq}}{a} = & 0.909 + 0.339485 \frac{S}{a} + 0.103946 \frac{a}{\ell} - 0.017881 \left(\frac{S}{a} \right)^2 - 0.045229 \left(\frac{S}{a} \right)^2 \frac{a}{\ell} \\ & + 0.000436 \left(\frac{S}{a} \right)^3 - 0.301805 \frac{S}{a} \left(\frac{a}{\ell} \right)^3 + 0.034664 \left(\frac{S}{\ell} \right)^2 + 0.001 \left(\frac{S}{a} \right)^3 \frac{a}{\ell} \end{aligned} \quad (12)$$

Limits: $0 \leq S/a \leq 20$
 $0 \leq a/\ell \leq 0.5$

$R^2 = 1.0$

where

- a_{eq} = Equivalent single axle radius of dual wheels, in.
- a = Radius of the applied load, in.
- S = Dual wheel spacing, in.
- ℓ = Radius of relative stiffness, in.

The use of the equivalent load radius in equation 10 gives results that closely match those of ILLI-SLAB analysis.

In the NCHRP 1-26 procedure, the load stress is determined by applying various adjustment factors to the edge stress calculated using Westergaard's equation (equation 10). The adjustments are made for the slab size effect, widened slab, tied concrete shoulder, and stabilized base. Regression equations are provided for determining each of these factors, but only the factor for widened slab was used in this evaluation for the following reasons:

- The adjustment factor for the slab size effect was not used, because the ILLI-SLAB analysis performed to validate all procedures used in this project showed that the use of this factor could result in overcompensation for the slab size effect. This factor was originally introduced because the load stress in short slabs can be significantly less than that in an infinite slab assumed in the Westergaard solution. The stresses are lower in short slabs because some of the load on short slabs is carried by the rigid body motion of the slab (i.e., slabs sinking into the subgrade).

If this rigid body motion is prevented, by the adjacent slabs for example, the stresses in short slabs can be even higher than that in infinite slabs. The analysis has shown that the response of a multiple slab system with even a poor load transfer efficiency (deflection LTE of 50 percent) at the transverse joints closely approximate that of an infinitely long slab.

- The effects of tied concrete shoulder were treated by directly considering the stress LTE. The stress LTE was determined from deflection LTE using equation 8 (Seiler 1993). The average LTE_{Δ} across the lane-shoulder joint in the tied concrete shoulder section was 84 percent. The corresponding LTE_{σ} at this joint is 28 percent according to equation 8. For the sections provided with tied concrete shoulder, the load stress was multiplied by the following factor to account for the edge support:

$$f_{LTE} = \frac{100}{100 + LTE_{\sigma}} \quad (13)$$

where

f_{ES} = Adjustment factor for edge support (= 1.0 if no edge support).
 LTE_{σ} = Stress LTE, percent.

Equation 13 gives f_{ES} of 0.78 for LTE_{σ} equal to 28 percent, meaning that the tied shoulder provides 22 percent reduction in edge stress.

- The effects of stabilized bases were ignored in this study for reliability considerations.

On widened slab sections, the critical location for fatigue damage is the bottom of the slab, directly under the wheelpath. Studies have shown that the slabs are almost never loaded at the outer edge on widened lane sections (Benekohal et al. 1990). Therefore, the following adjustment factor was used to obtain the maximum stress directly under the wheel load:

$$f_{WL} = 0.454147 + \frac{0.013211}{D/\ell} + 0.386201 \frac{a}{D} - 0.24565 \left(\frac{a}{D} \right)^2 + 0.053891 \left(\frac{a}{D} \right)^3 \quad (14)$$

where

f_{WL} = Adjustment factor for widen lane (= 1.0 if standard-width lane).
 a = Radius of loaded area, in.
 D = Mean wheel location, inches from outer edge.
 ℓ = Radius of relative stiffness, in.

The load stress can now be determined using the following equation:

$$\sigma_{Load} = f_{ES} f_{WL} \sigma_e \quad (15)$$

where

- σ_{Load} = Load stress, lbf/in².
- f_{ES} = Adjustment factor for edge support (equation 13).
- f_{WL} = Adjustment factor for widened slab (equation 14).
- σ_e = Westergaard's edge stress (equation 10), psi.

Curling Stress

The curling stress was determined using the following equation and then combined with the load stress using a regression coefficient in the NCHRP 1-26 procedure:

$$\sigma_c = \frac{C E \alpha_T \Delta T}{2} \quad (16)$$

where

- σ_c = Curling stress, psi.
- C = Curling stress coefficient.
- E = Concrete modulus of elasticity, psi.
- α_T = Concrete coefficient of thermal expansion (5.5×10^{-6}).
- ΔT = Temperature difference between the top and bottom of the slab, °F.

This equation was developed by Westergaard, and Bradbury developed the coefficients for solving this equation (Westergaard 1926; Bradbury 1938). For maximum stress at the longitudinal edge, the curling stress coefficient is given by the following equation (Salsili et al. 1993):

$$C = 1 - \frac{2 \cos \lambda \cosh \lambda}{\sin 2\lambda + \sinh 2\lambda} (\tan \lambda + \tanh \lambda) \quad (17)$$

where

$$\lambda = \frac{L}{\ell \sqrt{8}} \quad (18)$$

- L = Slab length, in.
- ℓ = Radius of relative stiffness, in.

Combined Stress

The combined stress due to load and curling was obtained using the following equation:

$$\sigma_{combined} = \sigma_{load} + R * \sigma_{curl} \quad (19)$$

where

- $\sigma_{combined}$ = Combined edge stress, psi.
- σ_{load} = Load stress, psi.
- R = Regression coefficient.
- σ_{curl} = Curling stress, psi.

The expression for the regression coefficient R is given below:

$$\begin{aligned} R = & 1.062 - 0.015757 dT - 0.0000876k - 1.068 \frac{L}{\ell} + 0.387317 dT \frac{L}{\ell} \\ & + 1.17 \times 10^{-11} E dT k - 1.81 \times 10^{-12} E dT^2 k - 1.051 \times 10^{-9} E \left(\frac{L}{\ell} \right)^2 k dT \\ & + 1.84 \times 10^{-11} E dT^2 \frac{L}{\ell} k - 1.7487 \left(\frac{L}{\ell} \right)^2 dT + 0.000034351 dT^3 \\ & + 86.97 \left(\frac{L}{\ell} \right)^3 - 0.00816396 dT^2 \frac{L}{\ell} \end{aligned} \quad (20)$$

where

- $dT = \alpha \Delta T \times 10^5$.
- α = PCC coefficient of thermal expansion, $\epsilon/^\circ\text{F}$.
- ΔT = Temperature difference through the slab, $^\circ\text{F}$.
- k = Subgrade modulus of reaction, psi/in
- L = Slab length, in.
- ℓ = Radius of relative stiffness, in (equation 11).
- E = Modulus of elasticity of PCC, psi.

The coefficient R is needed because the load and curling stresses are not directly additive. Curling causes various parts of the slab to lift off of the base, invalidating the full contact assumption made in the load stress calculation. The regression coefficient R provides the necessary adjustment to the curling stress to give the correct combined stress.

Fatigue Damage Calculation

The fatigue damage was determined using the linear damage accumulation approach proposed by Miner (Miner 1945):

$$FD = \sum_{i=1}^j \frac{n_i}{N_i} \quad (21)$$

where

- FD = Fatigue damage.
- n = Number of applied load applications at stress level *i*.
- N = Number of allowable load applications at stress level *i*.

In this study, the following fatigue damage model was used to determine N:

$$\log N = 2.13 SR^{-1.2} \quad (22)$$

where

- N = Number of allowable load applications.
- SR = Stress to strength ratio (σ/MR).
- σ = Critical tensile stress, psi.
- MR = PCC modulus of rupture, psi.

This model was developed at ERES based on the Corps of Engineers (COE) data from 51 full scale field sections, and it has given good results in both airfield and highway applications (Darter 1988).

Equation 21 is simple and straightforward, but it requires separate consideration of all cases that significantly affect N to obtain an accurate estimate of FD. The N is a function of SR. The main variable that affects SR on PCC pavements is the temperature gradients through the slab. The temperature gradients vary continuously throughout the day and from day to day throughout the year. Because the curling stresses resulting from the temperature gradients can significantly affect the combined stresses and N is an exponential function of SR, an adequate number of cases for different temperature conditions must be considered to obtain accurate results.

The n_i in equation 21 refers to the number of load applications that occurred at the SR corresponding to the N_i . The SR used to determine N_i in equation 22 is determined for the load placed directly at the longitudinal edge. Because the actual traffic wanders about the mean wheel path (which is typically 18 to 22 inches away from the pavement edge) and the edge stress is highly dependent on the load placement, the effective n_i must be determined that corresponds to all traffic passes that occurred at the SR_i . The

concept of pass-to-coverage ratio (p/c) is used in this study to determine the effective n_i that occurred at each stress level.

Temperature Distribution

In this study, a computer model was used to obtain the distribution of hourly temperature gradients through the slabs for the average year using 30-year average climatic data. The Climatic-Materials-Structural (CMS) program developed at the University of Illinois (Dempsey et al. 1986) generates the distribution of average hourly temperature gradients given temperature, wind speed, percent sunshine, and thermal properties of the pavement layer materials.

The results of CMS analysis for the conditions at the test site are shown in figure 37. The results give the frequency distribution of temperature gradients in 2 °F increments between the minimum and maximum temperature gradients calculated for the site (in this case, from -20 °F to +28 °F for the 11-in slab). Assuming that the traffic is evenly distributed across all temperature conditions, the frequencies shown in figure 37 were used to distribute traffic to different temperature conditions. The fatigue damage caused at each temperature condition was then determined and summed to obtain the total FD.

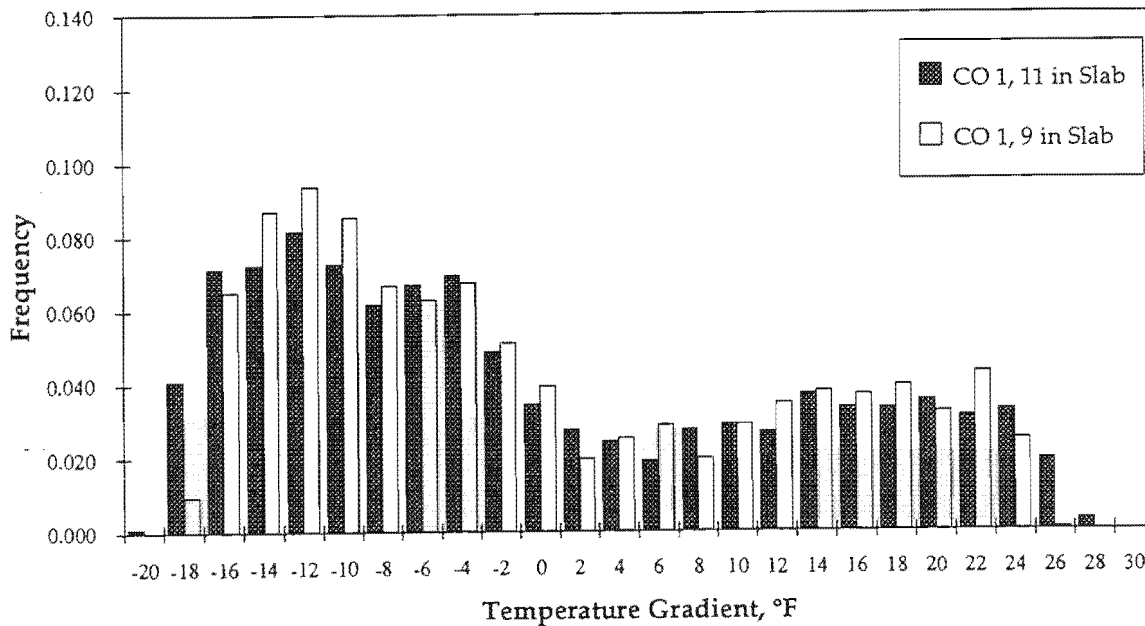


Figure 37. Distribution of hourly temperature gradients determined using CMS program.

Pass-to-Coverage Ratio

The p/c is the ratio that gives the number of traffic passes needed to produce the same amount of fatigue damage at the critical location as one traffic pass through the critical location (i.e., edge loading for the standard-width section). For example, if the p/c is 100, this means that it takes 100 traffic passes to cause the same amount of damage as 1 load placed directly at the edge. The p/c converts the applied traffic to an equivalent number of loading cycles (coverage) under the reference loading condition defined for the p/c. Because the p/c is used to facilitate the FD calculations, the reference loading condition is so selected because the stresses under that loading condition are easily determined. For the standard-width lanes, the most sensible reference condition is the edge-loading condition; for widened slabs, the use of the maximum stress under the load is convenient.

The p/c is commonly taken as a percentage of traffic that passes close to the pavement edge. In this approach, the traffic passing within a certain distance of the outer edge is assumed to cause one edge loading application. In this study, the concept of "fatigue damage per pass" (FD/Pass) was used to more precisely determined the amount of fatigue damage cause by the passing traffic. A more precise determination of p/c is warranted because the edge load stress on concrete slabs is extremely sensitive to the load location.

The edge load distribution due to a dual wheel load is illustrated in figure 38. Each line in this figure is the normalized stress at various locations across the slab due to the load placed at a certain distance from the edge. The load placement shown in figure 38 spans from 0 in from the outer edge to 36 in from the edge. As shown in this figure, the edge stress drops rapidly as the load is moved away from the edge. Even the load placed 2 in from the edge produces stresses that are considerably less (about 12 percent drop) than the load placed directly at the edge. In terms of fatigue damage, the stress trends shown in figure 38 are much more significant (figure 39). To accurately determine the accumulated fatigue damage at the critical location, the fatigue contribution by the traffic passing near the pavement edge needs to be determined more accurately.

The fatigue damage caused by the traffic at any point on a pavement slab may be determined using FD/Pass. The FD/Pass may be defined as follows:

$$FD_{D_i}/Pass = \sum_j P(COV_{D_j}) * FD_{D_{ij}} \quad (23)$$

where

- FD_{D_i}/Pass = Fatigue damage per pass at the damage location D_i.
- P(COV_{D_j}) = Probability that the load will pass through location D_j.
- FD_{D_{ij}} = Fatigue damage at location D_i due to the load at D_j.

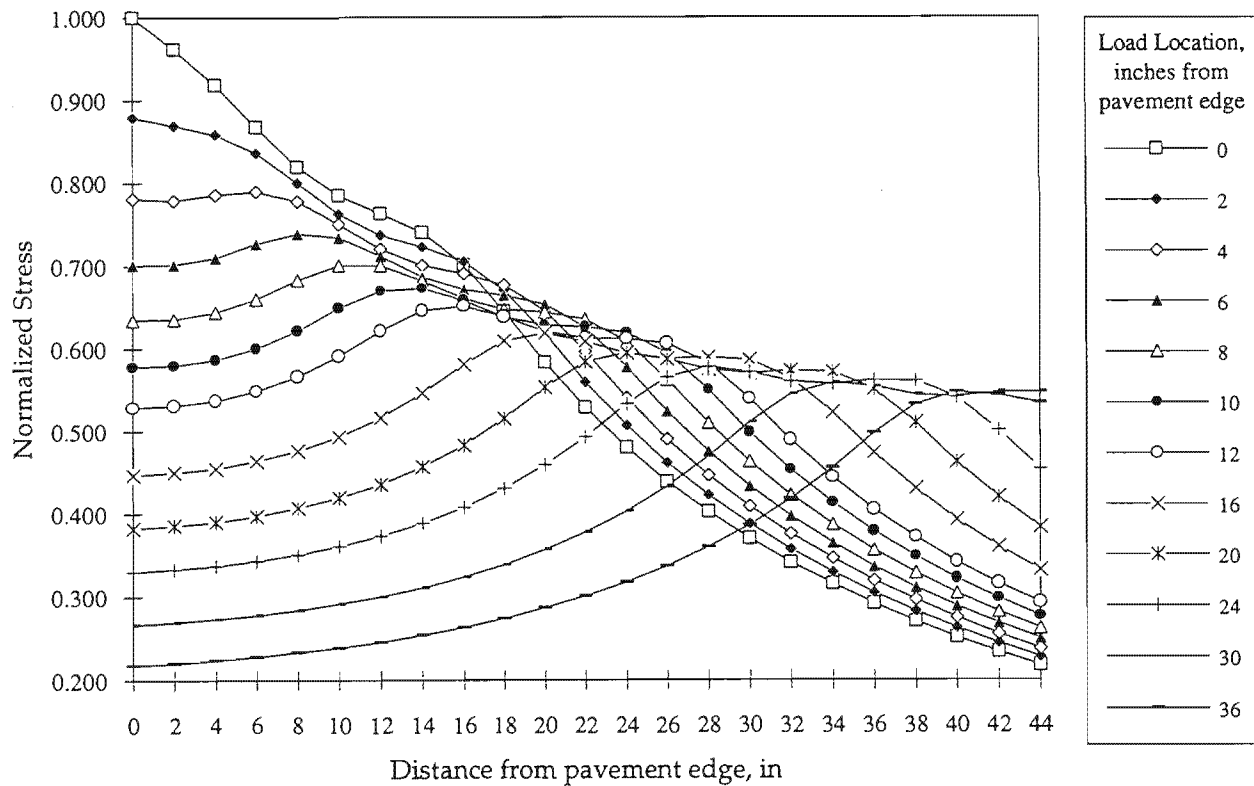


Figure 38. Edge load stress distribution across a pavement slab at midslab.

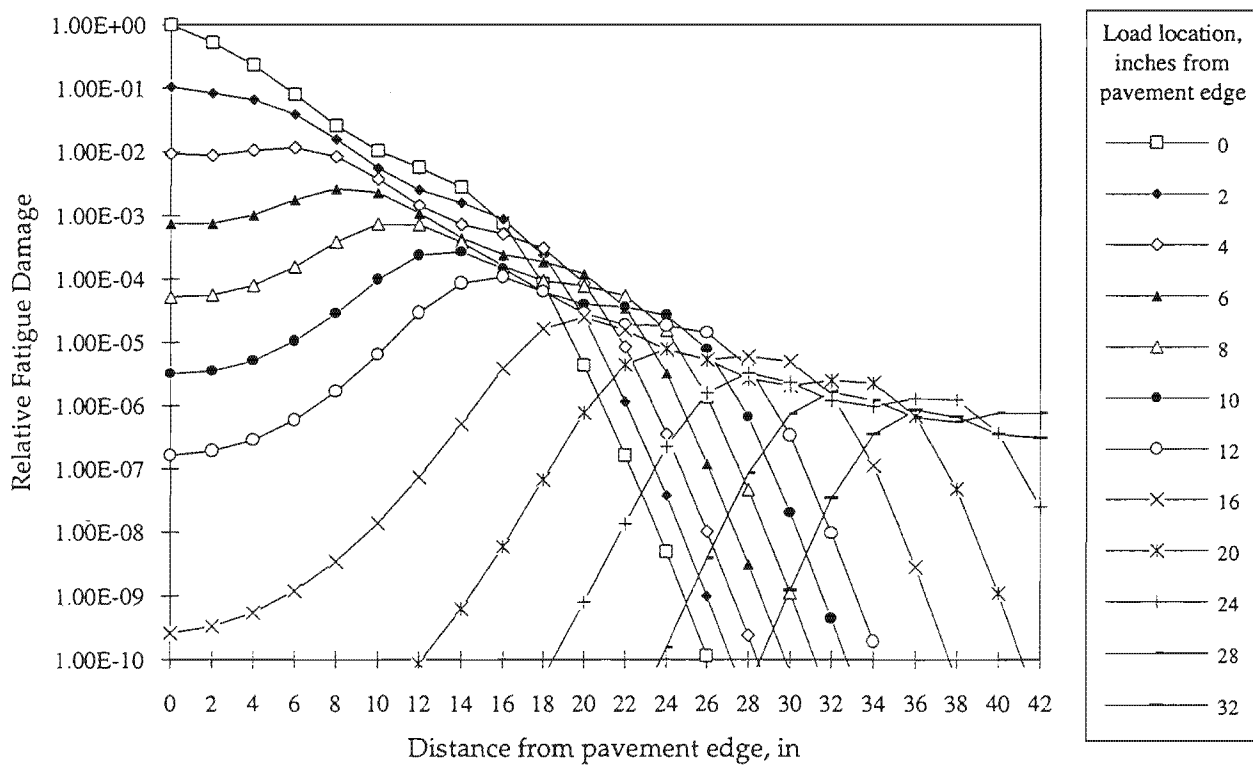


Figure 39. Fatigue damage distribution across a pavement slab due to the loads placed at various distances from the pavement edge.

This equation assumes normal distribution of the lateral traffic wander. Studies have shown that this assumption is reasonable (Benekohol et al. 1990). The FD/Pass as defined in equation 23 represents the probabilistic amount of damage caused at location D_i due to the applied traffic. It is important to note that FD/Pass is determined for a specific point on the pavement. To determine FD/Pass, the stress at the location of interest due to the loads placed at all relevant locations must be determined. Figure 38 is an example of the type of data needed to determine FD/Pass.

Once the FD/Pass is determined, this number can be used to define p/c which in turn can be used to convert the applied traffic to the number of equivalent load cycles under the reference condition (i.e., edge loading for standard-width lanes, maximum stress under the wheel at the mean wheel location for the widened slab) as follows:

$$p/c_{D_i} = \frac{FD_{D_{ii}}}{\sum_j P(COV_{D_j}) * FD_{D_{ij}}} \quad (24)$$

where

- p/c_{D_i} = p/c at location D_i .
- $FD_{D_{ii}}$ = Fatigue damage at location D_i due to the load at D_i .
- $P(COV_{D_j})$ = Probability that the load will pass through location D_j .
- $FD_{D_{ij}}$ = Fatigue damage at location D_i due to the load at D_j .

The subscript on p/c above denotes that the p/c determined above converts the traffic placed on the pavement to the equivalent number of load applications by the loads placed directly at D_i for fatigue damage at D_i . Again, this location is the longitudinal pavement edge for standard-width lanes and directly under the wheelpath for widened slab. Taking fatigue damage as $1/N$, this equation can be rewritten as follows:

$$p/c_{D_i} = \frac{1/N_{D_{ii}}}{\sum_j P(COV_{D_j}) * 1/N_{D_{ij}}} \quad (25)$$

where

- $N_{D_{ii}}$ = Allowable number of load applications based on stress at location D_i due to the load placed at D_i .
- $N_{D_{ij}}$ = Allowable number of load application based on stress at location D_i due to the load at D_j .

Equation 25 reduces to the following:

$$p/c_{Di} = \frac{1}{\sum_j P(\text{COV}_{Dj}) * \frac{N_{Dii}}{N_{Dij}}} \quad (26)$$

The p/c as defined in equation 26 involves a considerable amount of analysis; however, because it is a measure of relative damage caused by the loads placed at various locations, it is not very sensitive to the pavement structure. Therefore, p/c determined for the average case may be used. The p/c is, however, affected by several factors, including the following:

- Mean wheel location and standard deviation of traffic wander.
- Stress level.
- Temperature gradient.

The mean wheel location and standard deviation of traffic are somewhat variable, and both of these factors have a significant effect on p/c. In this study the following figures reported by Benekohol et al. (1990) were used:

- Average wheel location:
 - 22 in from pavement edge for standard-width section.
 - 20 in from paint stripe for widened-slab sections.
- Standard deviation = 8.4 in.

These results are based on 1,300 observations.

Both stress level and temperature gradient have significant effect on p/c for standard-width lanes. The stress level affects p/c because at higher stress ratios the stress due to traffic passes farther away from the edge become more significant. Temperature gradients influence the p/c by altering the stress distribution across the slab. When the temperature gradient is zero, the edge stress drops rapidly as the load is moved away from the pavement edge; however, when the slab is under high positive temperature gradient, a significant portion of the combined stress (as much as 50 percent or more) is due to curling stress, and the curling stress is slightly higher at the slab center than at the slab edge. The effects of temperature gradient and stress ratio on p/c are shown in figure 40.

As shown in this figure, at high stress ratios the p/c under high temperature gradients is significantly lower (fewer traffic passes required to cause one critical loading cycle) than at zero temperature gradient. The p/c versus SR relationship can be easily approximated by a regression equation; however, the dependence of this relationship on temperature gradients makes it difficult to model this relationship. To simplify the calculation process, a combined p/c versus SR relationship was developed that could be accurately represented by a regression equation:

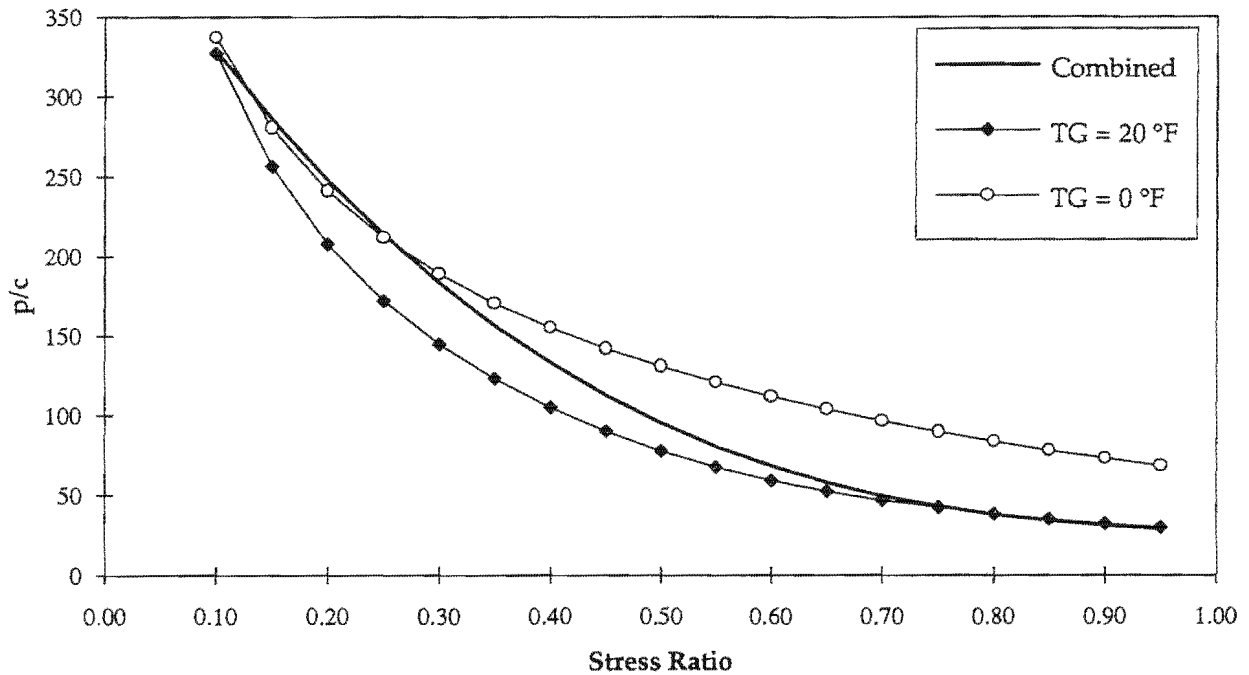


Figure 40. Effects of temperature gradient and SR on p/c.

- The high stress ratios in the pavement slabs are likely to occur only under high temperature gradients. Therefore, the p/c versus SR relationship should follow the curve for the highest temperature gradient at the high SRs.
- The SR due to load stress typically ranges from 0.3 to 0.5 on highway slabs. Therefore, at the lower SRs, the combined curve should follow the curve for the zero temperature gradient.
- The curling stresses due to negative temperature gradients actually reduce edge stresses, but the FD contribution at such low SR is practically zero (actually, only the traffic passes at the highest 5 or 6 positive temperature gradients are significant for the FD at the pavement edge). Hence, any error in p/c at low SRs (say, SR less than 0.4) is not significant.

The regression equation for the combined p/c versus SR curve shown in figure 40 is given below:

$$\begin{aligned}
 p/c &= 427.5 - 1086SR + 1001SR^2 - 315.1SR^3 && \text{for } SR < 1 \\
 p/c &= 84.86 - 92.42SR + 41.04SR^2 - 6.335SR^3 && \text{for } SR \geq 1
 \end{aligned}
 \tag{27}$$

$$R^2 = 1.00$$

where

SR = Ratio of stress to PCC modulus of rupture, σ/MR .

The effects of SR on p/c for widened-slab sections is shown in figure 41. As shown in this figure, the p/c for widened-slab sections is relatively insensitive to SR, especially in the range of SR that is normally significant for fatigue considerations (0.2 to 0.5). This is because the stress distribution across the slab at interior locations is fairly flat; that is, as the load is moved away from the critical location, the stress at the critical location does not rapidly drop off. In this study, the constant value of 2.6 was taken as the p/c for widened-slab sections.

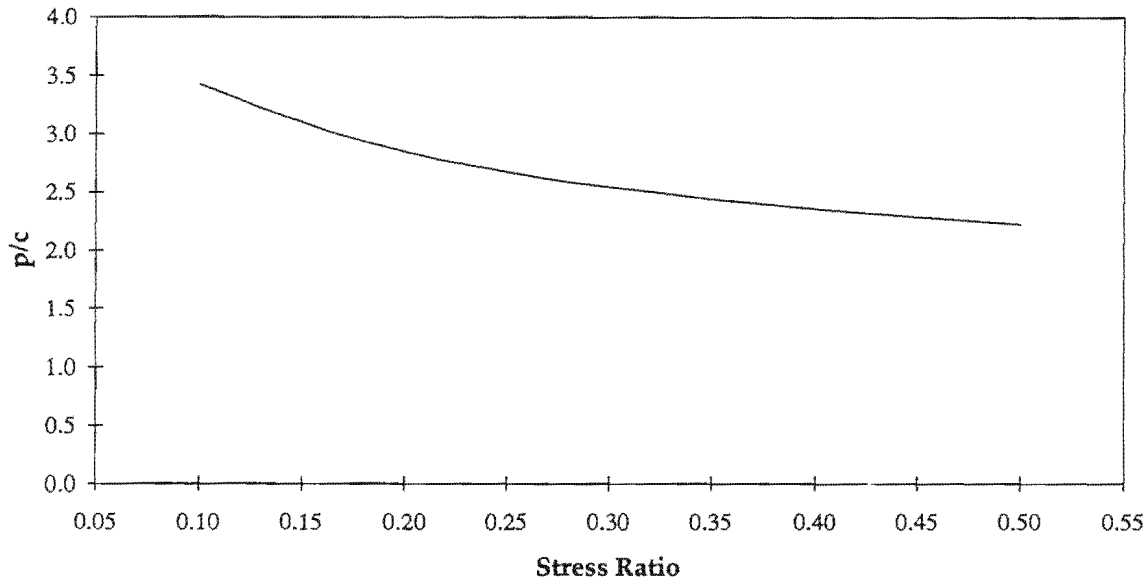


Figure 41. The effects of SR on p/c of widened-lane sections.

The FD calculation was performed on a spreadsheet using the equations and data presented in this section. An example calculation is shown in table 11. The FD caused at each temperature gradient is illustrated in figure 42. The traffic distribution is shown as white bars, and the FD distribution is shown as shaded bars. The cumulative FD is shown by the line. As shown in this figure, most of the damage is done by the small fraction of traffic passes that occurred during the highest 7 temperature gradients.

Fatigue Damage Distribution Across the Slab

The FD/Pass calculated using equation 23 can be used to determine the relative FD distribution across the slab and identify the location of critical damage. The FD distribution across the slab for standard-width and widened-slab sections are illustrated in figures 43 and 44. On standard-width lanes, the maximum FD does occur at the pavement edge, and the accumulated FD drops off rapidly as you move inward. On widened-slab sections, if the traffic never wanders out to the pavement edge as discussed in the reference by Benekohol et al. (1990), the maximum FD occurs directly under one of the traffic wheels at the mean wheel location, and the accumulated FD has a flatter distribution.

Table 11. Example fatigue damage calculation.

Ec, Mpsi = 3.2 Total Traffic = 15 MESAL D = 38
 MR, psi = 650 Wheel Load = 9,000 lbs F Damage = 0.289 D/l = 1.068
 Stress LTE = 0.2 Tire Pressure = 95 psi Cracking = 3.5% a/l = 0.193

h	Slab L, ft	Ec MPsi	k	Temp Diff	Freq	Traffic ESAL	Load Stress	Temp Stress	Stress L+T	FD ERES	P	p	a _{eq}	SR	l	C	R	L/l	.01 L/l	DT	Lam	p/c
10.0	15	3.20	170	-28.0	0.000	0	177.7	-179.3	69.8	0.000	9,000	95	6.87	0.11	35.6	0.73	0.602	5.1	0.051	-15.400	1.788	262.5
10.0	15	3.20	170	-26.0	0.000	0	177.7	-166.5	67.7	0.000	9,000	95	6.87	0.10	35.6	0.73	0.661	5.1	0.051	-14.300	1.788	263.3
10.0	15	3.20	170	-24.0	0.000	0	177.7	-153.7	68.0	0.000	9,000	95	6.87	0.10	35.6	0.73	0.714	5.1	0.051	-13.200	1.788	263.2
10.0	15	3.20	170	-22.0	0.000	0	177.7	-140.9	70.4	0.000	9,000	95	6.87	0.11	35.6	0.73	0.761	5.1	0.051	-12.100	1.788	262.2
10.0	15	3.20	170	-20.0	0.001	55	177.7	-128.1	74.7	0.000	9,000	95	6.87	0.11	35.6	0.73	0.804	5.1	0.051	-11.000	1.788	260.4
10.0	15	3.20	170	-18.0	0.041	2,372	177.7	-115.3	80.7	0.000	9,000	95	6.87	0.12	35.6	0.73	0.841	5.1	0.051	-9.900	1.788	257.7
10.0	15	3.20	170	-16.0	0.071	4,216	177.7	-102.4	88.1	0.000	9,000	95	6.87	0.14	35.6	0.73	0.874	5.1	0.051	-8.800	1.788	254.1
10.0	15	3.20	170	-14.0	0.072	4,353	177.7	-89.6	96.7	0.000	9,000	95	6.87	0.15	35.6	0.73	0.903	5.1	0.051	-7.700	1.788	249.5
10.0	15	3.20	170	-12.0	0.082	5,014	177.7	-76.8	106.4	0.000	9,000	95	6.87	0.16	35.6	0.73	0.928	5.1	0.051	-6.600	1.788	244.0
10.0	15	3.20	170	-10.0	0.073	4,600	177.7	-64.0	117.0	0.000	9,000	95	6.87	0.18	35.6	0.73	0.948	5.1	0.051	-5.500	1.788	237.5
10.0	15	3.20	170	-8.0	0.062	4,020	177.7	-51.2	128.2	0.000	9,000	95	6.87	0.20	35.6	0.73	0.965	5.1	0.051	-4.400	1.788	230.2
10.0	15	3.20	170	-6.0	0.067	4,531	177.7	-38.4	140.1	0.000	9,000	95	6.87	0.22	35.6	0.73	0.979	5.1	0.051	-3.300	1.788	222.1
10.0	15	3.20	170	-4.0	0.070	4,899	177.7	-25.6	152.3	0.000	9,000	95	6.87	0.23	35.6	0.73	0.990	5.1	0.051	-2.200	1.788	213.4
10.0	15	3.20	170	-2.0	0.049	3,582	177.7	-12.8	164.9	0.000	9,000	95	6.87	0.25	35.6	0.73	0.999	5.1	0.051	-1.100	1.788	204.1
10.0	15	3.20	170	0.0	0.034	2,657	177.7	0.0	177.7	0.000	9,000	95	6.87	0.27	35.6	0.73	1.004	5.1	0.051	0.000	1.788	194.5
10.0	15	3.20	170	2.0	0.028	2,235	177.7	12.8	190.6	0.000	9,000	95	6.87	0.29	35.6	0.73	1.008	5.1	0.051	1.100	1.788	184.6
10.0	15	3.20	170	4.0	0.024	2,096	177.7	25.6	203.5	0.000	9,000	95	6.87	0.31	35.6	0.73	1.010	5.1	0.051	2.200	1.788	174.6
10.0	15	3.20	170	6.0	0.019	1,736	177.7	38.4	216.5	0.000	9,000	95	6.87	0.33	35.6	0.73	1.010	5.1	0.051	3.300	1.788	164.6
10.0	15	3.20	170	8.0	0.027	2,661	177.7	51.2	229.4	0.000	9,000	95	6.87	0.35	35.6	0.73	1.009	5.1	0.051	4.400	1.788	154.7
10.0	15	3.20	170	10.0	0.029	2,984	177.7	64.0	242.1	0.000	9,000	95	6.87	0.37	35.6	0.73	1.007	5.1	0.051	5.500	1.788	145.0
10.0	15	3.20	170	12.0	0.027	2,970	177.7	76.8	254.8	0.001	9,000	95	6.87	0.39	35.6	0.73	1.004	5.1	0.051	6.600	1.788	135.6
10.0	15	3.20	170	14.0	0.037	4,381	177.7	89.6	267.3	0.003	9,000	95	6.87	0.41	35.6	0.73	1.000	5.1	0.051	7.700	1.788	126.5
10.0	15	3.20	170	16.0	0.033	4,255	177.7	102.4	279.7	0.006	9,000	95	6.87	0.43	35.6	0.73	0.996	5.1	0.051	8.800	1.788	117.8
10.0	15	3.20	170	18.0	0.033	4,526	177.7	115.3	292.1	0.012	9,000	95	6.87	0.45	35.6	0.73	0.993	5.1	0.051	9.900	1.788	109.4
10.0	15	3.20	170	20.0	0.035	5,225	177.7	128.1	304.3	0.027	9,000	95	6.87	0.47	35.6	0.73	0.989	5.1	0.051	11.000	1.788	101.3
10.0	15	3.20	170	22.0	0.031	4,948	177.7	140.9	316.6	0.044	9,000	95	6.87	0.49	35.6	0.73	0.986	5.1	0.051	12.100	1.788	93.7
10.0	15	3.20	170	24.0	0.033	5,671	177.7	153.7	328.9	0.085	9,000	95	6.87	0.51	35.6	0.73	0.984	5.1	0.051	13.200	1.788	86.4
10.0	15	3.20	170	26.0	0.019	3,610	177.7	166.5	341.4	0.088	9,000	95	6.87	0.53	35.6	0.73	0.983	5.1	0.051	14.300	1.788	79.4
10.0	15	3.20	170	28.0	0.003	588	177.7	179.3	354.1	0.023	9,000	95	6.87	0.54	35.6	0.73	0.984	5.1	0.051	15.400	1.788	72.7
10.0	15	3.20	170	30.0	0.000	0	177.7	192.1	367.1	0.000	9,000	95	6.87	0.56	35.6	0.73	0.986	5.1	0.051	16.500	1.788	66.4
10.0	15	3.20	170	32.0	0.000	0	177.7	204.9	380.6	0.000	9,000	95	6.87	0.59	35.6	0.73	0.991	5.1	0.051	17.600	1.788	60.3
10.0	15	3.20	170	34.0	0.000	0	177.7	217.7	394.7	0.000	9,000	95	6.87	0.61	35.6	0.73	0.997	5.1	0.051	18.700	1.788	54.6
SUM					1.000	8.82E+04	Total Fatigue Damage			0.289												
										Te		17.29										

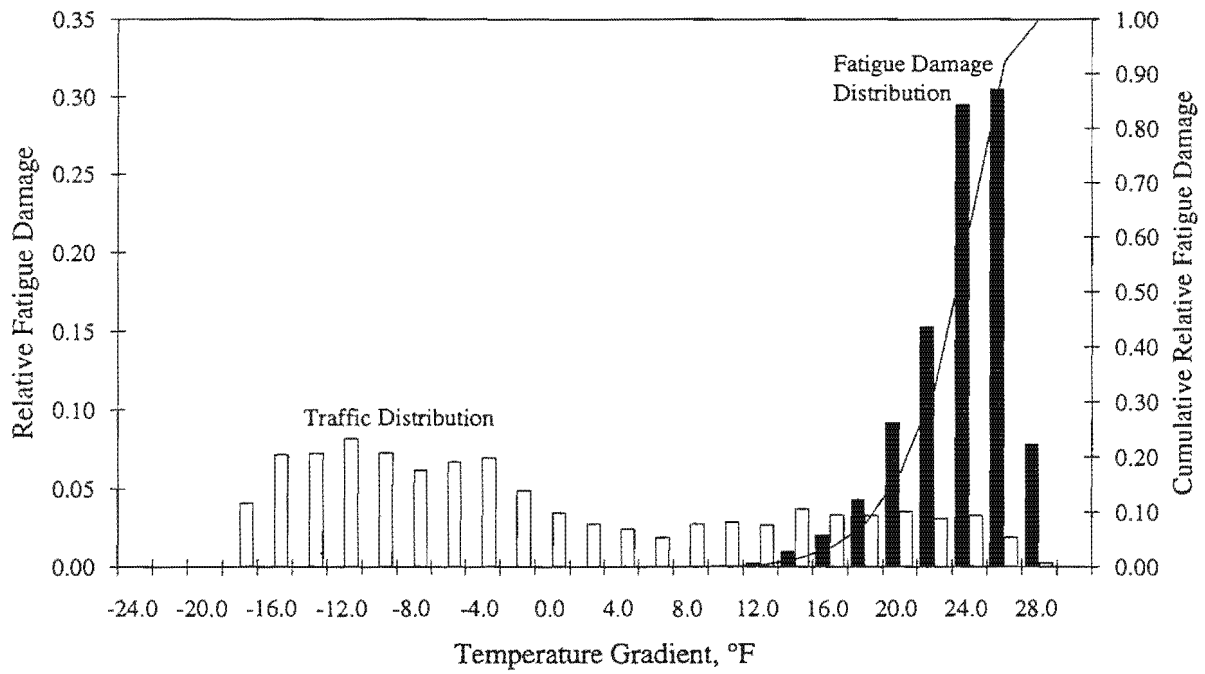


Figure 42. Fatigue damage distribution with respect to temperature gradient.

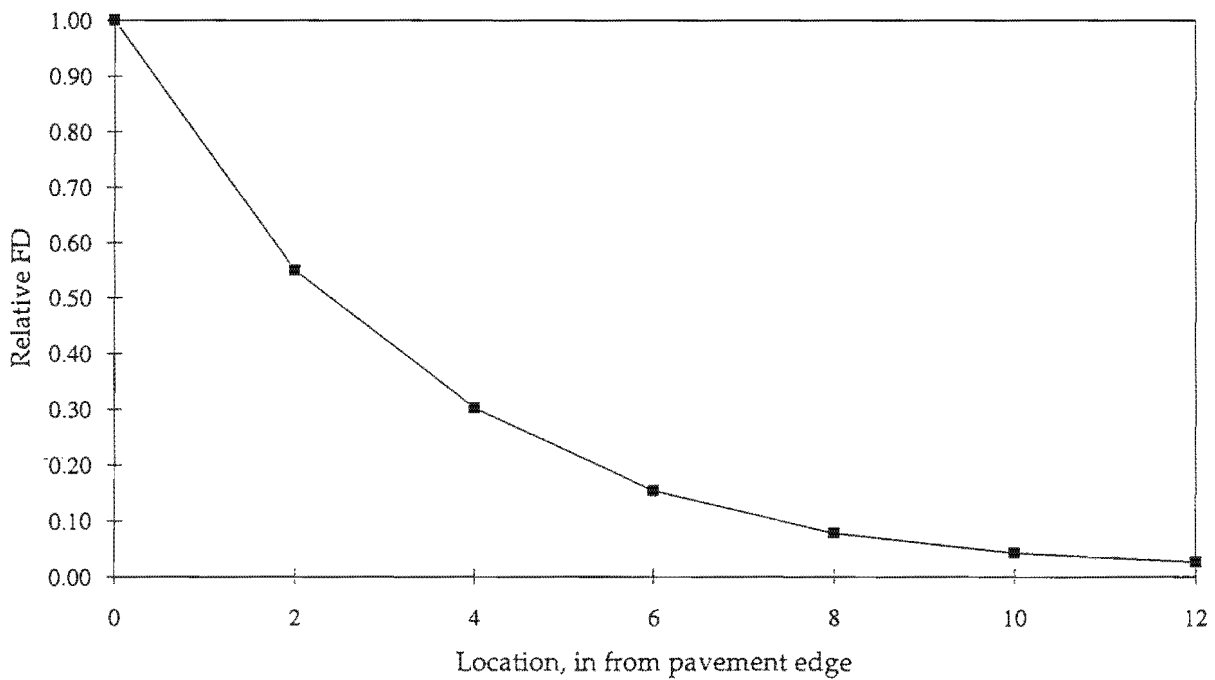


Figure 43. Typical distribution of fatigue damage across a standard-width slab.

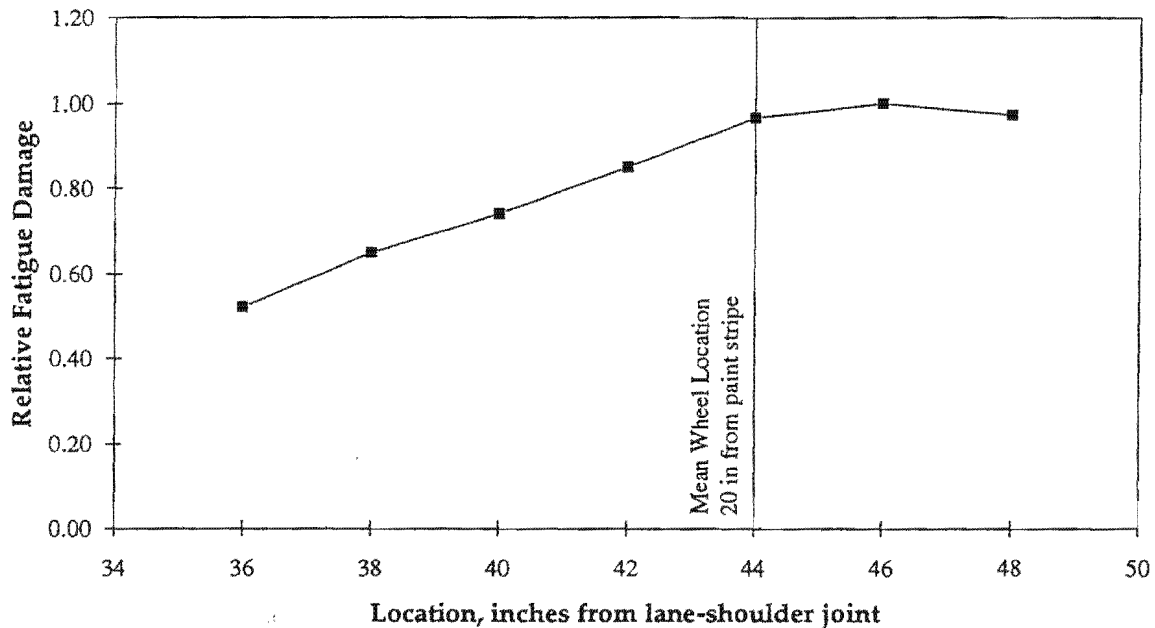


Figure 44. Typical distribution of fatigue damage across a widened-lane slab.

Effects of Built-in Upward Curling on Performance

The presence of significant built-in upward curling in the test sections was discussed in the first part of this report, where the analysis of the data from the instrumented slabs is described. The magnitude of the effective residual temperature gradient was estimated to be up to -20°F . The residual negative temperature gradients have the effect of shifting the entire temperature gradient distribution in the negative direction. This, in turn, simultaneously reduces the edge load stress and increases the corner load stress. The corner load stresses lead to fatigue cracking that initiates at the slab surface.

The effects of the temperature shifts on the critical stresses in the slab are illustrated in figure 45. Because negative temperature gradients occur much more frequently than positive temperature gradients, the corner load stress does not have to be greater than the edge stress for the top-down cracking to become critical. The corner load stress could be even higher in widened-slab sections if the loads were placed directly at the slab corner, because both the slab length and width affect the curling stresses at the slab corners. However, according to Benekohol et al. (1990) the traffic on widened-slab sections do not wander out to the pavement edge. Hence, the corner load stress for the widened lane was determined for a load placed 10 in from the pavement edge, based on field observations by Benekohol et al (1990). The edge stress for the widened slab shown in figure 45 is the maximum stress under the wheelpath.

Figure 45 shows that on widened-slab sections, if the effective residual temperature gradient is about -8°F or lower, the corner-load stress is more critical. The corner stresses become more critical if the effective residual temperature gradient is about -13°F or lower on standard-width lanes. Although the presence of the built-in curling may change the mode of failure, the amount of cracking resulting from top-down cracking is

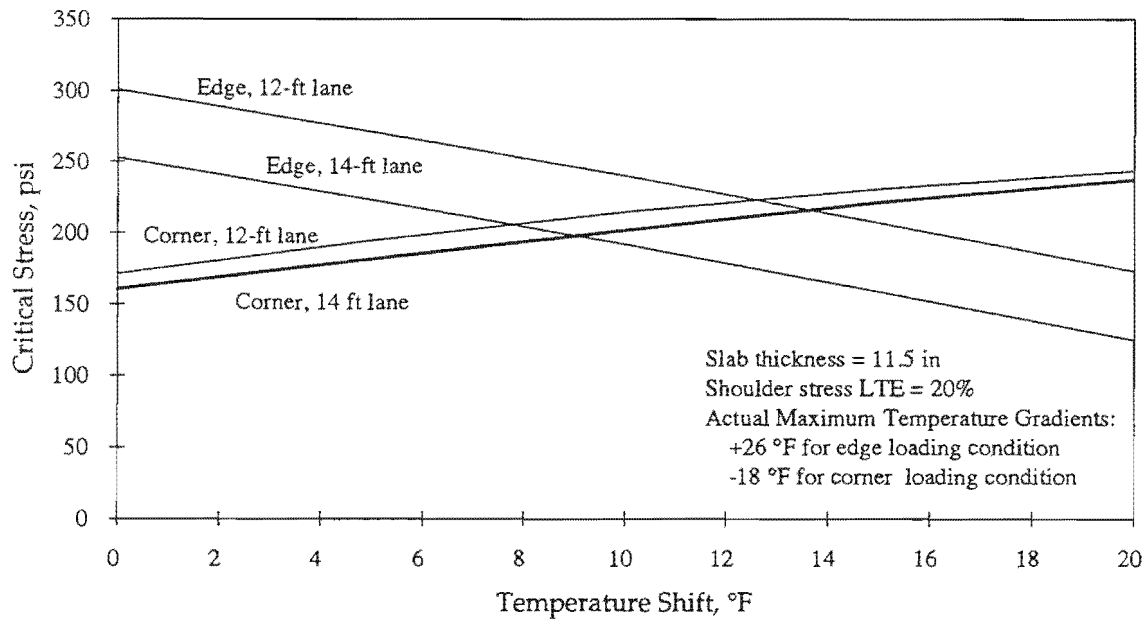


Figure 45. The effects of residual temperature gradients on critical stresses in PCC slabs.

not likely to exceed the level of cracking that would be predicted for bottom-up cracking (ignoring residual temperature gradients). In the particular cases being analyzed, the magnitude of stresses under corner loading, even if a large residual temperature gradient may be assumed, is less than the stresses under edge loading with no residual temperature gradients. This may not be the case if shorter slabs were involved, since edge-load stresses are far more sensitive to slab length than corner stresses.

Expected Performance

The expected fatigue performance was determined using the following slab cracking model, developed at ERES (Smith et al. 1995b):

$$\text{Percent Cracking} = \frac{100}{1 + 4.15FD^{-1.52}} \quad (28)$$

$$\begin{aligned} R^2 &= 0.91 \\ \text{SEE} &= 7.1 \\ n &= 465 \end{aligned}$$

where

$$FD = \text{Accumulated fatigue damage } (\sum n/N).$$

This model was developed based on the performance of 465 in-service PCC pavement sections. Figure 46 shows a plot of this model, along with the data points that the model is based on.

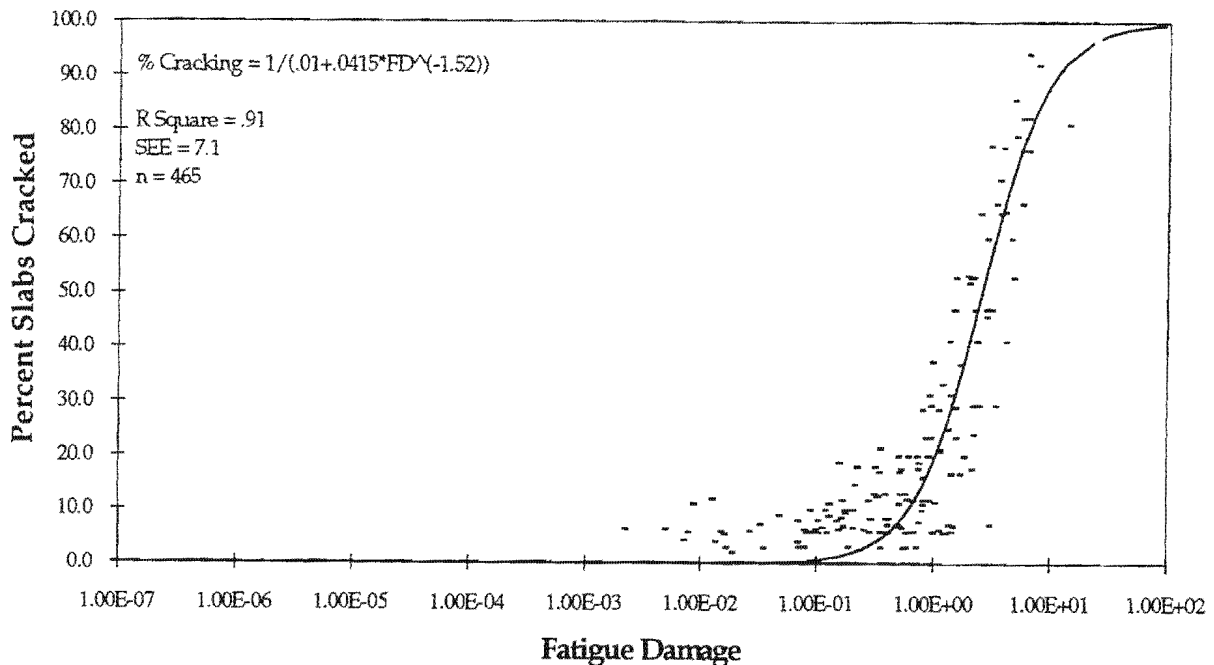


Figure 46. The fatigue cracking model.

Several sensitivity plots were developed to evaluate the expected performance of the test sections. These plots show the expected level of cracking as a function of traffic. The factors evaluated include the following:

- Slab thickness.
- Shoulder type.
- Widened slab.
- Shoulder LTE.
- PCC modulus of rupture.

In this section, no distinctions are made between the two widened slab sections because the type of shoulder does not significantly affect fatigue performance of widened slab sections.

The effects of slab thickness on performance are shown in figures 47 and 48 for tied PCC shoulder and widened-slab sections, respectively. As shown in these figures, the expected fatigue life of either of the two designs (tied PCC shoulder, and widened slab with any type of shoulder) is well beyond the 15.4 million ESALs expected on the test pavement. Virtually no fatigue cracking is expected on these sections up to 100 million ESALs.

The expected performance of a similar pavement section constructed with standard-width slabs and AC shoulders is shown in figure 49. The performance trends shown in

figures 47, 48, and 49 follow the characteristic S-shape of the slab cracking versus FD shown in figure 46. An important feature of this S-shaped characteristic curve is that the amount of slab cracking remains nearly zero for a long period; however, once the FD reaches a certain point, rapid deterioration to failure takes place.

This trend is reflected in the sensitivity plots. For example, the curve for the 9-in slab in figure 49 shows over a 60 percent increase in the amount of slab cracking as the traffic is increased from 1 million to 10 million ESALs. Over the same interval, the change in the amount of slab cracking for the 10-in slab is only about 12 percent and the amount of slab cracking remains close to zero for the 11-in slab.

A comparison of the performance given by different slab designs for 10-in slabs is shown in figure 50. This figure shows that the addition of a tied PCC shoulder (on standard-width slabs) or widened slab can lead to significant improvement in performance. A comparison of figures 47, 48, and 49 shows that the structural benefit offered by either a tied concrete shoulder or widened slab (with any type of shoulder) is roughly equivalent to 1 inch of additional slab thickness.

Figure 50 also shows that tied concrete shoulders and widened slabs may be expected to provide similar performance; however, a widened slab is likely to provide more reliable performance because the performance of a tied concrete shoulder section depends on the LTE across the lane-shoulder joint. It is not uncommon for the LTE at any joint to deteriorate over time. The effect of LTE on performance is shown in figure 51. If the LTE drops significantly over the course of the pavement life, a substantially higher than expected amount of cracking can result.

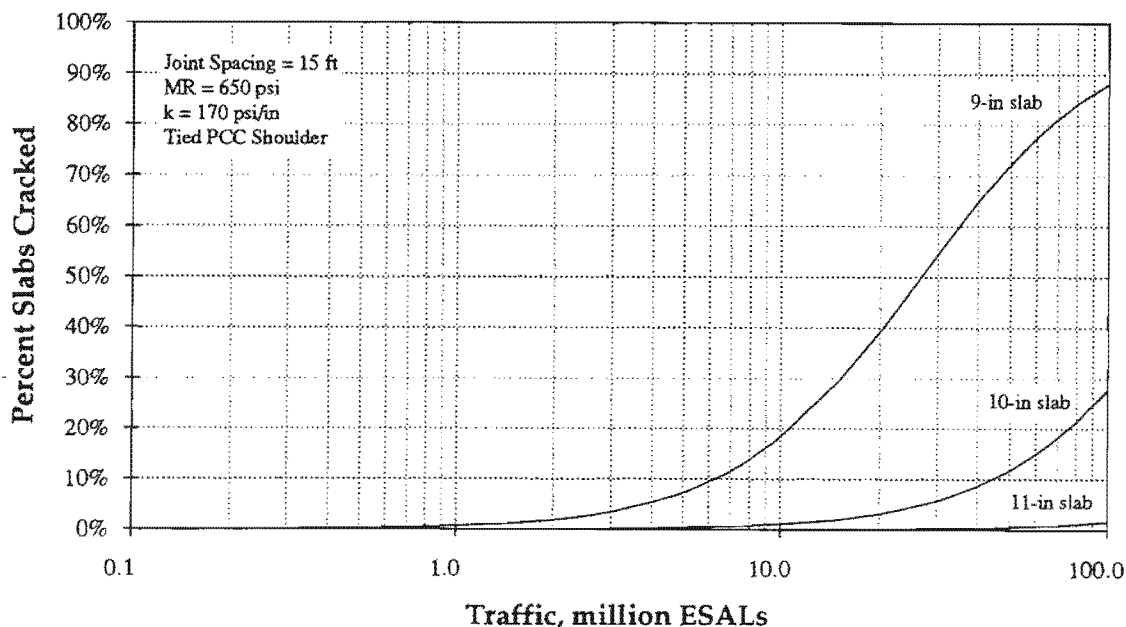


Figure 47. The effects of slab thickness on fatigue cracking in tied concrete shoulder sections.

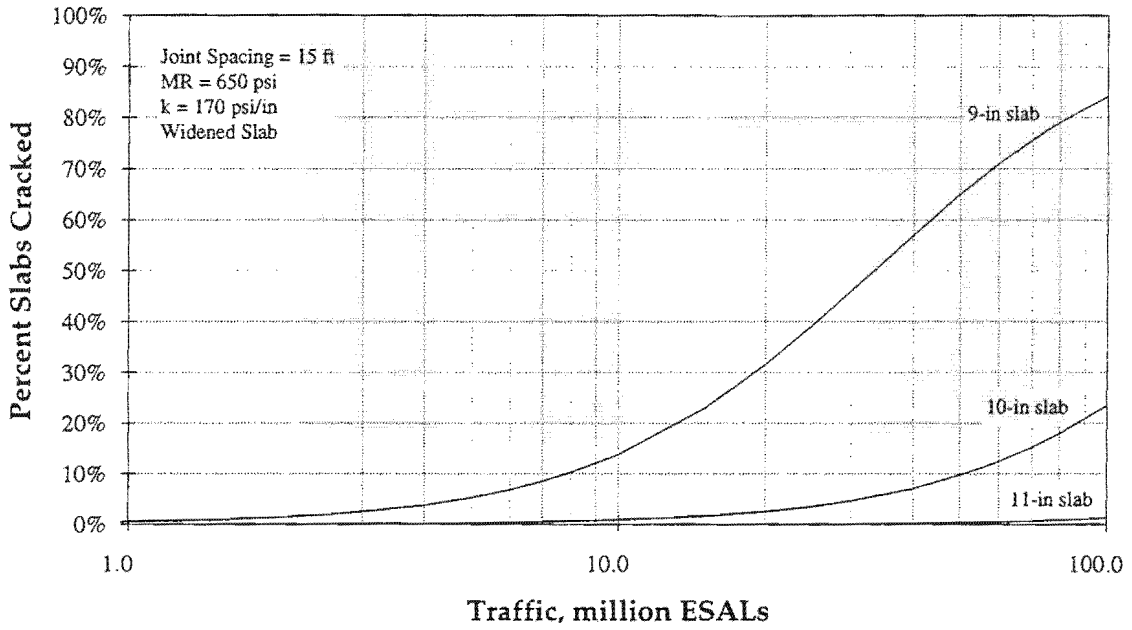


Figure 48. The effects of slab thickness on fatigue cracking in widened-lane sections.

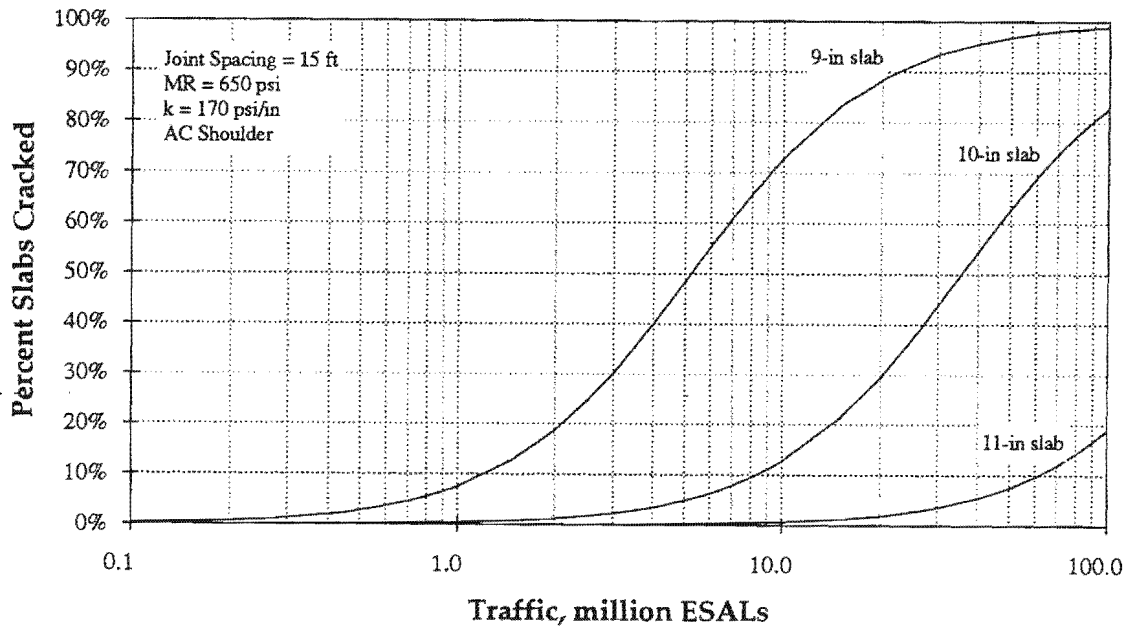


Figure 49. The effects of slab thickness on fatigue cracking in AC shoulder sections.

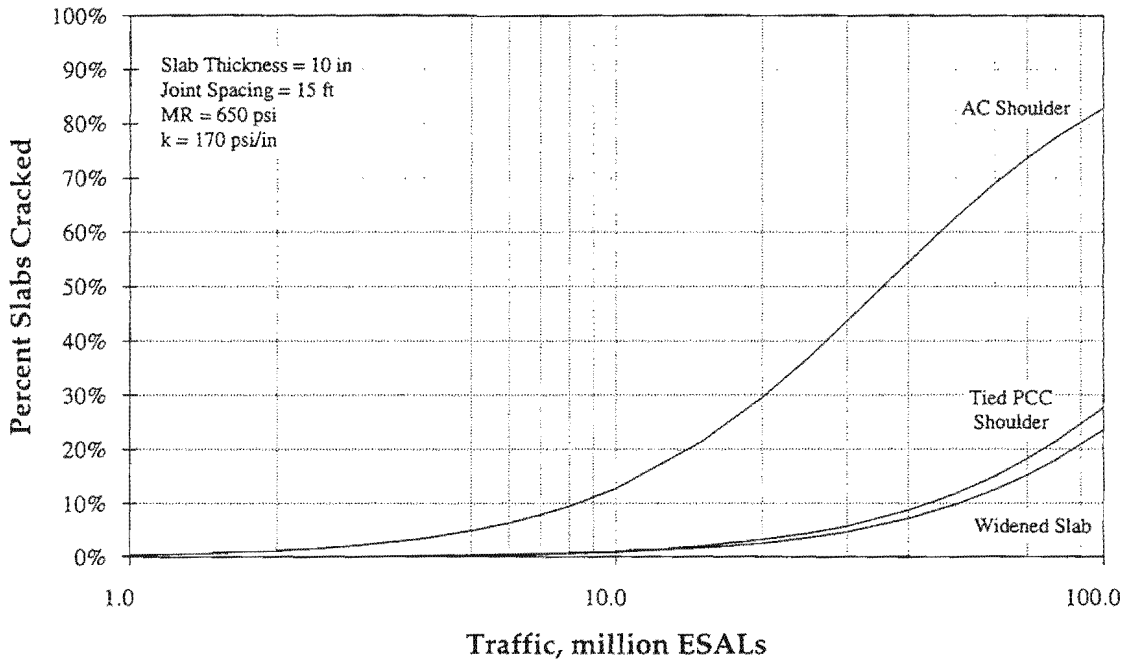


Figure 50. The effects of different PCC pavement design features on fatigue cracking.

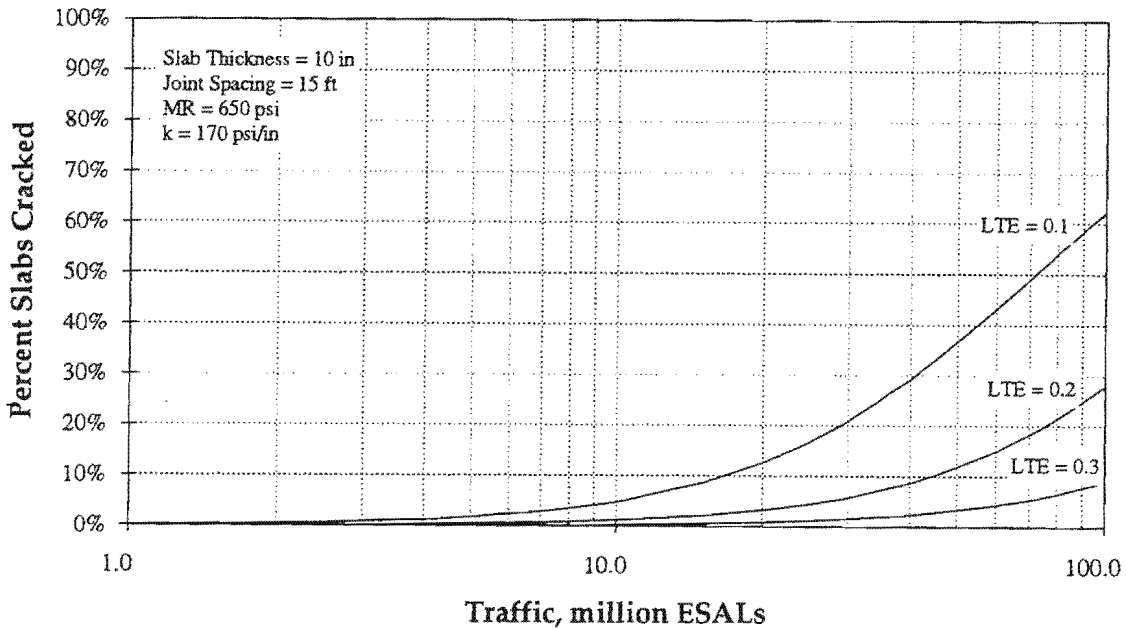


Figure 51. The effects of shoulder load transfer efficiency on fatigue cracking.

The last sensitivity plot (figure 52) shows the effects of PCC modulus of elasticity on performance. This figure shows the possibility of the stresses in PCC slabs increasing over time as the PCC modulus of elasticity increase with age, resulting in greater amount of cracking. However, the increase in PCC modulus is likely to be accompanied by increase in strength, which has a much more significant effect on FD. Therefore, PCC slabs are not likely to become more susceptible to cracking as a result of PCC becoming stiffer with age.

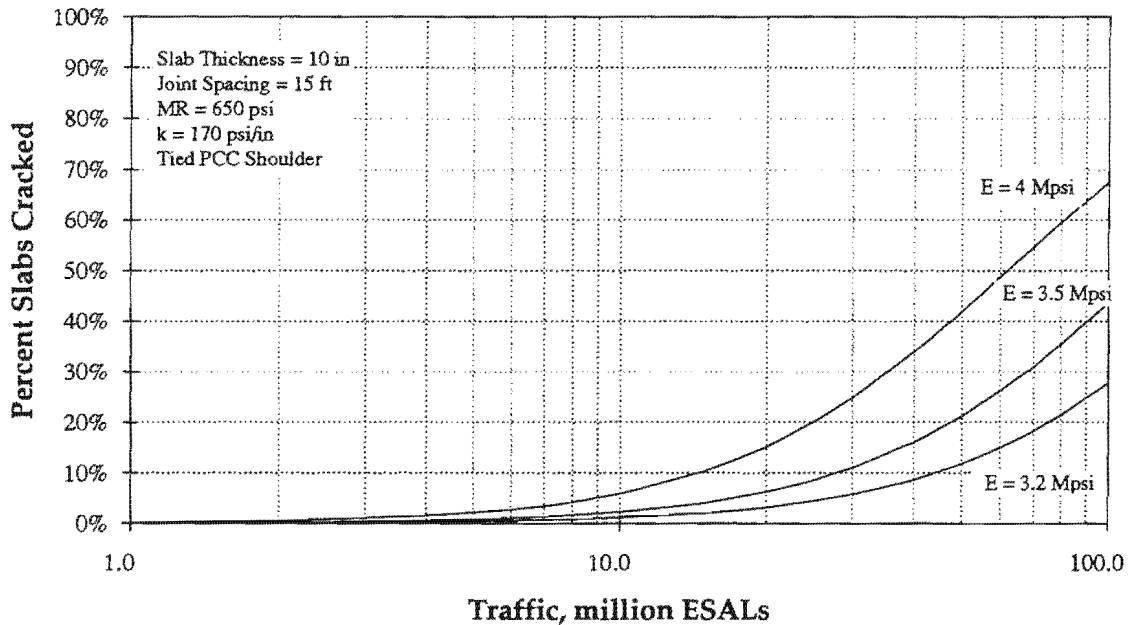


Figure 52. The effects of PCC modulus of elasticity on fatigue cracking.

Long-Term Monitoring

Continued monitoring of the test sections is recommended to evaluate the long-term performance of each design. Because the test sections are expected to provide excellent performance, a 2- to 3-year interval between field surveys may be adequate. If any unusual distresses were observed during the routine surveys, more frequent surveys (e.g., annual) may be appropriate. The routine surveys should consist of the following:

- Visual distress survey:
 - Record all visible distresses.
 - Measure faulting at transverse joints.
 - Photograph representative distresses and any unusual distresses or conditions.
- FWD testing:
 - Load transfer efficiency testing across lane-shoulder joints.
 - Load transfer efficiency testing across transverse joints.
 - Basin testing for deflection monitoring and backcalculation.

The FWD testing is an important aspect of the long-term monitoring program to identify any changes in the shoulder LTE and the structural response of the PCC slab-AC base system.

SUMMARY

The objectives of this study were twofold:

- Instrument and test in-place PCC slabs to characterize the structural response of these slabs and to verify that the deflections and stresses in PCC pavements can be adequately determined by analytical means.
- Evaluate the effects of widened slab and tied concrete shoulders on performance of JCP. The effects that widened slab and tied concrete shoulders have on the critical stresses and deflections in PCC slabs were examined to determine how the pavement performance is affected by these design features.

Field Testing and Data Analysis

The field work for this study was performed in two parts:

- The first part in July 1994 to instrument and test pavement slabs to obtain curling and load response data.
- The second part in May 1995 to obtain deflection data for the use in the development of performance predictions.

A thorough analysis was performed on the collected data. The results of the analysis of the data collected from the instrumented slabs showed the following:

- The measured curling is consistent with the calculated values, if the slabs are assumed curled up in their relaxed state. Such a phenomenon is not uncommon, and may be the result of the temperature conditions at placement, or presence of moisture gradients, or both. The amount of equivalent temperature gradient needed to produce the initial curling necessary to match the field data was about -20 °F.
- A PCC pavement constructed on a stiff base can present itself as a different structure to different loading conditions. The slab may separate from the base when curling upward, but the slab and the base can act together as if they are bonded when acted upon by a heavy wheel load. The latter condition results in significantly reduced stresses in the PCC slabs, with corresponding substantial increase in fatigue life.
- Load strains at all locations can be adequately determined by analytical means.

An examination of the measured pavement responses raised several apparent anomalies. For example, the measured deflections were substantially higher than the calculated values (about 40 percent higher), but the measured strains were only about 50 percent of the calculated values. If the 7-in AC base is assumed to be fully bonded to the PCC surface, the calculated strain values are in line with the measured values; however,

in that case the calculated deflections would be lower, which would lead to an even greater discrepancy between the calculated and measured deflections.

The only way to explain the seemingly conflicting measured responses appears to be that under certain loading conditions the PCC slab can separate from the stabilized base, but under other loading conditions the pavement system behaves as if the base is bonded to the slab. The high curling deflections measured at the slab corners and at the longitudinal edge are possible only if the slab is free to lift off of the base and if the slab is initially curled up (i.e., the slab is curled up at zero temperature gradient). The most reasonable explanation for the low measured strains is the bonded response of the PCC slab and the AC base.

The finding that the PCC pavement is curled up at zero temperature gradient, translating to having a significant amount of built-in negative temperature gradient, has a great impact on estimated fatigue life of the test sections. Curling caused by high positive temperature gradients can easily double the critical edge stresses in most highway pavements. If this positive temperature gradient is largely offset by the built-in negative temperature gradient, the curling stress would become insignificant, resulting in a substantial increase in estimated fatigue life.

The analysis of the instrumented slabs showed that the edge stresses in the test sections are very low because of the structural contribution of the 7-in AC base. The stresses are so low that fatigue of concrete is highly unlikely to control the service life of the test sections. The composite action of the base and the slab has an even greater effect on the reduction of the edge stresses than either the tied concrete shoulder or the widened slab on the structures evaluated; however, the AC base may not reliably provide the structural benefit at all locations in the project, and the base may not provide the same support level over the life of the pavement.

Expected Performance

The second part of this study focused on fatigue analysis to determine the structural benefits of tied concrete shoulders and widened slab. A thorough analysis was conducted to provide an accurate account of the effects of temperature gradients and lateral traffic wander on fatigue damage at the critical locations. Sensitivity plots were then developed to evaluate the effects of various design features on concrete pavement performance. Conclusions from this analysis include the following:

- Tied concrete shoulders and widened slab can significantly improve fatigue life of concrete pavements.
- The structural benefits of tied concrete shoulder and widened-slab were found to be similar, but for the tied PCC shoulder to provide significant structural benefit, high LTE across the lane-shoulder joint must be achieved (deflection LTE greater than 80 percent). The required level of LTE across the lane-shoulder joint may be achieved by providing adequate-sized tiebars at close intervals (e.g., #5 bars at 30-in spacing).

- In the cases evaluated, the effective structural contribution of tied PCC shoulders and widened slabs were equivalent to about 1 inch of slab thickness.

The sensitivity plots showed that the test sections on I-70 are not expected to develop any fatigue cracking over their life. These estimates are based on very conservative assumptions, and the structural contribution of the 7-in AC layer beneath the slabs was ignored in these predictions. The doweled joints provided at 15-ft intervals and sealed with silicone should also provide excellent joint performance (e.g. no pumping, faulting, or spalling). If durability or any other material problems do not develop, the pavement should provide excellent performance well beyond its design life.

Recommendations

Tied PCC shoulders and widened slabs can be used to significantly improve the performance of PCC pavements. The performance of standard-width, tied PCC sections are sensitive to the LTE across the lane-shoulder joint. Because the LTE across the lane-shoulder joint can deteriorate with age, widened slab sections are expected to provide more reliable performance. The performance of in-service JCPs with tied PCC shoulders is mixed because of the sensitivity of the design to the LTE across the lane-shoulder joint. This should not imply that tied PCC shoulder is not a good design; it simply means that if tied PCC shoulders are to be used, adequate measures must be taken to ensure that high levels of LTE across the lane-shoulder joint will be maintained.

Where the use of tied PCC shoulders is being considered, widened slabs may be provided at no additional cost to obtain more reliable performance. This can be achieved by simply moving the lane-shoulder joint 2 ft further out toward the shoulder than the standard. The width of widening of 2 ft is recommended for several reasons:

- The widening of pavement slabs by less than 2 ft does not offer the level of stress reduction possible to obtain significantly improved performance. An important factor for consideration on widened slab sections is keeping the traffic from wandering out to the pavement edge. If sufficiently wide slabs are not provided, it may not be possible to keep all traffic off of the slab edge.
- The 2 ft widening is adequate to obtain most of the benefits of using widened slabs, especially when tied PCC shoulders are used in conjunction with the widened slabs. Even on AC shoulder sections, the widening of the mainline slabs beyond 2 ft (14-ft slabs) does not provide significant further reduction of the critical stresses.
- Excessive curling stress can develop in the transverse direction if much wider slabs are used. The excessive curling stresses in the transverse direction can lead to longitudinal cracking.

On both tied PCC shoulder and widened slab sections, proper and timely sawing of the lane-shoulder joint is extremely important to prevent longitudinal cracking. This joint may have to be sawed to a greater depth to ensure that the joint does form at the proper location, because the curling stresses that cause the cracking at the saw cuts (thus

forming the contraction joint) are significantly lower in the transverse direction. The curling stress responsible for the formation of longitudinal joints in PCC pavements is the greatest at the midpoint between the two free edges (near the centerline joint) and decreases to zero at the free edge (outer edge of the shoulder). Thus, the stresses needed to cause the controlled cracking is much less at the lane-shoulder joint than at any other joints. When the lane-shoulder joint is moved even further out toward the free edge, the joint-forming stresses are even lower. Therefore, proper sawing of this joint is even more critical when both widened slab and tied PCC shoulders are provided.

The potential problem with longitudinal cracking along the lane-shoulder joint on widened slab sections may be avoided by providing AC shoulders on widened slab sections. However, when both widened slabs and tied PCC shoulders are used, the LTE at the lane-shoulder joint is of little importance; therefore, this joint may be sawed very deep without the concern for any performance penalties. If PCC shoulders are used on PCC pavements, the shoulder should be tied to the mainline pavement to prevent lane-shoulder separation that can lead to other problems (e.g., moisture-related problems).

Other factors for consideration when selecting the shoulder type and slab width include the following:

- Construction:
 - Widened slabs are easier to construct than tied PCC shoulders.
 - Tied PCC shoulders require the construction and maintenance of another joint.

- Location:
 - In rural areas, widened slabs would provide the desired performance without the requirement of maintaining another pavement joint.
 - In urban areas, tied shoulders may be advantageous to accommodate disabled vehicles and lane closures. Widened slabs may also be provided in addition to the tied shoulder at no additional cost in such cases.

REFERENCES

- Benekohal, R.F., K.T. Hall, and H.W. Miller, "Effects of Lane Widening on Lateral Distribution of Truck Wheels," *Transportation Research Record 1286*, Transportation Research Board, Washington, DC, 1990.
- Bradbury, R.D., *Reinforced Concrete Pavements*, Wire Reinforcement Institute, 1938.
- Darter, M.I., *A Comparison Between Corps of Engineers and ERES Consultants, Inc. Rigid Pavement Design Procedures*, Technical Report Prepared for the United States Air Force SAC, Urbana, IL, 1988.
- Dempsey, B.J., W.A. Herlache, and A.J. Patel, *The Climatic-Materials-Structural Pavement Analysis Program User's Manual*, FHWA/RD-82/126, Federal Highway Administration, Washington, DC, 1986.
- Eisenmann, J., and G. Leykauf, "Effects of Paving Temperatures on Pavement Performance," *Proceedings*, 2nd International Workshop on the Theoretical Design of Concrete Pavements, Spain, 1990a.
- Eisenmann, J., and G. Leykauf, "Simplified Calculation Method of Slab Curling Caused by Surface Shrinkage," *Proceedings*, 2nd International Workshop on the Theoretical Design of Concrete Pavements, Spain, 1990b.
- Ioannides, A.M., L. Khazanovich, and J.L. Becque, "Structural Evaluation of Base Layers in Concrete Pavement Systems," Paper presented at the 1992 Annual Meeting of the TRB, Transportation Research Board, Washington, DC, 1992.
- Khazanovich, L., *Structural Analysis of Multi-Layered Concrete Pavement Systems*, Ph.D. Thesis, University of Illinois, Urbana, IL, 1994.
- Miner, M.A., "Cumulative Damage in Fatigue," *Transactions*, ASME, Volume 67, 1945.
- Salsilli, R.A., E.J. Barenberg, and M.I. Darter, "Calibrated Mechanistic Design Procedure to Prevent Transverse Cracking of Jointed Plain Concrete Pavements," *Proceedings of the 5th International Conference on Concrete Pavement Design and Rehabilitation*, Purdue University, 1993.
- Seiler, W.J., "Expedient Stress Analysis of Jointed Concrete Pavement Loaded by Aircraft with Multiwheel Gear," *Transportation Research Record 1370*, Transportation Research Board, Washington, DC, 1993.
- Smith, K.D., M.J. Wade, D.G. Peshkin, L. Khazanovich, H.T. Yu, and M.I. Darter, *Performance of Concrete Pavements Volume II — Evaluation of Inservice Concrete Pavements*, Final Report, Contract DTFH61-91-C-00053, Federal Highway Administration, McLean, VA, 1995.

Smith, K.D. et al. *Performance of Concrete Pavements Volume III — Improving Concrete Pavement Performance*, Final Report, Contract DTFH61-91-C-00053, Federal Highway Administration, McLean, VA, 1995b.

Totsky, O.N., *Behavior of Multi-Layered Plates on Winkler Foundation*, *Stroitel'naya Mekhanika i Raschet Sooruzhenii*, No. 6, Moscow, 1981, pp.54-58 (in Russian).

Westergaard, H.M., "Analysis of Stresses in Concrete Pavements Due to Variations of Temperature," *Proceedings, Sixth Annual Meeting*, Highway Research Board, Washington, DC, 1926.

Westergaard, H.M., "New Formulas for Stresses in Concrete Pavements of Airfields," *Transactions, American Society of Civil Engineers*, Volume 113, 1948.

Whiting, D., M. Nagi, P. Okamoto, T. Yu, D. Peshkin, K. Smith, M. Darter, J. Clifton, L. Kaetzel, *Optimization of Highway Concrete Technology*, Final Report, Report SHRP-C-373, SHRP, National Research Council, Washington, DC, 1994.

APPENDIX A: CORE TESTING RESULTS



COMMERCIAL TESTING LABORATORIES

A DIVISION OF CTL/THOMPSON, INC.

August 2, 1994

Colorado Department of Transportation
4201 East Arkansas Avenue
Room A-100
Denver, Colorado 80222

Attention: Mr. Ahmad Ardani

Subject: Results of Testing
Modulus of Elasticity, 6-inch Cores
CDOT Project ACIM 070-5 (53)
Job No. 9370

Gentlemen:

This report presents results of tests conducted on six 6-inch cores delivered to our laboratory for testing. We understand that these cores were extracted from pavement at the Burlington to Kansas project, but were not informed as to the dates of placement. The cores were soaked for 40 hours in lime water, and tested for Modulus of Elasticity (MOE) and Compressive Strength.

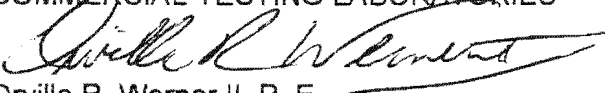
The tests were conducted in accordance with ASTM C 469 using a mechanical frame to monitor stain versus stress. As specified, an initial stress reading was taken when a strain of 0.00005 was achieved, and additional strain readings were taken at 5000 load pound increments up to 50% of the anticipated ultimate load. After two duplicate runs were achieved on each specimen, the frame was removed, and the core was tested for compressive strength.

The MOE was calculated based on the stress-strain differential between the initial load and 40% of the ultimate load. One core exhibited atypical elastic properties, in that it achieved only 2570 psi compressive strength and 2.05×10^6 psi MOE. The other five cores achieved values from 3990 psi to 4920 psi for compressive strength and 2.88×10^6 psi to 3.30×10^6 psi MOE. Results are presented in Table No. 1. In our experience, MOE's of concrete made with local materials are not as high as predicted by the American Concrete Institute and other industry literature. Moreover, we have noticed that cores tend to yield lower MOE's than cast cylinders from the same materials. However, the MOE's of these cores are slightly lower than we expected for Class P concrete.

If you have any questions regarding this report, or if we can be of further assistance, please do not hesitate to call.

Very truly yours,

COMMERCIAL TESTING LABORATORIES


Orville R. Werner II, P. E.
Principal Consultant

ORW/orw3

cc CDOT District 1 Materials Engineer (Gerald Peterson)

Table No. 1

MODULUS OF ELASTICITY AND COMPRESSIVE STRENGTH OF CONCRETE CORES

<u>Sample ID.</u>	<u>Diameter (in)</u>	<u>Length (in)</u>	<u>Ultimate Load (lb)</u>	<u>Load at 0.00005 Strain (lb)</u>	<u>Load at 40% f_c (lb)</u>	<u>Strain at 40% f_c</u>	<u>Modulus of Elasticity</u>	<u>Compressive Strength (psi)</u>
1-2	5.90	11.48	134,500	4875	53,800	0.000546	3.30x10 ⁶	4920
1-3	5.89	11.60	125,000	4775	50,000	0.000581	2.88x10 ⁶	4590
2-1	5.89	11.61	70,000	3400	28,000	0.000445	2.05x10 ⁶	2570
2-2	5.87	11.58	108,000	4500	43,000	0.000495	2.91x10 ⁶	3990
3-3	5.90	11.76	115,000	4730	46,000	0.000503	3.02x10 ⁶	4210
3-4	5.89	11.55	114,500	4800	46,000	0.000507	2.99x10 ⁶	4200

Tested after 40 hours soaking in lime water. Tested on July 29, 1994.

DENSITY OF CONCRETE CORES

<u>Sample ID.</u>	<u>Dimensional Volume (ft.³)</u>	<u>SSD Wt. (g)</u>	<u>Density (pcf)</u>
1-2	0.178	11,490	142.3
1-3	0.181	11,660	142.0
2-1	0.181	11,429	139.2
2-2	0.180	11,444	140.2
3-3	0.182	11,744	142.3
3-4	0.180	11,467	140.4

August 2, 1994
Job No. 9370



APPENDIX B: SUMMARY OF FIELD STRAIN DATA

Tied PCC Shoulders - 14 ft Lanes						
Load			Strain Measurement			
Time	Wheel Path	Speed	Long. Distance From Midspan, in.	Strain Location	Long. Distance From Midspan, in.	Strain, millionths
7:00	edge	creep	0	edge	0	19.4
				shoulder	0	9.9
				edge	12	5.5
				shoulder	12	5.5
				edge	24	4.8
				shoulder	24	3.4
			12	edge	12	15.4
				shoulder	12	9.0
				edge	0	8.4
				shoulder	0	7.5
				edge	24	8.0
				shoulder	24	8.2
			24	edge	24	21.6
				shoulder	24	10.3
				edge	0	3.9
				shoulder	0	3.7
				edge	12	5.2
				shoulder	12	6.6
9:10	edge	creep	0	edge	0	13.6
				shoulder	0	4.5
				edge	12	1.7
				shoulder	12	3.7
				edge	24	-3.5
				shoulder	24	-1.9
			12	edge	12	12.5
				shoulder	12	4.1
				edge	0	3.0
				shoulder	0	1.7
				edge	24	1.5
				shoulder	24	1.8
			24	edge	24	13.3
				shoulder	24	2.5
				edge	0	-0.6
				shoulder	0	-2.7
				edge	12	3.5
				shoulder	12	3.9

Tied PCC Shoulders - 14 ft Lanes						
Load			Strain Measurement			
Time	Wheel Path	Speed	Long. Distance From Midspan, in.	Strain Location	Long. Distance From Midspan, in.	Strain, millionths
11:25	edge	creep	0	edge	0	12.4
				shoulder	0	1.0
			12	edge	12	-1.3
				shoulder	12	-0.3
			24	edge	24	-3.9
				shoulder	24	-7.3
			12	edge	12	13.1
				shoulder	12	3.5
			0	edge	0	-1.1
				shoulder	0	-2.6
			24	edge	24	0.4
				shoulder	24	-2.3
			24	edge	24	12.8
				shoulder	24	-1.4
			0	edge	0	-3.5
				shoulder	0	-6.7
12	edge	12	0.4			
	shoulder	12	-1.2			
15:10	edge	creep	0	edge	0	14.3
				shoulder	0	3.6
			12	edge	12	3.4
				shoulder	12	1.9
			24	edge	24	-2.6
				shoulder	24	-3.2
			12	edge	12	15.7
				shoulder	12	5.6
			0	edge	0	3.2
				shoulder	0	1.0
			24	edge	24	1.8
				shoulder	24	0.8
			24	edge	24	15.1
				shoulder	24	4.1
			0	edge	0	-1.2
				shoulder	0	-2.2
12	edge	12	5.1			
	shoulder	12	2.6			

Tied PCC Shoulders - 14 ft Lanes									
Load			Strain Measurement						
Time	Wheel Path	Speed	Long. Distance From Midspan, in.	Strain Location	Long. Distance From Midspan, in.	Strain, millionths			
17:10	edge	creep	0	edge	0	25.3			
				shoulder	0	14.4			
				edge	12	8.3			
						12	shoulder	12	9.7
							edge	24	5.3
							shoulder	24	0.4
						12	edge	12	23.9
							shoulder	12	13.9
							edge	0	11.5
						24	shoulder	0	7.1
							edge	24	9.0
							shoulder	24	4.6
						24	edge	24	26.9
							shoulder	24	11.5
							edge	0	5.1
				shoulder	0	6.0			
				edge	12	9.1			
				shoulder	12	10.5			
7:00	edge	static	0	edge	0	22.6			
				shoulder	0	11.6			
				edge	12	7.5			
				shoulder	12	9.1			
				edge	24	5.4			
				shoulder	24	2.5			
9:10	edge	static	0	edge	0	11.8			
				shoulder	0	1.2			
				edge	12	-1.6			
				shoulder	12	-1.4			
				edge	24	-7.0			
				shoulder	24	-6.9			
11:25	edge	static	0	edge	0	8.3			
				shoulder	0	-5.9			
				edge	12	-4.5			
				shoulder	12	-5.5			
				edge	24	-13.9			
				shoulder	24	-12.6			

Tied PCC Shoulders - 14 ft Lanes						
Load				Strain Measurement		
Time	Wheel Path	Speed	Long. Distance From Midspan, in.	Strain Location	Long. Distance From Midspan, in.	Strain, millionths
15:10	edge	static	0	edge	0	8.1
				shoulder	0	-2.2
				edge	12	-4.8
				shoulder	12	-4.6
				edge	24	-13.8
				shoulder	24	-13.7
17:10	edge	static	0	edge	0	18.7
				shoulder	0	11.5
				edge	12	6.3
				shoulder	12	8.1
				edge	24	3.1
				shoulder	24	2.5
7:00	24 in.	creep	0	24 in.	0	14.8
				edge	0	5.2
				shoulder	0	2.3
9:10	24 in.	creep	0	24 in.	0	11.1
				edge	0	5.7
				shoulder	0	2.5
11:25	24 in.	creep	0	24 in.	0	10.7
				edge	0	4.0
				shoulder	0	3.3
15:10	24 in.	creep	0	24 in.	0	13.4
				edge	0	4.7
				shoulder	0	7.1
17:10	24 in.	creep	0	24 in.	0	16.5
				edge	0	2.0
				shoulder	0	3.7
7:00	24 in.	static	0	24 in.	0	15.3
				edge	0	5.9
				shoulder	0	5.3
9:10	24 in.	static	0	24 in.	0	10.5
				edge	0	3.9
				shoulder	0	4.7
11:25	24 in.	static	0	24 in.	0	7.0
				edge	0	4.6
				shoulder	0	4.2
15:10	24 in.	static	0	24 in.	0	16.4
				edge	0	1.7
				shoulder	0	-0.9

Tied PCC Shoulders - 14 ft Lanes						
Load				Strain Measurement		
Time	Wheel Path	Speed	Long. Distance From Midspan, in.	Strain Location	Long. Distance From Midspan, in.	Strain, millionths
17:10	24 in.	static	0	24 in.	0	16.0
				edge	0	5.9
				shoulder	0	1.7
7:00	42 in.	creep	0	42 in.	0	20.2
				24 in.	0	7.1
				edge	0	4.3
				shoulder		0.6
9:10	42 in.	creep	0	42 in.	0	12.7
				24 in.	0	8.9
				edge	0	3.0
				shoulder		0.9
11:25	42 in.	creep	0	42 in.	0	10.5
				24 in.	0	3.5
				edge	0	3.7
				shoulder		4.6
15:10	42 in.	creep	0	42 in.	0	13.3
				24 in.	0	9.3
				edge	0	5.9
				shoulder		4.4
17:10	42 in.	creep	0	42 in.	0	16.3
				24 in.	0	8.6
				edge	0	5.9
				shoulder		2.2
7:00	42 in.	static	0	42 in.	0	18.9
				24 in.	0	7.5
				edge	0	4.0
				shoulder	0	3.3
9:10	42 in.	static	0	42 in.	0	6.7
				24 in.	0	8.4
				edge	0	1.4
				shoulder	0	-0.8
11:25	42 in.	static	0	42 in.	0	1.0
				24 in.	0	-2.2
				edge	0	-2.9
				shoulder	0	-3.8
15:10	42 in.	static	0	42 in.	0	16.5
				24 in.	0	8.7
				edge	0	2.8
				shoulder	0	0.8

Tied PCC Shoulders - 14 ft Lanes						
Load				Strain Measurement		
Time	Wheel Path	Speed	Long. Distance From Midspan, in.	Strain Location	Long. Distance From Midspan, in.	Strain, millionths
17:10	42 in.	static	0	42 in.	0	17.7
				24 in.	0	7.9
				edge	0	4.1
				shoulder	0	0.8

Nontied PCC Shoulders - 14 ft Lanes									
Load				Strain Measurement					
Time	Wheel Path	Speed	Long. Distance From Midspan, in.	Strain Location	Long. Distance From Midspan, in.	Strain, millionths			
7:46	edge	creep	0	edge	0	25.6			
				shoulder	0	2.2			
				edge	12	7.2			
						12	shoulder	12	4.4
							edge	24	-2.2
							shoulder	24	4.9
						24	edge	12	22.0
							shoulder	12	5.4
							edge	0	11.4
						24	shoulder	0	2.0
							edge	24	4.2
							shoulder	24	6.4
						24	edge	24	17.2
							shoulder	24	6.1
							edge	0	5.9
						24	shoulder	0	0.7
			edge	12	10.7				
			shoulder	12	4.1				
9:50		creep	0	edge	0	19.0			
				shoulder	0	-2.3			
				edge	12	2.8			
						12	shoulder	12	-1.6
							edge	24	-6.4
							shoulder	24	-3.2
						24	edge	12	18.1
							shoulder	12	-0.1
							edge	0	4.5
						24	shoulder	0	-0.9
							edge	24	-1.9
							shoulder	24	-0.6
						24	edge	24	11.7
							shoulder	24	-1.4
							edge	0	-1.6
						24	shoulder	0	-3.6
			edge	12	5.7				
			shoulder	12	-2.6				

Nontied PCC Shoulders - 14 ft Lanes						
Load			Strain Measurement			
Time	Wheel Path	Speed	Long. Distance From Midspan, in.	Strain Location	Long. Distance From Midspan, in.	Strain, millionths
12:08		creep	0	edge	0	17.7
				shoulder	0	-3.2
				edge	12	2.3
				shoulder	12	-3.1
				edge	24	-6.0
				shoulder	24	-3.7
			12	edge	12	15.5
				shoulder	12	-2.8
				edge	0	6.3
				shoulder	0	-3.4
				edge	24	-2.4
				shoulder	24	-3.5
			24	edge	24	11.6
				shoulder	24	-3.3
				edge	0	-4.4
				shoulder	0	-4.7
				edge	12	5.2
				shoulder	12	-4.1
15:50		creep	0	edge	0	20.9
				shoulder	0	5.1
				edge	12	8.6
				shoulder	12	4.5
				edge	24	1.8
				shoulder	24	4.6
			12	edge	12	21.4
				shoulder	12	3.9
				edge	0	9.2
				shoulder	0	4.3
				edge	24	7.5
				shoulder	24	6.9
			24	edge	24	21.5
				shoulder	24	8.4
				edge	0	4.7
				shoulder	0	1.8
				edge	12	11.3
				shoulder	12	2.4

Nontied PCC Shoulders - 14 ft Lanes									
Load				Strain Measurement					
Time	Wheel Path	Speed	Long. Distance From Midspan, in.	Strain Location	Long. Distance From Midspan, in.	Strain, millionths			
17:36		creep	0	edge	0	24.2			
				shoulder	0	3.7			
			12	edge	12	8.1			
				shoulder	12	5.6			
			24	edge	24	0.2			
				shoulder	24	4.9			
				edge	12	23.7			
				shoulder	12	5.6			
				edge	0	13.6			
				shoulder	0	3.7			
			7:46	edge	static	0	edge	0	27.8
							shoulder	0	3.6
						12	edge	12	7.0
							shoulder	12	3.4
						24	edge	24	-2.5
							shoulder	24	2.2
edge	12	11.0							
shoulder	12	5.7							
9:50	edge	static	0	edge	0	16.0			
				shoulder	0	-7.3			
			12	edge	12	0.1			
				shoulder	12	-7.3			
			24	edge	24	-7.5			
				shoulder	24	-8.2			
12:08	edge	static	0	edge	0	11.6			
				shoulder	0	-13.0			
			12	edge	12	-5.2			
				shoulder	12	-10.9			
			24	edge	24	-13.9			
				shoulder	24	-14.1			

Nontied PCC Shoulders - 14 ft Lanes						
Load				Strain Measurement		
Time	Wheel Path	Speed	Long. Distance From Midspan, in.	Strain Location	Long. Distance From Midspan, in.	Strain, millionths
15:50	edge	static	0	edge	0	23.7
				shoulder	0	1.1
				edge	12	7.3
				shoulder	12	1.4
				edge	24	-0.7
				shoulder	24	-0.2
17:36	edge	static	0	edge	0	29.8
				shoulder	0	3.7
				edge	12	10.8
				shoulder	12	4.0
				edge	24	2.6
				shoulder	24	2.2
7:46	24 in.	creep	0	24 in.	0	14.0
				edge	0	6.9
				shoulder	0	1.2
9:50	24 in.	creep	0	24 in.	0	12.2
				edge	0	7.2
				shoulder	0	0.4
12:08	24 in.	creep	0	24 in.	0	16.0
				edge	0	6.5
				shoulder	0	1.4
15:50	24 in.	creep	0	24 in.	0	17.5
				edge	0	8.1
				shoulder	0	2.7
17:36	24 in.	creep	0	24 in.	0	19.2
				edge	0	7.3
				shoulder	0	1.3
7:46	24 in.	static	0	24 in.	0	17.2
				edge	0	8.3
				shoulder	0	2.4
9:50	24 in.	static	0	24 in.	0	11.0
				edge	0	9.3
				shoulder	0	2.3
12:08	24 in.	static	0	24 in.	0	7.5
				edge	0	7.7
				shoulder	0	-0.9
15:50	24 in.	static	0	24 in.	0	17.4
				edge	0	8.3
				shoulder	0	-0.9

Nontied PCC Shoulders - 14 ft Lanes						
Load				Strain Measurement		
Time	Wheel Path	Speed	Long. Distance From Midspan, in.	Strain Location	Long. Distance From Midspan, in.	Strain, millionths
17:36	24 in.	static	0	24 in.	0	19.1
				edge	0	4.7
				shoulder	0	1.0
7:46	42 in.	creep	0	42 in.	0	12.5
				24 in.	0	8.2
				edge	0	4.4
				shoulder	0	1.6
9:50	42 in.	creep	0	42 in.	0	7.6
				24 in.	0	5.8
				edge	0	5.7
				shoulder	0	0.5
12:08	42 in.	creep	0	42 in.	0	13.4
				24 in.	0	7.5
				edge	0	4.8
				shoulder	0	1.8
15:50	42 in.	creep	0	42 in.	0	17.2
				24 in.	0	12.5
				edge	0	6.1
				shoulder	0	0.1
17:36	42 in.	creep	0	42 in.	0	18.8
				24 in.	0	8.7
				edge	0	3.7
				shoulder	0	-2.2
7:46	42 in.	static	0	42 in.	0	13.9
				24 in.	0	8.8
				edge	0	4.0
				shoulder	0	0.2
9:50	42 in.	static	0	42 in.	0	8.8
				24 in.	0	7.5
				edge	0	6.4
				shoulder	0	1.8
12:08	42 in.	static	0	42 in.	0	8.8
				24 in.	0	7.5
				edge	0	6.4
				shoulder	0	1.8
15:50	42 in.	static	0	42 in.	0	17.0
				24 in.	0	10.6
				edge	0	5.1
				shoulder	0	0.1

Nontied PCC Shoulders - 14 ft Lanes						
Load				Strain Measurement		
Time	Wheel Path	Speed	Long. Distance From Midspan, in.	Strain Location	Long. Distance From Midspan, in.	Strain, millionths
17:36	42 in	static	0	42 in.	0	15.0
				24 in.	0	8.6
				edge	0	3.8
				shoulder	0	0.6

Tied PCC Shoulders - 12 ft Lanes						
Load			Strain Measurement			
Time	Wheel Path	Speed	Long. Distance From Midspan, in.	Strain Location	Long. Distance From Midspan, in.	Strain, millionths
6:15	edge	creep	0	edge	0	19.6
				shoulder	0	9.6
			12	edge	12	6.4
				shoulder	12	7.8
			24	edge	24	2.9
				shoulder	24	1.9
			12	edge	12	17.3
				shoulder	12	11.3
			0	edge	0	10.2
				shoulder	0	7.9
			24	edge	24	6.4
				shoulder	24	6.4
			24	edge	24	19.3
				shoulder	24	9.8
			0	edge	0	5.1
				shoulder	0	5.7
12	edge	12	6.0			
	shoulder	12	7.9			
8:15	edge	creep	0	edge	0	17.8
				shoulder	0	10.4
			12	edge	12	5.4
				shoulder	12	8.8
			24	edge	24	4.2
				shoulder	24	1.1
			12	edge	12	16.0
				shoulder	12	10.1
			0	edge	0	5.9
				shoulder	0	5.0
			24	edge	24	6.4
				shoulder	24	6.1
			24	edge	24	18.3
				shoulder	24	9.4
			0	edge	0	3.2
				shoulder	0	2.7
12	edge	12	6.2			
	shoulder	12	8.0			

Tied PCC Shoulders - 12 ft Lanes									
Load				Strain Measurement					
Time	Wheel Path	Speed	Long. Distance From Midspan, in.	Strain Location	Long. Distance From Midspan, in.	Strain, millionths			
10:30	edge	creep	0	edge	0	15.4			
				shoulder	0	5.6			
				edge	12	4.6			
						12	shoulder	12	4.4
							edge	24	0.7
							shoulder	24	0.6
						24	edge	12	16.6
							shoulder	12	8.6
							edge	0	4.2
						24	shoulder	0	3.4
							edge	24	5.8
							shoulder	24	5.1
						24	edge	24	18.4
							shoulder	24	9.0
							edge	0	-1.6
						24	shoulder	0	-2.3
							edge	12	4.6
							shoulder	12	4.5
			14:20	edge	creep	0	edge	0	17.9
shoulder	0	10.3							
edge	12	5.1							
						12	shoulder	12	8.5
							edge	24	4.2
							shoulder	24	3.4
						12	edge	12	17.8
							shoulder	12	12.4
							edge	0	6.6
						24	shoulder	0	6.1
							edge	24	9.8
							shoulder	24	8.6
						24	edge	24	19.7
							shoulder	24	11.9
							edge	0	2.8
						24	shoulder	0	2.8
							edge	12	7.3
							shoulder	12	8.3

Tied PCC Shoulders - 12 ft Lanes							
Load				Strain Measurement			
Time	Wheel Path	Speed	Long. Distance From Midspan, in.	Strain Location	Long. Distance From Midspan, in.	Strain, millionths	
16:30	edge	creep	0	edge	0	21.8	
				shoulder	0	12.0	
					edge	12	8.8
					shoulder	12	10.6
					edge	24	2.8
					shoulder	24	2.5
				12	edge	12	21.4
					shoulder	12	13.8
					edge	0	9.5
					shoulder	0	8.3
					edge	24	9.1
					shoulder	24	8.8
			24	edge	24	21.0	
				shoulder	24	10.9	
				edge	0	4.1	
				shoulder	0	3.9	
				edge	12	9.6	
				shoulder	12	12.3	
6:15	edge	static	0	edge	0	18.0	
				shoulder	0	9.6	
	edge	static			edge	12	8.8
					shoulder	12	6.6
	edge	static			edge	24	3.1
					shoulder	24	2.2
8:15	edge	static	0	edge	0	15.7	
				shoulder	0	9.7	
	edge	static	0		edge	12	5.7
					shoulder	12	4.9
edge	static	0		edge	24	1.5	
				shoulder	24	2.2	
10:30	edge	static	0	edge	0	12.3	
				shoulder	0	3.4	
	edge	static	0		edge	12	4.0
					shoulder	12	-0.3
	edge	static	0		edge	24	-1.0
					shoulder	24	-0.8
14:20	edge	static	0	edge	0	12.8	
				shoulder	0	5.2	
	edge	static	0		edge	12	7.2
					shoulder	12	5.2
	edge	static	0		edge	24	1.1
					shoulder	24	1.1

Tied PCC Shoulders - 12 ft Lanes						
Load				Strain Measurement		
Time	Wheel Path	Speed	Long. Distance From Midspan, in.	Strain Location	Long. Distance From Midspan, in.	Strain, millionths
16:30	edge	static	0	edge	0	18.3
				shoulder	0	11.3
	edge	static	0	edge	12	7.8
				shoulder	12	6.1
	edge	static	0	edge	24	2.2
				shoulder	24	2.2
6:15	24 in.	creep	0	24 in.	0	17.2
				edge	0	9.4
				shoulder	0	3.8
8:15	24 in.	creep	0	24 in.	0	13.2
				edge	0	7.0
				shoulder	0	3.8
10:30	24 in.	creep	0	24 in.	0	13.9
				edge	0	6.6
				shoulder	0	1.6
14:20	24 in.	creep	0	24 in.	0	15.7
				edge	0	7.6
				shoulder	0	6.8
16:30	24 in.	creep	0	24 in.	0	17.8
				edge	0	5.1
				shoulder	0	3.3
6:15	24 in.	static	0	24 in.	0	18.4
				edge	0	9.1
				shoulder	0	4.9
8:15	24 in.	static	0	24 in.	0	15.2
				edge	0	9.3
				shoulder	0	6.0
10:30	24 in.	static	0	24 in.	0	8.4
				edge	0	2.5
				shoulder	0	-3.4
14:20	24 in.	static	0	24 in.	0	11.7
				edge	0	11.2
				shoulder	0	6.6
16:30	24 in.	static	0	24 in.	0	14.6
				edge	0	9.3
				shoulder	0	4.3

Free Edge												
Load			Strain Measurement									
Time	Wheel Path	Speed	Long. Distance From Midspan, in.	Strain Location	Long. Distance From Midspan, in.	Strain, millionths						
6:25	edge	creep	0	edge	0	26.6						
					12	15.9						
					24	5.1						
			12	edge		12	edge	12	28.6			
								0	16.3			
								24	12.3			
						24	edge		24	edge	24	26.9
											0	8.5
											12	18.1
8:30	edge	creep	0	edge	0	24.3						
					12	11.8						
					24	2.2						
			12	edge		12	edge	12	26.2			
								0	12.5			
								24	11.1			
						24	edge		24	edge	24	25.1
											0	5.4
											12	13.4
10:42	edge	creep	0	edge	0	26.1						
					12	12.1						
					24	4.1						
			12	edge		12	edge	12	27.8			
								0	13.3			
								24	8.9			
						24	edge		24	edge	24	24.5
											0	4.4
											12	14.1
14:30	edge	creep	0	edge	0	31.4						
					12	17.3						
					24	6.0						
			12	edge		12	edge	12	34.4			
								0	15.6			
								24	15.0			
						24	edge		24	edge	24	30.0
											0	7.5
											12	18.0

Free Edge						
Load			Strain Measurement			
Time	Wheel Path	Speed	Long. Distance From Midspan, in.	Strain Location	Long. Distance From Midspan, in.	Strain, millionths
16:50	edge	creep	0	edge	0	30.3
					12	17.6
					24	4.9
			12	edge	12	33.3
					0	17.7
					24	17.8
			24	edge	24	31.0
					0	8.4
					12	18.7
6:25	edge	static	0	edge	0	26.3
					12	15.1
					24	3.3
8:30	edge	static	0	edge	0	24.5
					12	12.3
					24	4.2
10:42	edge	static	0	edge	0	27.9
					12	13.6
					24	-1.2
14:30	edge	static	0	edge	0	30.0
					12	18.7
					24	5.1
16:50	edge	static	0	edge	0	31.2
					12	20.8
					24	10.2
6:25	18 in.	creep	0	18 in.	0	17.7
				edge	0	13.0
8:30	18 in.	creep	0	18 in.	0	16.9
				edge	0	11.8
10:42	18 in.	creep	0	18 in.	0	18.6
				edge	0	13.1
14:30	18 in.	creep	0	18 in.	0	17.5
				edge	0	14.3
16:50	18 in.	creep	0	18 in.	0	22.1
				edge	0	16.9
6:25	18 in.	static	0	18 in.	0	21.5
				edge	0	13.0
8:30	18 in.	static	0	18 in.	0	16.4
				edge	0	13.1
10:42	18 in.	static	0	18 in.	0	16.2
				edge	0	12.3

Free Edge						
Load				Strain Measurement		
Time	Wheel Path	Speed	Long. Distance From Midspan, in.	Strain Location	Long. Distance From Midspan, in.	Strain, millionths
14:30	18 in.	static	0	18 in. edge	0	18.8
					0	13.5
16:50	18 in.	static	0	18 in. edge	0	21.3
					0	14.6

APPENDIX C: FWD DATA

Table C1. Interior deflections measured using FWD.

Sec	Stn ft	Test	Drop	Load lbf	Measured Deflections, mils						Deflections Normalized to 9,000 lb Load, mils						Time hh:mm:ss	Temp °F
					0	12	18	26	36	60	0	12	18	26	36	60		
1	0	Basin	1	9,021	2.77	2.57	2.40	2.26	1.98	1.39	2.76	2.56	2.39	2.25	1.98	1.39	16:07:18	54
1	0	Basin	2	12,109	3.68	3.38	3.19	2.98	2.56	1.99	2.74	2.51	2.37	2.21	1.90	1.48	16:07:28	54
1	0	Basin	3	16,028	4.75	4.47	4.14	3.91	3.35	2.44	2.67	2.51	2.32	2.20	1.88	1.37	16:07:36	54
1	15	Basin	1	8,984	2.87	2.63	2.48	2.32	1.99	1.37	2.88	2.63	2.48	2.32	1.99	1.37	16:08:35	54
1	15	Basin	2	12,146	3.81	3.51	3.32	3.10	2.64	1.91	2.82	2.60	2.46	2.30	1.96	1.42	16:08:44	54
1	15	Basin	3	16,052	5.03	4.70	4.36	4.07	3.50	2.43	2.82	2.64	2.44	2.28	1.96	1.36	16:08:51	54
1	30	Basin	1	8,972	2.90	2.70	2.57	2.38	2.04	1.41	2.91	2.71	2.58	2.39	2.05	1.41	16:09:34	54
1	30	Basin	2	11,914	3.79	3.50	3.36	3.11	2.64	1.95	2.86	2.64	2.54	2.35	1.99	1.47	16:09:45	54
1	30	Basin	3	15,906	4.96	4.75	4.39	4.08	3.50	2.48	2.81	2.69	2.48	2.31	1.98	1.40	16:09:53	54
1	45	Basin	1	8,936	2.95	2.78	2.57	2.40	2.06	1.43	2.97	2.80	2.59	2.42	2.07	1.44	16:10:32	54
1	45	Basin	2	11,914	3.91	3.59	3.37	3.18	2.68	1.99	2.95	2.71	2.55	2.40	2.02	1.50	16:10:39	54
1	45	Basin	3	15,808	5.12	4.86	4.40	4.13	3.58	2.48	2.91	2.77	2.51	2.35	2.04	1.41	16:10:45	54
1	60	Basin	1	8,850	2.71	2.54	2.37	2.24	1.96	1.40	2.76	2.58	2.41	2.28	1.99	1.42	16:11:27	54
1	60	Basin	2	11,865	3.57	3.35	3.16	2.97	2.59	1.98	2.71	2.54	2.40	2.25	1.96	1.50	16:11:36	54
1	60	Basin	3	15,942	4.69	4.46	4.14	3.92	3.39	2.49	2.65	2.52	2.34	2.21	1.91	1.41	16:11:44	54
1	75	Basin	1	9,058	2.77	2.56	2.42	2.25	1.96	1.37	2.75	2.54	2.40	2.24	1.95	1.36	16:12:24	54
1	75	Basin	2	11,987	3.64	3.33	3.21	3.00	2.57	1.91	2.73	2.50	2.41	2.25	1.93	1.43	16:12:33	54
1	75	Basin	3	16,089	4.82	4.40	4.22	3.93	3.35	2.43	2.70	2.46	2.36	2.20	1.87	1.36	16:12:40	54
1	90	Basin	1	9,033	2.75	2.51	2.43	2.27	1.95	1.38	2.74	2.50	2.42	2.26	1.94	1.37	16:13:23	54
1	90	Basin	2	12,048	3.60	3.30	3.15	2.96	2.51	1.80	2.69	2.47	2.35	2.21	1.88	1.34	16:13:31	54
1	90	Basin	3	15,991	4.72	4.31	4.09	3.85	3.33	2.38	2.66	2.43	2.30	2.17	1.87	1.34	16:13:38	54
1	105	Basin	1	8,997	2.97	2.75	2.63	2.47	2.11	1.51	2.97	2.75	2.63	2.47	2.11	1.51	16:14:19	54
1	105	Basin	2	12,122	3.94	3.68	3.49	3.28	2.79	2.01	2.93	2.73	2.59	2.44	2.07	1.49	16:14:28	54
1	105	Basin	3	16,089	5.13	4.83	4.55	4.27	3.68	2.69	2.87	2.70	2.55	2.39	2.06	1.50	16:14:34	54
1	120	Basin	1	9,045	3.00	2.78	2.62	2.46	2.06	1.44	2.99	2.77	2.61	2.45	2.05	1.43	16:15:18	54
1	120	Basin	2	11,914	3.95	3.68	3.47	3.25	2.79	1.99	2.98	2.78	2.62	2.46	2.11	1.50	16:15:28	54
1	120	Basin	3	15,930	5.15	4.86	4.60	4.28	3.72	2.61	2.91	2.75	2.60	2.42	2.10	1.47	16:15:35	54
1	135	Basin	1	8,948	2.79	2.52	2.40	2.26	1.88	1.36	2.81	2.53	2.41	2.27	1.89	1.37	16:16:32	54
1	135	Basin	2	12,061	3.71	3.44	3.19	3.03	2.59	1.92	2.77	2.57	2.38	2.26	1.93	1.43	16:16:42	54
1	135	Basin	3	16,028	4.80	4.53	4.21	3.90	3.36	2.46	2.70	2.54	2.36	2.19	1.89	1.38	16:16:49	54
2	0	Basin	1	8,984	2.47	2.22	2.15	2.01	1.79	1.32	2.47	2.22	2.15	2.01	1.79	1.32	16:21:36	54
2	0	Basin	2	12,073	3.27	2.97	2.82	2.72	2.35	1.92	2.44	2.21	2.10	2.03	1.75	1.43	16:21:46	54
2	0	Basin	3	15,991	4.15	3.91	3.65	3.50	3.06	2.30	2.34	2.20	2.05	1.97	1.72	1.29	16:21:54	54
2	15	Basin	1	8,911	2.43	2.21	2.14	2.02	1.77	1.29	2.45	2.23	2.16	2.04	1.79	1.30	16:22:34	54
2	15	Basin	2	12,036	3.30	3.03	2.86	2.75	2.39	1.77	2.47	2.27	2.14	2.06	1.79	1.32	16:22:44	54
2	15	Basin	3	16,162	4.23	3.96	3.70	3.55	3.11	2.34	2.36	2.21	2.06	1.98	1.73	1.30	16:22:52	54

Table C1. Interior deflections measured using FWD, continued.

Sec	Stn ft	Test	Drop	Load lbf	Measured Deflections, mils						Deflections Normalized to 9,000 lb Load, mils						Time hh:mm:ss	Temp °F
					0	12	18	26	36	60	0	12	18	26	36	60		
2	30	Basin	1	8,936	2.53	2.36	2.25	2.17	1.89	1.37	2.55	2.38	2.27	2.19	1.90	1.38	16:23:30	54
2	30	Basin	2	12,134	3.41	3.20	3.04	2.91	2.53	1.97	2.53	2.37	2.25	2.16	1.88	1.46	16:23:40	54
2	30	Basin	3	16,125	4.37	4.23	3.93	3.78	3.30	2.48	2.44	2.36	2.19	2.11	1.84	1.38	16:23:47	54
2	45	Basin	1	8,936	2.36	2.16	2.06	1.99	1.71	1.29	2.38	2.18	2.07	2.00	1.72	1.30	16:24:26	54
2	45	Basin	2	12,183	3.19	2.95	2.78	2.67	2.35	1.95	2.36	2.18	2.05	1.97	1.74	1.44	16:24:37	54
2	45	Basin	3	16,101	4.06	3.83	3.63	3.42	3.03	2.31	2.27	2.14	2.03	1.91	1.69	1.29	16:24:45	54
2	60	Basin	1	8,960	2.60	2.39	2.27	2.15	1.84	1.34	2.61	2.40	2.28	2.16	1.85	1.35	16:25:27	54
2	60	Basin	2	12,085	3.49	3.25	3.06	2.90	2.57	2.00	2.60	2.42	2.28	2.16	1.91	1.49	16:25:38	54
2	60	Basin	3	16,125	4.54	4.35	4.01	3.78	3.38	2.49	2.53	2.43	2.24	2.11	1.89	1.39	16:25:46	54
2	75	Basin	1	8,875	2.61	2.46	2.34	2.23	1.93	1.35	2.65	2.49	2.37	2.26	1.96	1.37	16:26:24	54
2	75	Basin	2	11,987	3.51	3.33	3.14	3.00	2.61	1.91	2.64	2.50	2.36	2.25	1.96	1.43	16:26:33	54
2	75	Basin	3	15,808	4.53	4.30	4.08	3.88	3.37	2.49	2.58	2.45	2.32	2.21	1.92	1.42	16:26:41	54
2	90	Basin	1	9,094	2.72	2.52	2.42	2.31	2.03	1.47	2.69	2.49	2.39	2.29	2.01	1.45	16:27:47	54
2	90	Basin	2	11,902	3.57	3.31	3.17	3.00	2.65	2.05	2.70	2.50	2.40	2.27	2.00	1.55	16:28:00	54
2	90	Basin	3	15,967	4.59	4.30	4.09	3.90	3.42	2.52	2.59	2.42	2.31	2.20	1.93	1.42	16:28:07	54
2	105	Basin	1	8,862	2.78	2.52	2.39	2.22	1.94	1.37	2.82	2.56	2.43	2.25	1.97	1.39	16:28:55	54
2	105	Basin	2	11,914	3.75	3.45	3.22	3.01	2.68	1.92	2.83	2.61	2.43	2.27	2.02	1.45	16:29:05	54
2	105	Basin	3	15,796	4.89	4.52	4.17	3.89	3.41	2.51	2.79	2.58	2.38	2.22	1.94	1.43	16:29:14	54
2	120	Basin	1	8,875	2.76	2.54	2.42	2.32	1.99	1.50	2.80	2.58	2.45	2.35	2.02	1.52	16:29:59	54
2	120	Basin	2	12,183	3.74	3.54	3.28	3.16	2.76	2.22	2.76	2.62	2.42	2.33	2.04	1.64	16:30:11	54
2	120	Basin	3	15,906	4.72	4.46	4.17	3.98	3.48	2.65	2.67	2.52	2.36	2.25	1.97	1.50	16:30:17	54
2	135	Basin	1	8,948	2.61	2.42	2.28	2.19	1.93	1.43	2.63	2.43	2.29	2.20	1.94	1.44	16:31:09	54
2	135	Basin	2	11,975	3.52	3.18	3.08	2.95	2.56	1.94	2.65	2.39	2.31	2.22	1.92	1.46	16:31:18	54
2	135	Basin	3	16,052	4.51	4.23	4.01	3.82	3.37	2.57	2.53	2.37	2.25	2.14	1.89	1.44	16:31:26	54
3	0	Basin	1	9,045	3.18	2.93	2.80	2.65	2.30	1.65	3.16	2.92	2.79	2.64	2.29	1.64	16:35:40	54
3	0	Basin	2	12,097	4.20	3.89	3.69	3.49	3.03	2.37	3.12	2.89	2.75	2.60	2.25	1.76	16:35:49	54
3	0	Basin	3	15,991	5.37	5.09	4.78	4.52	3.93	2.84	3.02	2.86	2.69	2.54	2.21	1.60	16:35:55	54
3	15	Basin	1	9,009	3.05	2.79	2.68	2.55	2.19	1.61	3.05	2.79	2.68	2.55	2.19	1.61	16:36:35	54
3	15	Basin	2	12,146	4.05	3.71	3.57	3.37	2.95	2.29	3.00	2.75	2.65	2.50	2.19	1.70	16:36:43	54
3	15	Basin	3	16,064	5.19	4.84	4.60	4.35	3.82	2.75	2.91	2.71	2.58	2.44	2.14	1.54	16:36:50	54
3	30	Basin	1	9,021	2.98	2.82	2.66	2.54	2.23	1.58	2.97	2.81	2.65	2.53	2.22	1.58	16:37:30	54
3	30	Basin	2	12,073	3.97	3.74	3.52	3.34	3.15	2.38	2.96	2.79	2.62	2.49	2.35	1.77	16:37:38	54
3	30	Basin	3	15,918	5.11	4.85	4.59	4.35	3.78	2.72	2.89	2.74	2.60	2.46	2.14	1.54	16:37:45	54
3	45	Basin	1	8,960	2.92	2.76	2.60	2.48	2.18	1.57	2.93	2.77	2.61	2.49	2.19	1.58	16:38:44	54
3	45	Basin	2	12,109	3.93	3.67	3.47	3.29	2.91	2.27	2.92	2.73	2.58	2.45	2.16	1.69	16:38:54	54
3	45	Basin	3	15,930	5.03	4.76	4.49	4.25	3.74	2.71	2.84	2.69	2.54	2.40	2.11	1.53	16:39:01	54
3	60	Basin	1	8,997	3.21	2.95	2.85	2.66	2.29	1.64	3.21	2.95	2.85	2.66	2.29	1.64	16:39:41	54

Table C1. Interior deflections measured using FWD, continued.

Sec	Stn ft	Test	Drop	Load lbf	Measured Deflections, mils						Deflections Normalized to 9,000 lb Load, mils						Time hh:mm:ss	Temp °F
					0	12	18	26	36	60	0	12	18	26	36	60		
3	60	Basin	2	12,061	4.26	3.93	3.78	3.51	3.03	2.32	3.18	2.93	2.82	2.62	2.26	1.73	16:39:49	54
3	60	Basin	3	15,918	5.47	5.16	4.86	4.56	3.93	2.80	3.09	2.92	2.75	2.58	2.22	1.58	16:39:56	54
3	75	Basin	1	8,923	3.06	2.90	2.75	2.62	2.32	1.69	3.09	2.93	2.77	2.64	2.34	1.70	16:40:31	54
3	75	Basin	2	12,097	4.11	3.83	3.63	3.46	3.03	2.39	3.06	2.85	2.70	2.57	2.25	1.78	16:40:39	54
3	75	Basin	3	15,918	5.27	4.97	4.71	4.47	3.90	2.88	2.98	2.81	2.66	2.53	2.21	1.63	16:40:46	54
3	90	Basin	1	9,021	3.20	3.01	2.84	2.69	2.34	1.70	3.19	3.00	2.83	2.68	2.33	1.70	16:41:25	54
3	90	Basin	2	12,000	4.23	3.97	3.74	3.53	3.05	2.32	3.17	2.98	2.81	2.65	2.29	1.74	16:41:33	54
3	90	Basin	3	15,930	5.45	5.06	4.85	4.58	3.96	2.90	3.08	2.86	2.74	2.59	2.24	1.64	16:41:40	54
3	105	Basin	1	9,009	3.22	3.01	2.82	2.67	2.29	1.63	3.22	3.01	2.82	2.67	2.29	1.63	16:42:15	54
3	105	Basin	2	11,914	4.30	3.96	3.78	3.56	3.34	2.44	3.25	2.99	2.86	2.69	2.52	1.84	16:42:22	54
3	105	Basin	3	15,991	5.53	5.20	4.90	4.58	3.95	2.85	3.11	2.93	2.76	2.58	2.22	1.60	16:42:28	54
3	120	Basin	1	8,997	3.32	3.12	2.97	2.81	2.42	1.66	3.32	3.12	2.97	2.81	2.42	1.66	16:43:07	54
3	120	Basin	2	11,902	4.34	4.10	3.87	3.67	3.17	2.30	3.28	3.10	2.93	2.78	2.40	1.74	16:43:15	54
3	120	Basin	3	16,089	5.76	5.43	5.15	4.84	4.18	2.89	3.22	3.04	2.88	2.71	2.34	1.62	16:43:21	54
3	135	Basin	1	8,887	3.05	2.91	2.70	2.57	2.27	1.68	3.09	2.95	2.73	2.60	2.30	1.70	16:43:58	54
3	135	Basin	2	11,975	3.97	3.71	3.50	3.32	2.92	2.38	2.98	2.79	2.63	2.50	2.19	1.79	16:44:07	54
3	135	Basin	3	15,918	5.09	4.80	4.52	4.28	3.76	2.81	2.88	2.71	2.56	2.42	2.13	1.59	16:44:14	54

Table C2. Deflections and load transfer efficiencies (LTE) at transverse edge measured using FWD.

Sec	Stn ft	Test	Drop	Load lbf	Measured Deflections, mils							Deflections Normalized to 9,000 lb Load, mils							LTE	Average LTE	Time hh:mm:ss	Temp °F
					0	-12	12	18	26	36	60	0	-12	12	18	26	36	60				
1	0	LTE-L	1	9,167	3.51	2.68	3.05	2.79	2.55	2.19	1.46	3.45	2.63	2.99	2.74	2.50	2.15	1.43	76.4%	77%	12:41:21	56
1	0	LTE-L	2	12,061	4.57	3.44	3.94	3.59	3.29	2.80	1.97	3.41	2.57	2.94	2.68	2.46	2.09	1.47	75.3%		12:41:31	56
1	0	LTE-L	3	15,820	5.99	4.48	5.16	4.68	4.26	3.68	2.55	3.41	2.55	2.94	2.66	2.42	2.09	1.45	74.8%		12:41:39	56
1	0	LTE-A	1	9,277	3.38	2.67	2.90	2.67	2.49	2.08	1.46	3.28	2.59	2.81	2.59	2.42	2.02	1.42	79.0%		12:42:27	56
1	0	LTE-A	2	12,158	4.34	3.45	3.72	3.44	3.19	2.71	2.00	3.21	2.55	2.75	2.55	2.36	2.01	1.48	79.5%		12:42:35	56
1	0	LTE-A	3	15,967	5.64	4.49	4.86	4.51	4.14	3.50	2.44	3.18	2.53	2.74	2.54	2.33	1.97	1.38	79.6%		12:42:42	56
1	15	LTE-L	1	9,131	3.52	2.70	2.95	2.74	2.51	2.06	1.45	3.47	2.66	2.91	2.70	2.47	2.03	1.43	76.7%	75%	12:43:41	56
1	15	LTE-L	2	12,085	4.55	3.50	3.88	3.55	3.25	2.74	1.95	3.39	2.61	2.89	2.64	2.42	2.04	1.45	76.9%		12:43:50	56
1	15	LTE-L	3	15,820	6.06	4.60	5.15	4.74	4.34	3.60	2.47	3.45	2.62	2.93	2.70	2.47	2.05	1.41	75.9%		12:43:57	56
1	15	LTE-A	1	8,984	3.50	2.61	3.01	2.79	2.56	2.14	1.48	3.51	2.61	3.02	2.79	2.56	2.14	1.48	74.6%		12:44:29	56
1	15	LTE-A	2	11,926	4.57	3.41	3.95	3.61	3.34	2.80	1.96	3.45	2.57	2.98	2.72	2.52	2.11	1.48	74.6%		12:44:38	56
1	15	LTE-A	3	15,820	6.08	4.46	5.29	4.81	4.39	3.67	2.53	3.46	2.54	3.01	2.74	2.50	2.09	1.44	73.4%		12:44:45	56
1	30	LTE-L	1	9,167	3.25	2.59	2.76	2.60	2.42	2.05	1.47	3.19	2.54	2.71	2.55	2.38	2.01	1.44	79.7%	81%	12:46:31	56
1	30	LTE-L	2	12,036	4.24	3.33	3.59	3.37	3.16	2.68	2.06	3.17	2.49	2.68	2.52	2.36	2.00	1.54	78.5%		12:47:06	56
1	30	LTE-L	3	16,040	5.62	4.46	4.83	4.48	4.15	3.54	2.58	3.15	2.50	2.71	2.51	2.33	1.99	1.45	79.4%		12:47:14	56
1	30	LTE-A	1	8,948	3.12	2.56	2.79	2.55	2.40	2.09	1.47	3.14	2.57	2.81	2.56	2.41	2.10	1.48	82.1%		12:47:49	56
1	30	LTE-A	2	11,926	4.08	3.35	3.77	3.36	3.15	2.74	2.10	3.08	2.53	2.85	2.54	2.38	2.07	1.58	82.1%		12:47:57	56
1	30	LTE-A	3	15,894	5.40	4.49	4.98	4.44	4.20	3.55	2.61	3.06	2.54	2.82	2.51	2.38	2.01	1.48	83.1%		12:48:04	56
1	45	LTE-L	1	9,058	3.16	2.47	2.70	2.54	2.39	2.04	1.45	3.14	2.45	2.68	2.52	2.37	2.03	1.44	78.2%	80%	12:49:07	56
1	45	LTE-L	2	12,036	4.11	3.26	3.58	3.32	3.11	2.68	1.90	3.07	2.44	2.68	2.48	2.33	2.00	1.42	79.3%		12:49:16	56
1	45	LTE-L	3	16,052	5.53	4.36	4.75	4.46	4.15	3.55	2.57	3.10	2.44	2.66	2.50	2.33	1.99	1.44	78.8%		12:49:25	56
1	45	LTE-A	1	9,009	3.12	2.54	2.73	2.57	2.42	2.06	1.49	3.12	2.54	2.73	2.57	2.42	2.06	1.49	81.4%		12:50:05	56
1	45	LTE-A	2	11,877	4.07	3.33	3.58	3.33	3.16	2.84	2.19	3.08	2.52	2.71	2.52	2.39	2.15	1.66	81.8%		12:50:14	56
1	45	LTE-A	3	15,930	5.47	4.43	4.81	4.49	4.22	3.57	2.60	3.09	2.50	2.72	2.54	2.38	2.02	1.47	81.0%		12:50:22	56
1	60	LTE-L	1	9,106	3.50	2.84	2.86	2.65	2.47	2.06	1.45	3.46	2.81	2.83	2.62	2.44	2.04	1.43	81.1%	80%	12:51:28	56
1	60	LTE-L	2	11,902	4.54	3.69	3.75	3.45	3.22	2.76	2.03	3.43	2.79	2.84	2.61	2.43	2.09	1.54	81.3%		12:51:38	56
1	60	LTE-L	3	15,942	6.17	4.90	5.12	4.72	4.34	3.71	2.58	3.48	2.77	2.89	2.66	2.45	2.09	1.46	79.4%		12:51:44	56
1	60	LTE-A	1	8,984	3.23	2.57	2.81	2.63	2.46	2.10	1.47	3.24	2.57	2.82	2.63	2.46	2.10	1.47	79.6%		12:52:33	56
1	60	LTE-A	2	11,755	4.17	3.33	3.64	3.38	3.17	2.69	1.91	3.19	2.55	2.79	2.59	2.43	2.06	1.46	79.9%		12:52:43	56
1	60	LTE-A	3	15,869	5.63	4.50	4.95	4.56	4.25	3.72	2.65	3.19	2.55	2.81	2.59	2.41	2.11	1.50	79.9%		12:52:50	56
1	75	LTE-L	1	9,033	3.60	2.89	3.06	2.81	2.63	2.21	1.57	3.59	2.88	3.05	2.80	2.62	2.20	1.56	80.3%	81%	12:53:39	56
1	75	LTE-L	2	11,951	4.64	3.82	4.05	3.69	3.42	2.89	2.08	3.49	2.88	3.05	2.78	2.58	2.18	1.57	82.3%		12:53:48	56
1	75	LTE-L	3	15,942	6.26	5.05	5.41	4.96	4.57	3.86	2.69	3.53	2.85	3.05	2.80	2.58	2.18	1.52	80.7%		12:53:55	56
1	75	LTE-A	1	9,033	3.39	2.74	2.98	2.77	2.58	2.22	1.56	3.38	2.73	2.97	2.76	2.57	2.21	1.55	80.8%		12:56:10	56
1	75	LTE-A	2	12,048	4.44	3.56	3.87	3.62	3.38	2.92	2.04	3.32	2.66	2.89	2.70	2.52	2.18	1.52	80.2%		12:56:20	56
1	75	LTE-A	3	15,918	5.87	4.72	5.13	4.79	4.46	3.77	2.70	3.32	2.67	2.90	2.71	2.52	2.13	1.53	80.4%		12:56:27	56

Table C2. Deflections and load transfer efficiencies (LTE) at transverse edge measured using FWD, continued.

Sec	Stn ft	Test	Drop	Load lbf	Measured Deflections, mils							Deflections Normalized to 9,000 lb Load, mils							LTE	Average LTE	Time hh:mm:ss	Temp °F
					0	-12	12	18	26	36	60	0	-12	12	18	26	36	60				
1	90	LTE-L	1	9,021	3.25	2.60	2.85	2.65	2.46	2.08	1.46	3.24	2.59	2.84	2.64	2.45	2.08	1.46	80.0%	80%	12:57:16	56
1	90	LTE-L	2	11,987	4.23	3.36	3.68	3.43	3.18	2.68	2.01	3.18	2.52	2.76	2.58	2.39	2.01	1.51	79.4%		12:57:24	56
1	90	LTE-L	3	15,942	5.67	4.47	4.92	4.58	4.22	3.55	2.57	3.20	2.52	2.78	2.59	2.38	2.00	1.45	78.8%		12:57:32	56
1	90	LTE-A	1	9,119	3.23	2.61	2.78	2.61	2.46	2.09	1.49	3.19	2.58	2.74	2.58	2.43	2.06	1.47	80.8%		12:58:54	56
1	90	LTE-A	2	12,061	4.18	3.34	3.67	3.40	3.19	2.71	2.06	3.12	2.49	2.74	2.54	2.38	2.02	1.54	79.9%		12:59:03	56
1	90	LTE-A	3	15,991	5.59	4.43	4.90	4.55	4.20	3.57	2.49	3.15	2.49	2.76	2.56	2.36	2.01	1.40	79.2%		12:59:10	56
1	105	LTE-L	1	9,070	3.22	2.65	2.88	2.67	2.55	2.20	1.58	3.20	2.63	2.86	2.65	2.53	2.18	1.57	82.3%	81%	13:00:00	56
1	105	LTE-L	2	12,012	4.23	3.49	3.74	3.50	3.32	2.87	2.19	3.17	2.61	2.80	2.62	2.49	2.15	1.64	82.5%		13:00:10	56
1	105	LTE-L	3	15,918	5.60	4.57	4.94	4.71	4.37	3.78	2.76	3.17	2.58	2.79	2.66	2.47	2.14	1.56	81.6%		13:00:17	56
1	105	LTE-A	1	9,082	3.28	2.65	2.94	2.78	2.62	2.28	1.61	3.25	2.63	2.91	2.75	2.60	2.26	1.60	80.8%		13:00:53	56
1	105	LTE-A	2	11,963	4.25	3.42	3.81	3.54	3.34	2.89	2.20	3.20	2.57	2.87	2.66	2.51	2.17	1.66	80.5%		13:01:03	56
1	105	LTE-A	3	15,942	5.63	4.54	5.07	4.71	4.44	4.00	2.77	3.18	2.56	2.86	2.66	2.51	2.26	1.56	80.6%		13:01:10	56
1	120	LTE-L	1	9,045	4.29	3.23	2.86	2.67	2.50	2.13	1.52	4.27	3.21	2.85	2.66	2.49	2.12	1.51	75.3%	70%	13:01:58	56
1	120	LTE-L	2	11,853	5.72	4.37	3.77	3.55	3.35	2.85	2.10	4.34	3.32	2.86	2.70	2.54	2.16	1.59	76.4%		13:02:07	56
1	120	LTE-L	3	15,894	7.47	5.70	4.80	4.51	4.33	3.68	2.60	4.23	3.23	2.72	2.55	2.45	2.08	1.47	76.3%		13:02:15	56
1	120	LTE-A	1	9,009	4.12	2.69	3.49	3.24	2.99	2.48	1.79	4.12	2.69	3.49	3.24	2.99	2.48	1.79	65.3%		13:03:15	56
1	120	LTE-A	2	11,951	5.39	3.45	4.62	4.20	3.85	3.23	2.21	4.06	2.60	3.48	3.16	2.90	2.43	1.66	64.0%		13:03:24	56
1	120	LTE-A	3	15,796	7.18	4.46	6.14	5.62	5.10	4.29	2.87	4.09	2.54	3.50	3.20	2.91	2.44	1.64	62.1%		13:03:31	56
1	135	LTE-L	1	9,009	3.87	2.93	3.18	2.92	2.69	2.25	1.53	3.87	2.93	3.18	2.92	2.69	2.25	1.53	75.7%	76%	13:04:14	56
1	135	LTE-L	2	11,938	5.02	3.81	4.11	3.78	3.48	2.94	2.02	3.78	2.87	3.10	2.85	2.62	2.22	1.52	75.9%		13:04:23	56
1	135	LTE-L	3	15,881	6.70	5.09	5.54	5.07	4.66	3.88	2.68	3.80	2.88	3.14	2.87	2.64	2.20	1.52	76.0%		13:04:28	56
1	135	LTE-A	1	9,021	3.68	2.83	3.14	2.90	2.68	2.27	1.56	3.67	2.82	3.13	2.89	2.67	2.26	1.56	76.9%		13:05:13	56
1	135	LTE-A	2	12,000	4.80	3.67	4.14	3.81	3.48	2.96	2.02	3.60	2.75	3.11	2.86	2.61	2.22	1.52	76.5%		13:05:22	56
1	135	LTE-A	3	15,930	6.42	4.89	5.51	5.10	4.64	3.92	2.68	3.63	2.76	3.11	2.88	2.62	2.21	1.51	76.2%		13:05:31	56
2	0	LTE-L	1	9,021	3.10	2.50	2.73	2.53	2.35	1.99	1.42	3.09	2.49	2.72	2.52	2.34	1.99	1.42	80.6%	81%	13:13:01	56
2	0	LTE-L	2	12,109	4.10	3.31	3.61	3.37	3.13	2.67	1.93	3.05	2.46	2.68	2.50	2.33	1.98	1.43	80.7%		13:13:10	56
2	0	LTE-L	3	15,894	5.42	4.33	4.75	4.42	4.13	3.48	2.61	3.07	2.45	2.69	2.50	2.34	1.97	1.48	79.9%		13:13:17	56
2	0	LTE-A	1	8,972	2.99	2.42	2.64	2.45	2.29	1.96	1.39	3.00	2.43	2.65	2.46	2.30	1.97	1.39	80.9%		13:14:38	56
2	0	LTE-A	2	11,877	3.96	3.21	3.49	3.23	3.00	2.58	1.82	3.00	2.43	2.64	2.45	2.27	1.96	1.38	81.1%		13:14:47	56
2	0	LTE-A	3	15,710	5.26	4.26	4.56	4.26	4.01	3.44	2.49	3.01	2.44	2.61	2.44	2.30	1.97	1.43	81.0%		13:14:53	56
2	15	LTE-L	1	9,058	2.88	2.34	2.50	2.32	2.22	1.91	1.36	2.86	2.33	2.48	2.31	2.21	1.90	1.35	81.3%	82%	13:16:24	56
2	15	LTE-L	2	12,061	3.80	3.09	3.33	3.11	2.91	2.52	1.99	2.84	2.31	2.48	2.32	2.17	1.88	1.48	81.3%		13:16:34	56
2	15	LTE-L	3	15,942	5.00	4.02	4.47	4.12	3.83	3.32	2.44	2.82	2.27	2.52	2.33	2.16	1.87	1.38	80.4%		13:16:42	56
2	15	LTE-A	1	8,948	2.76	2.27	2.45	2.27	2.17	1.89	1.37	2.78	2.28	2.46	2.28	2.18	1.90	1.38	82.2%		13:17:18	56
2	15	LTE-A	2	11,987	3.66	3.02	3.28	3.06	2.89	2.51	1.84	2.75	2.27	2.46	2.30	2.17	1.88	1.38	82.5%		13:17:27	56
2	15	LTE-A	3	15,784	4.79	3.97	4.26	4.01	3.75	3.24	2.45	2.73	2.26	2.43	2.29	2.14	1.85	1.40	82.9%		13:17:36	56

Table C2. Deflections and load transfer efficiencies (LTE) at transverse edge measured using FWD, continued.

Sec	Stn ft	Test	Drop	Load lbf	Measured Deflections, mils							Deflections Normalized to 9,000 lb Load, mils							Average LTE	Time hh:mm:ss	Temp °F	
					0	-12	12	18	26	36	60	0	-12	12	18	26	36	60				LTE
2	30	LTE-L	1	8,972	3.23	2.61	2.81	2.62	2.44	2.09	1.48	3.24	2.62	2.82	2.63	2.45	2.10	1.48	80.8%	80%	13:18:29	49
2	30	LTE-L	2	11,865	4.19	3.39	3.70	3.41	3.16	2.79	2.12	3.18	2.57	2.81	2.59	2.40	2.12	1.61	80.9%		13:18:38	49
2	30	LTE-L	3	15,918	5.65	4.44	4.93	4.58	4.26	3.63	2.57	3.19	2.51	2.79	2.59	2.41	2.05	1.45	78.6%		13:18:45	49
2	30	LTE-A	1	9,033	3.17	2.55	2.76	2.56	2.40	2.06	1.47	3.16	2.54	2.75	2.55	2.39	2.05	1.46	80.4%		13:19:21	49
2	30	LTE-A	2	11,975	4.16	3.36	3.64	3.39	3.17	2.71	1.95	3.13	2.53	2.74	2.55	2.38	2.04	1.47	80.8%		13:19:30	49
2	30	LTE-A	3	15,967	5.43	4.41	4.78	4.47	4.16	3.56	2.63	3.06	2.49	2.69	2.52	2.34	2.01	1.48	81.2%		13:19:37	49
2	45	LTE-L	1	8,887	2.97	2.42	2.53	2.38	2.25	1.96	1.38	3.01	2.45	2.56	2.41	2.28	1.98	1.40	81.5%	81%	13:20:23	49
2	45	LTE-L	2	11,914	3.93	3.19	3.38	3.17	3.00	2.59	1.89	2.97	2.41	2.55	2.39	2.27	1.96	1.43	81.2%		13:20:33	49
2	45	LTE-L	3	15,942	5.21	4.31	4.49	4.22	3.98	3.44	2.54	2.94	2.43	2.53	2.38	2.25	1.94	1.43	82.7%		13:20:42	49
2	45	LTE-A	1	8,826	2.86	2.32	2.52	2.35	2.25	1.92	1.41	2.92	2.37	2.57	2.40	2.29	1.96	1.44	81.1%		13:21:19	49
2	45	LTE-A	2	11,853	3.81	3.09	3.39	3.14	2.97	2.56	1.88	2.89	2.35	2.57	2.38	2.26	1.94	1.43	81.1%		13:21:29	49
2	45	LTE-A	3	16,052	5.02	4.08	4.45	4.14	3.91	3.42	2.55	2.81	2.29	2.50	2.32	2.19	1.92	1.43	81.3%		13:21:37	49
2	60	LTE-L	1	9,131	2.85	2.31	2.56	2.39	2.28	1.97	1.44	2.81	2.28	2.52	2.36	2.25	1.94	1.42	81.1%	83%	13:22:21	49
2	60	LTE-L	2	12,134	3.81	3.13	3.48	3.21	3.02	2.59	2.03	2.83	2.32	2.58	2.38	2.24	1.92	1.51	82.2%		13:22:30	49
2	60	LTE-L	3	16,016	4.95	4.05	4.53	4.22	3.98	3.37	2.58	2.78	2.28	2.55	2.37	2.24	1.89	1.45	81.8%		13:22:37	49
2	60	LTE-A	1	8,899	2.77	2.31	2.45	2.33	2.19	1.93	1.41	2.80	2.34	2.48	2.36	2.21	1.95	1.43	83.4%		13:23:11	49
2	60	LTE-A	2	11,853	3.71	3.11	3.35	3.12	2.96	2.53	1.87	2.82	2.36	2.54	2.37	2.25	1.92	1.42	83.8%		13:23:21	49
2	60	LTE-A	3	15,686	4.83	4.03	4.42	4.06	3.85	3.47	2.49	2.77	2.31	2.54	2.33	2.21	1.99	1.43	83.4%		13:23:29	49
2	75	LTE-L	1	10,535	4.09	3.19	3.45	3.18	2.98	2.50	1.79	3.49	2.73	2.95	2.72	2.55	2.14	1.53	78.0%	79%	13:25:44	49
2	75	LTE-L	2	14,050	5.29	4.15	4.46	4.14	3.87	3.35	2.53	3.39	2.66	2.86	2.65	2.48	2.15	1.62	78.4%		13:25:53	49
2	75	LTE-L	3	19,312	7.03	5.48	6.02	5.53	5.14	4.36	3.11	3.28	2.55	2.81	2.58	2.40	2.03	1.45	78.0%		13:26:09	49
2	75	LTE-A	1	10,364	3.74	3.00	3.26	3.07	2.89	2.46	1.71	3.25	2.61	2.83	2.67	2.51	2.14	1.48	80.2%		13:26:45	49
2	75	LTE-A	2	12,073	4.38	3.51	3.81	3.57	3.37	2.87	2.04	3.27	2.62	2.84	2.66	2.51	2.14	1.52	80.1%		13:26:53	49
2	75	LTE-A	3	19,324	6.68	5.41	5.88	5.44	5.09	4.42	3.15	3.11	2.52	2.74	2.53	2.37	2.06	1.47	81.0%		13:26:59	49
2	90	LTE-L	1	9,155	3.30	2.61	2.91	2.72	2.54	2.16	1.52	3.24	2.57	2.86	2.67	2.50	2.12	1.49	79.1%	79%	13:27:41	49
2	90	LTE-L	2	12,231	4.40	3.52	3.92	3.64	3.39	2.89	2.13	3.24	2.59	2.88	2.68	2.49	2.13	1.57	80.0%		13:27:50	49
2	90	LTE-L	3	15,771	5.58	4.47	4.95	4.63	4.34	3.70	2.62	3.18	2.55	2.82	2.64	2.48	2.11	1.50	80.1%		13:27:57	49
2	90	LTE-A	1	9,058	3.30	2.59	2.87	2.68	2.52	2.14	1.54	3.28	2.57	2.85	2.66	2.50	2.13	1.53	78.5%		13:28:47	49
2	90	LTE-A	2	11,829	4.30	3.40	3.69	3.44	3.26	2.76	2.09	3.27	2.59	2.81	2.62	2.48	2.10	1.59	79.1%		13:28:55	49
2	90	LTE-A	3	15,820	5.73	4.53	5.02	4.65	4.32	3.69	2.65	3.26	2.58	2.86	2.65	2.46	2.10	1.51	79.1%		13:29:01	49
2	105	LTE-L	1	9,167	3.43	2.77	2.94	2.77	2.58	2.20	1.57	3.37	2.72	2.89	2.72	2.53	2.16	1.54	80.8%	81%	13:29:46	49
2	105	LTE-L	2	11,938	4.43	3.59	3.81	3.60	3.37	2.88	2.11	3.34	2.71	2.87	2.71	2.54	2.17	1.59	81.0%		13:29:55	49
2	105	LTE-L	3	16,052	5.85	4.70	5.07	4.76	4.44	3.77	2.75	3.28	2.64	2.84	2.67	2.49	2.11	1.54	80.3%		13:30:02	49
2	105	LTE-A	1	9,192	3.30	2.70	2.92	2.72	2.56	2.17	1.55	3.23	2.64	2.86	2.66	2.51	2.12	1.52	81.8%		13:30:34	49
2	105	LTE-A	2	12,024	4.28	3.53	3.83	3.55	3.34	2.86	2.05	3.20	2.64	2.87	2.66	2.50	2.14	1.53	82.5%		13:30:42	49
2	105	LTE-A	3	16,064	5.61	4.60	5.06	4.68	4.40	3.73	2.78	3.14	2.58	2.83	2.62	2.47	2.09	1.56	82.0%		13:30:48	49

Table C2. Deflections and load transfer efficiencies (LTE) at transverse edge measured using FWD, continued.

Sec	Stn ft	Test	Drop	Load lbf	Measured Deflections, mils							Deflections Normalized to 9,000 lb Load, mils							Average LTE	Time hh:mm:ss	Temp °F	
					0	-12	12	18	26	36	60	0	-12	12	18	26	36	60				LTE
2	120	LTE-L	1	9,045	3.08	2.54	2.83	2.63	2.48	2.16	1.57	3.06	2.53	2.82	2.62	2.47	2.15	1.56	82.5%	82%	13:31:37	49
2	120	LTE-L	2	11,914	4.06	3.32	3.74	3.45	3.25	2.83	2.05	3.07	2.51	2.83	2.61	2.46	2.14	1.55	81.8%		13:31:47	49
2	120	LTE-L	3	16,040	5.34	4.32	4.93	4.54	4.27	3.66	2.75	3.00	2.42	2.77	2.55	2.40	2.05	1.54	80.9%		13:31:54	49
2	120	LTE-A	1	9,021	3.05	2.54	2.74	2.56	2.43	2.09	1.53	3.04	2.53	2.73	2.55	2.42	2.09	1.53	83.3%		13:32:29	49
2	120	LTE-A	2	11,926	4.05	3.36	3.59	3.39	3.20	2.79	2.05	3.06	2.54	2.71	2.56	2.41	2.11	1.55	83.0%		13:32:41	49
2	120	LTE-A	3	16,064	5.33	4.42	4.79	4.49	4.23	3.67	2.81	2.99	2.48	2.68	2.52	2.37	2.06	1.57	82.9%		13:32:50	49
2	135	LTE-L	1	9,009	3.52	2.76	3.04	2.85	2.64	2.23	1.57	3.52	2.76	3.04	2.85	2.64	2.23	1.57	78.4%	79%	13:33:56	49
2	135	LTE-L	2	11,951	4.55	3.58	4.00	3.73	3.47	2.93	2.20	3.43	2.70	3.01	2.81	2.61	2.21	1.66	78.7%		13:34:05	49
2	135	LTE-L	3	16,089	6.07	4.76	5.34	4.99	4.63	3.92	2.80	3.40	2.66	2.99	2.79	2.59	2.19	1.57	78.4%		13:34:11	49
2	135	LTE-A	1	8,862	3.44	2.73	2.94	2.78	2.58	2.21	1.57	3.49	2.77	2.99	2.82	2.62	2.24	1.59	79.4%		13:34:44	49
2	135	LTE-A	2	11,755	4.54	3.60	3.93	3.63	3.42	2.88	2.22	3.48	2.76	3.01	2.78	2.62	2.21	1.70	79.3%		13:34:52	49
2	135	LTE-A	3	15,771	6.02	4.75	5.20	4.83	4.50	3.83	2.81	3.44	2.71	2.97	2.76	2.57	2.19	1.60	78.9%		13:34:59	49
3	0	LTE-L	1	9,119	4.80	3.78	4.28	3.92	3.57	2.92	1.95	4.74	3.73	4.22	3.87	3.52	2.88	1.92	78.8%	80%	13:41:27	49
3	0	LTE-L	2	12,097	6.28	4.96	5.67	5.17	4.68	3.84	2.66	4.67	3.69	4.22	3.85	3.48	2.86	1.98	79.0%		13:41:32	49
3	0	LTE-L	3	16,113	8.29	6.51	7.51	6.85	6.19	5.14	3.42	4.63	3.64	4.19	3.83	3.46	2.87	1.91	78.5%		13:41:38	49
3	0	LTE-A	1	9,009	4.70	3.75	4.06	3.76	3.52	3.17	2.20	4.70	3.75	4.06	3.76	3.52	3.17	2.20	79.8%		13:43:13	47
3	0	LTE-A	2	12,012	6.19	4.98	5.40	4.95	4.54	3.81	2.57	4.64	3.73	4.05	3.71	3.40	2.85	1.93	80.5%		13:43:19	47
3	0	LTE-A	3	16,077	8.18	6.66	7.20	6.57	6.01	5.03	3.45	4.58	3.73	4.03	3.68	3.36	2.82	1.93	81.4%		13:43:24	47
3	15	LTE-L	1	9,082	4.73	3.72	4.12	3.79	3.46	2.94	2.13	4.69	3.69	4.08	3.76	3.43	2.91	2.11	78.6%	80%	13:44:07	47
3	15	LTE-L	2	11,902	6.12	4.84	5.35	4.93	4.50	3.80	2.73	4.63	3.66	4.05	3.73	3.40	2.87	2.06	79.1%		13:44:14	47
3	15	LTE-L	3	16,138	8.24	6.54	7.16	6.59	6.02	5.07	3.49	4.60	3.65	3.99	3.68	3.36	2.83	1.95	79.4%		13:44:18	47
3	15	LTE-A	1	9,082	4.66	3.73	4.05	3.74	3.49	2.94	2.17	4.62	3.70	4.01	3.71	3.46	2.91	2.15	80.0%		13:44:53	47
3	15	LTE-A	2	12,036	6.06	4.84	5.30	4.93	4.56	3.87	2.66	4.53	3.62	3.96	3.69	3.41	2.89	1.99	79.9%		13:45:00	47
3	15	LTE-A	3	16,077	7.95	6.39	6.98	6.49	5.97	5.06	3.54	4.45	3.58	3.91	3.63	3.34	2.83	1.98	80.4%		13:45:04	47
3	30	LTE-L	1	8,984	4.52	3.57	3.76	3.47	3.25	2.79	2.04	4.53	3.58	3.77	3.48	3.26	2.79	2.04	79.0%	79%	13:45:47	47
3	30	LTE-L	2	11,975	5.97	4.68	5.03	4.65	4.28	3.71	2.70	4.49	3.52	3.78	3.49	3.22	2.79	2.03	78.4%		13:45:55	47
3	30	LTE-L	3	16,223	7.94	6.18	6.67	6.22	5.71	5.00	3.38	4.40	3.43	3.70	3.45	3.17	2.77	1.88	77.8%		13:46:00	47
3	30	LTE-A	1	9,021	4.41	3.44	3.91	3.61	3.35	2.84	2.04	4.40	3.43	3.90	3.60	3.34	2.83	2.04	78.0%		13:46:35	47
3	30	LTE-A	2	12,048	5.77	4.56	5.09	4.74	4.41	3.75	2.59	4.31	3.41	3.80	3.54	3.29	2.80	1.93	79.0%		13:46:42	47
3	30	LTE-A	3	16,150	7.60	5.99	6.74	6.26	5.79	4.92	3.49	4.24	3.34	3.76	3.49	3.23	2.74	1.94	78.8%		13:46:47	47
3	45	LTE-L	1	8,911	4.77	3.70	4.00	3.65	3.33	2.80	1.96	4.82	3.74	4.04	3.69	3.36	2.83	1.98	77.6%	77%	13:47:28	47
3	45	LTE-L	2	12,000	6.37	4.95	5.39	4.93	4.46	4.08	2.86	4.78	3.71	4.04	3.70	3.35	3.06	2.15	77.7%		13:47:34	47
3	45	LTE-L	3	16,064	8.43	6.52	7.13	6.53	5.90	4.91	3.31	4.72	3.65	3.99	3.66	3.31	2.75	1.85	77.3%		13:47:38	47
3	45	LTE-A	1	8,899	4.77	3.56	4.13	3.76	3.47	2.91	2.06	4.82	3.60	4.18	3.80	3.51	2.94	2.08	74.6%		13:48:13	47
3	45	LTE-A	2	11,914	6.34	4.80	5.50	5.01	4.60	3.91	2.71	4.79	3.63	4.15	3.78	3.47	2.95	2.05	75.7%		13:48:19	47
3	45	LTE-A	3	16,174	8.51	6.49	7.48	6.73	6.17	5.21	3.56	4.74	3.61	4.16	3.74	3.43	2.90	1.98	76.3%		13:48:24	47

Table C2. Deflections and load transfer efficiencies (LTE) at transverse edge measured using FWD, continued.

Sec	Stn ft	Test	Drop	Load lbf	Measured Deflections, mils							Deflections Normalized to 9,000 lb Load, mils							LTE	Average LTE	Time hh:mm:ss	Temp °F
					0	-12	12	18	26	36	60	0	-12	12	18	26	36	60				
3	60	LTE-L	1	8,984	4.34	3.42	3.64	3.35	3.08	2.60	1.86	4.35	3.43	3.65	3.36	3.09	2.60	1.86	78.8%	79%	13:49:06	47
3	60	LTE-L	2	12,097	5.76	4.57	4.87	4.50	4.13	3.45	2.53	4.29	3.40	3.62	3.35	3.07	2.57	1.88	79.3%		13:49:13	47
3	60	LTE-L	3	16,248	7.59	6.03	6.48	5.98	5.46	4.56	3.18	4.20	3.34	3.59	3.31	3.02	2.53	1.76	79.4%		13:49:19	47
3	60	LTE-A	1	8,618	4.09	3.23	3.61	3.34	3.10	2.62	1.88	4.27	3.37	3.77	3.49	3.24	2.74	1.96	79.0%		13:49:49	47
3	60	LTE-A	2	11,621	5.38	4.26	4.75	4.45	4.07	3.68	2.64	4.17	3.30	3.68	3.45	3.15	2.85	2.04	79.2%		13:49:56	47
3	60	LTE-A	3	15,540	7.17	5.68	6.46	5.81	5.41	4.62	3.36	4.15	3.29	3.74	3.36	3.13	2.68	1.95	79.2%		13:50:00	47
3	75	LTE-L	1	9,070	4.73	3.69	3.98	3.66	3.35	2.85	2.03	4.69	3.66	3.95	3.63	3.32	2.83	2.01	78.0%	77%	13:52:05	47
3	75	LTE-L	2	12,305	6.33	4.95	5.42	4.97	4.54	3.82	2.70	4.63	3.62	3.96	3.64	3.32	2.79	1.97	78.2%		13:52:11	47
3	75	LTE-L	3	15,784	8.12	6.33	6.92	6.37	5.80	4.86	3.33	4.63	3.61	3.95	3.63	3.31	2.77	1.90	78.0%		13:52:16	47
3	75	LTE-A	1	8,850	4.55	3.46	3.97	3.67	3.40	2.87	2.00	4.63	3.52	4.04	3.73	3.46	2.92	2.03	76.0%		13:52:47	47
3	75	LTE-A	2	11,926	6.07	4.63	5.28	4.88	4.51	3.87	2.84	4.58	3.49	3.98	3.68	3.40	2.92	2.14	76.3%		13:52:53	47
3	75	LTE-A	3	16,028	8.07	6.14	6.97	6.52	5.99	5.05	3.59	4.53	3.45	3.91	3.66	3.36	2.84	2.02	76.1%		13:52:58	47
3	90	LTE-L	1	9,009	4.58	3.66	3.90	3.60	3.32	2.78	1.93	4.58	3.66	3.90	3.60	3.32	2.78	1.93	79.9%	79%	13:53:45	47
3	90	LTE-L	2	12,109	6.04	4.82	5.19	4.79	4.40	3.72	2.58	4.49	3.58	3.86	3.56	3.27	2.76	1.92	79.8%		13:53:53	47
3	90	LTE-L	3	16,138	7.98	6.26	6.76	6.26	5.74	4.84	3.37	4.45	3.49	3.77	3.49	3.20	2.70	1.88	78.4%		13:53:59	47
3	90	LTE-A	1	8,936	4.52	3.52	3.95	3.67	3.38	2.86	1.99	4.55	3.55	3.98	3.70	3.40	2.88	2.00	77.9%		13:54:34	47
3	90	LTE-A	2	12,048	5.95	4.70	5.23	4.83	4.46	4.09	2.96	4.44	3.51	3.91	3.61	3.33	3.06	2.21	79.0%		13:54:42	47
3	90	LTE-A	3	16,125	7.80	6.14	6.81	6.32	5.84	4.95	3.49	4.35	3.43	3.80	3.53	3.26	2.76	1.95	78.7%		13:54:47	47
3	105	LTE-L	1	8,911	4.60	3.58	3.92	3.60	3.31	2.79	1.99	4.65	3.62	3.96	3.64	3.34	2.82	2.01	77.8%	81%	13:55:31	47
3	105	LTE-L	2	11,975	6.05	4.76	5.21	4.75	4.39	3.68	2.66	4.55	3.58	3.92	3.57	3.30	2.77	2.00	78.7%		13:55:38	47
3	105	LTE-L	3	15,967	8.12	6.33	7.03	6.36	5.84	4.95	3.42	4.58	3.57	3.96	3.58	3.29	2.79	1.93	78.0%		13:55:44	47
3	105	LTE-A	1	8,997	4.23	3.52	3.77	3.51	3.27	2.79	2.07	4.23	3.52	3.77	3.51	3.27	2.79	2.07	83.2%		13:56:17	47
3	105	LTE-A	2	12,048	5.63	4.69	4.96	4.66	4.33	3.83	2.83	4.21	3.50	3.71	3.48	3.23	2.86	2.11	83.3%		13:56:26	47
3	105	LTE-A	3	16,174	7.39	6.12	6.58	6.11	5.67	4.85	3.47	4.11	3.41	3.66	3.40	3.16	2.70	1.93	82.8%		13:56:32	47
3	120	LTE-L	1	8,972	4.33	3.47	3.78	3.51	3.24	2.74	1.92	4.34	3.48	3.79	3.52	3.25	2.75	1.93	80.1%	80%	13:57:13	47
3	120	LTE-L	2	12,109	5.74	4.61	5.00	4.65	4.30	3.63	2.70	4.27	3.43	3.72	3.46	3.20	2.70	2.01	80.3%		13:57:21	47
3	120	LTE-L	3	16,223	7.54	5.99	6.58	6.09	5.62	4.73	3.35	4.18	3.32	3.65	3.38	3.12	2.62	1.86	79.4%		13:57:26	47
3	120	LTE-A	1	8,997	4.27	3.41	3.79	3.50	3.28	2.77	1.94	4.27	3.41	3.79	3.50	3.28	2.77	1.94	79.9%		13:58:03	47
3	120	LTE-A	2	12,073	5.62	4.51	4.94	4.62	4.29	3.64	2.72	4.19	3.36	3.68	3.44	3.20	2.71	2.03	80.2%		13:58:11	47
3	120	LTE-A	3	16,089	7.33	5.89	6.51	6.03	5.57	4.77	3.41	4.10	3.29	3.64	3.37	3.12	2.67	1.91	80.4%		13:58:17	47
3	135	LTE-L	1	9,045	4.75	3.82	4.08	3.77	3.44	2.87	2.05	4.73	3.80	4.06	3.75	3.42	2.86	2.04	80.4%	81%	13:59:00	47
3	135	LTE-L	2	11,987	6.25	5.10	5.39	4.97	4.57	3.81	2.69	4.69	3.83	4.05	3.73	3.43	2.86	2.02	81.6%		13:59:07	47
3	135	LTE-L	3	16,016	8.18	6.54	7.09	6.54	5.94	5.00	3.40	4.60	3.68	3.98	3.68	3.34	2.81	1.91	80.0%		13:59:12	47
3	135	LTE-A	1	9,021	4.49	3.68	3.95	3.65	3.38	2.89	2.11	4.48	3.67	3.94	3.64	3.37	2.88	2.11	82.0%		13:59:50	47
3	135	LTE-A	2	12,097	5.88	4.83	5.18	4.81	4.46	3.78	2.65	4.37	3.59	3.85	3.58	3.32	2.81	1.97	82.1%		13:59:58	47
3	135	LTE-A	3	16,003	7.65	6.26	6.72	6.23	5.75	4.88	3.45	4.30	3.52	3.78	3.50	3.23	2.74	1.94	81.8%		14:00:05	47

Table C3. Deflections and load transfer efficiencies (LTE) at the lane-shoulder edge measured using FWD, continued.

Sec	Stn ft	Test	Drop	Load lbf	Measured Deflections, mils							Deflections Normalized to 9,000 lb Load, mils							LTE	Average LTE	Time hh:mm:ss	Temp °F
					0	-12	12	18	26	36	60	0	-12	12	18	26	36	60				
1	0	Shoulder	1	9,058	3.47	2.97	3.15	2.97	2.82	2.47	1.94	3.45	2.95	3.13	2.95	2.80	2.45	1.93	84.2%	85%	14:31:25	52
1	0	Shoulder	2	12,122	4.49	3.91	4.10	3.92	3.69	3.21	2.42	3.33	2.90	3.04	2.91	2.74	2.38	1.80	85.1%		14:31:32	52
1	0	Shoulder	3	16,040	5.89	5.10	5.38	5.09	4.81	4.20	3.09	3.30	2.86	3.02	2.86	2.70	2.36	1.73	84.6%		14:31:38	52
1	15	Shoulder	1	9,021	2.94	2.60	2.75	2.63	2.51	2.23	1.68	2.93	2.59	2.74	2.62	2.50	2.22	1.68	84.4%	85%	14:34:06	52
1	15	Shoulder	2	11,951	3.80	3.39	3.55	3.39	3.26	2.88	2.32	2.86	2.55	2.67	2.55	2.46	2.17	1.75	85.3%		14:34:15	52
1	15	Shoulder	3	15,967	4.96	4.45	4.69	4.49	4.25	3.76	2.94	2.80	2.51	2.64	2.53	2.40	2.12	1.66	84.7%		14:34:22	52
1	30	Shoulder	1	8,936	3.13	2.78	2.96	2.81	2.72	2.40	1.64	3.15	2.80	2.98	2.83	2.74	2.42	1.65	83.9%	85%	14:35:38	52
1	30	Shoulder	2	11,914	4.09	3.62	3.79	3.66	3.52	3.08	2.30	3.09	2.73	2.86	2.76	2.66	2.33	1.74	85.3%		14:35:47	52
1	30	Shoulder	3	15,869	5.30	4.79	5.05	4.81	4.61	4.06	2.79	3.01	2.72	2.86	2.73	2.61	2.30	1.58	84.7%		14:35:56	52
1	45	Shoulder	1	8,911	3.16	2.76	2.97	2.82	2.68	2.30	1.68	3.19	2.79	3.00	2.85	2.71	2.32	1.70	83.0%	83%	14:37:07	52
1	45	Shoulder	2	11,902	4.15	3.67	3.90	3.72	3.50	3.06	2.45	3.14	2.78	2.95	2.81	2.65	2.31	1.85	84.0%		14:37:19	52
1	45	Shoulder	3	16,003	5.44	4.86	5.25	4.93	4.65	4.06	2.98	3.06	2.73	2.95	2.77	2.62	2.28	1.68	82.7%		14:37:24	52
1	60	Shoulder	1	8,984	2.94	2.55	2.70	2.56	2.42	2.11	1.51	2.95	2.55	2.70	2.56	2.42	2.11	1.51	84.3%	85%	14:38:46	52
1	60	Shoulder	2	11,987	3.86	3.37	3.53	3.35	3.16	2.74	2.09	2.90	2.53	2.65	2.52	2.37	2.06	1.57	85.2%		14:38:56	52
1	60	Shoulder	3	15,906	4.96	4.35	4.62	4.33	4.08	3.55	2.59	2.81	2.46	2.61	2.45	2.31	2.01	1.47	84.1%		14:39:03	52
1	75	Shoulder	1	8,911	2.72	2.31	2.43	2.32	2.17	1.89	1.32	2.75	2.33	2.45	2.34	2.19	1.91	1.33	84.9%	83%	14:41:27	52
1	75	Shoulder	2	11,914	3.57	3.05	3.34	3.02	2.83	2.42	1.92	2.70	2.30	2.52	2.28	2.14	1.83	1.45	81.5%		14:41:36	52
1	75	Shoulder	3	15,820	4.58	3.95	4.26	3.94	3.72	3.19	2.41	2.61	2.25	2.42	2.24	2.12	1.81	1.37	82.8%		14:41:44	52
2	0	Shoulder	1	8,728	2.77	2.40	2.57	2.40	2.31	2.03	1.48	2.86	2.47	2.65	2.47	2.38	2.09	1.53	83.4%	83%	14:53:41	54
2	0	Shoulder	2	11,743	3.73	3.25	3.49	3.22	3.12	2.76	1.99	2.86	2.49	2.67	2.47	2.39	2.12	1.53	83.1%		14:53:50	54
2	0	Shoulder	3	15,552	4.85	4.24	4.56	4.26	4.07	3.56	2.65	2.81	2.45	2.64	2.47	2.36	2.06	1.53	83.0%		14:53:56	54
2	45	Shoulder	1	8,838	3.56	2.95	3.31	3.15	3.01	2.64	2.01	3.63	3.00	3.37	3.21	3.07	2.69	2.05	79.6%	79%	14:56:15	54
2	45	Shoulder	2	11,963	4.77	3.98	4.48	4.24	4.08	3.60	2.90	3.59	2.99	3.37	3.19	3.07	2.71	2.18	79.3%		14:56:23	54
2	45	Shoulder	3	15,906	6.20	5.17	5.88	5.57	5.31	4.69	3.59	3.51	2.93	3.33	3.15	3.00	2.65	2.03	78.5%		14:56:29	54
2	90	Shoulder	1	8,850	4.02	3.35	3.74	3.56	3.41	2.99	2.23	4.09	3.41	3.80	3.62	3.47	3.04	2.27	80.0%	80%	14:59:17	54
2	90	Shoulder	2	11,902	5.35	4.49	4.97	4.78	4.56	4.02	3.01	4.05	3.40	3.76	3.61	3.45	3.04	2.28	80.7%		14:59:21	54
2	90	Shoulder	3	15,930	7.08	5.91	6.59	6.28	6.01	5.32	4.03	4.00	3.34	3.72	3.55	3.40	3.01	2.28	80.1%		14:59:26	54
2	135	Shoulder	1	9,094	4.06	3.46	3.78	3.62	3.46	3.07	2.33	4.02	3.42	3.74	3.58	3.42	3.04	2.31	81.7%	81%	15:01:19	54
2	135	Shoulder	2	11,865	5.30	4.55	4.99	4.69	4.51	3.93	3.12	4.02	3.45	3.79	3.56	3.42	2.98	2.37	81.4%		15:01:24	54
2	135	Shoulder	3	15,918	6.90	5.96	6.59	6.18	5.92	5.22	3.98	3.90	3.37	3.73	3.49	3.35	2.95	2.25	80.8%		15:01:29	54
2	180	Shoulder	1	8,826	4.27	3.69	4.11	3.92	3.76	3.44	2.73	4.35	3.76	4.19	4.00	3.83	3.51	2.78	80.2%	80%	15:08:20	54
2	180	Shoulder	2	12,012	5.81	5.03	5.55	5.28	5.08	4.52	3.48	4.35	3.77	4.16	3.96	3.81	3.39	2.61	80.9%		15:08:24	54
2	180	Shoulder	3	15,735	7.36	6.39	7.17	6.76	6.49	5.90	4.48	4.21	3.65	4.10	3.87	3.71	3.37	2.56	79.6%		15:08:28	54
2	225	Shoulder	1	8,813	2.83	2.47	2.62	2.51	2.39	2.13	1.57	2.89	2.52	2.68	2.56	2.44	2.18	1.60	84.2%	85%	15:15:28	54
2	225	Shoulder	2	11,902	3.75	3.32	3.46	3.33	3.18	2.79	2.26	2.84	2.51	2.62	2.52	2.40	2.11	1.71	85.7%		15:15:38	54
2	225	Shoulder	3	15,784	4.71	4.17	4.44	4.24	4.05	3.58	2.70	2.69	2.38	2.53	2.42	2.31	2.04	1.54	83.9%		15:15:44	54

Table C3. Deflections and load transfer efficiencies (LTE) at the lane-shoulder edge measured using FWD, continued.

Sec	Stn ft	Test	Drop	Load lbf	Measured Deflections, mils							Deflections Normalized to 9,000 lb Load, mils							LTE	Average LTE	Time hh:mm:ss	Temp °F
					0	-12	12	18	26	36	60	0	-12	12	18	26	36	60				
3	0	Shoulder	1	9,229	3.85	3.40	3.57	3.48	3.29	2.90	2.08	3.75	3.32	3.48	3.39	3.21	2.83	2.03	85.0%	85%	15:26:50	54
3	0	Shoulder	2	12,109	4.91	4.42	4.59	4.46	4.25	3.72	2.73	3.65	3.29	3.41	3.31	3.16	2.76	2.03	86.0%		15:26:55	54
3	0	Shoulder	3	16,113	6.42	5.69	5.96	5.74	5.45	4.84	3.59	3.59	3.18	3.33	3.21	3.04	2.70	2.01	85.2%		15:27:00	54
3	45	Shoulder	1	9,143	4.13	3.57	3.90	3.69	3.47	3.18	2.41	4.07	3.51	3.84	3.63	3.42	3.13	2.37	81.7%	82%	15:28:40	54
3	45	Shoulder	2	11,877	5.33	4.66	5.02	4.71	4.47	4.00	2.84	4.04	3.53	3.80	3.57	3.39	3.03	2.15	82.9%		15:28:44	54
3	45	Shoulder	3	15,784	6.95	6.11	6.65	6.16	5.91	5.42	3.72	3.96	3.48	3.79	3.51	3.37	3.09	2.12	82.0%		15:28:48	54
3	90	Shoulder	1	9,192	3.79	3.31	3.57	3.38	3.21	2.80	2.05	3.71	3.24	3.50	3.31	3.14	2.74	2.01	82.8%	84%	15:39:09	54
3	90	Shoulder	2	12,097	4.88	4.32	4.57	4.33	4.12	3.60	2.83	3.63	3.21	3.40	3.22	3.07	2.68	2.11	84.4%		15:39:16	54
3	90	Shoulder	3	16,187	6.51	5.69	6.05	5.68	5.41	4.78	3.51	3.62	3.16	3.36	3.16	3.01	2.66	1.95	84.0%		15:39:22	54
3	135	Shoulder	1	9,241	3.93	3.51	3.69	3.50	3.32	2.86	2.02	3.83	3.42	3.59	3.41	3.23	2.79	1.97	84.9%	86%	15:44:47	54
3	135	Shoulder	2	12,073	5.10	4.59	4.78	4.54	4.30	3.74	2.88	3.80	3.42	3.56	3.38	3.21	2.79	2.15	85.7%		15:44:53	54
3	135	Shoulder	3	16,113	6.63	6.04	6.24	5.95	5.61	4.86	3.48	3.70	3.37	3.49	3.32	3.13	2.71	1.94	86.4%		15:44:58	54
3	180	Shoulder	1	9,155	3.75	3.19	3.47	3.29	3.10	2.69	1.94	3.69	3.14	3.41	3.23	3.05	2.64	1.91	82.1%	83%	15:49:14	54
3	180	Shoulder	2	12,048	4.86	4.20	4.49	4.27	4.03	3.51	2.66	3.63	3.14	3.35	3.19	3.01	2.62	1.99	83.5%		15:49:21	54
3	180	Shoulder	3	16,199	6.31	5.47	5.94	5.59	5.28	4.57	3.32	3.51	3.04	3.30	3.11	2.93	2.54	1.84	82.2%		15:49:26	54
3	225	Shoulder	1	9,155	3.43	3.03	3.23	3.09	2.95	2.59	1.88	3.37	2.98	3.18	3.04	2.90	2.55	1.85	83.8%	84%	15:53:25	54
3	225	Shoulder	2	12,158	4.50	4.02	4.26	4.06	3.87	3.40	2.56	3.33	2.98	3.15	3.01	2.86	2.52	1.90	84.3%		15:53:34	54
3	225	Shoulder	3	16,223	5.85	5.23	5.52	5.31	5.02	4.41	3.26	3.25	2.90	3.06	2.95	2.78	2.45	1.81	84.6%		15:53:40	54